North Gale Landform and the Volcanic Sources of Sediment in Gale Crater, Mars

By

Jeff Churchill, BSc.

Brock University

Submitted in partial fulfillment

of the requirements for the degree of

Master of Science in Earth Sciences

Faculty of Earth Sciences, Brock University

St. Catharines, Ontario

Master of Science (2018) Brock University

(Earth Sciences) St Catharines, ON, Canada

TITLE: Volcanic Sources of Sediment in Gale Crater, Mars

AUTHOR: Jeffrey Churchill, Honours BSc.

(Brock University, St. Catharines, Ontario, Canada, 2016)

SUPERVISOR: Professor, Dr. Mariek E. Schmidt

COMMITTEE: Dr. Frank Fueten, Dr. Kevin Turner

NUMBER OF PAGES: 138

Abstract

An investigation into the origins of a previously unidentified landform north of Gale Crater, Mars (North Gale Landform, NGL) using remotely sensed datasets and morphological mapping has determined that it is a volcanic construct that collapsed and produced a hummocky terrain deposit to the south. Volcaniclastic sediments have been detected in the sedimentary rocks of Gale Crater by APXS. They can be grouped into distinct classes: Jake_M and Bathurst_Inlet. Jake_M are float rocks and cobbles made of igneous sediments with evolved, alkaline compositions and pitted, dusty surfaces. Bathurst_Inlet are least altered potassic basaltic sediments in siltstone sandstone to matrix-supported conglomerates. Simple petrologic models demonstrate there is a need for more than one distinct crystalline source. Bathurst_Inlet class targets are not mantle melts and Jake_M class targets are not differentiated from Bathurst_Inlet or Adirondack. NGL may be one source for the volcaniclastic sediments in Gale Crater.

Key words: Mars, Gale Crater, volcanology, geochemistry, petrological modelling

Acknowledgements

I'd like to thank my thesis supervisor Mariek Schmidt for all the help and support that she has given me for the past 2+ years. Mariek has helped me to live out a dream of mine to work in another planet and hopefully contribute something useful to the planetary science community. I'd like to acknowledge the support, advice and ideas that I have received from the rest of my committee: Frank Fueten, and Kevin Turner. I'd like to thank Jon Walmsley for providing me with the imagery and DEMs to get me started. Thanks to my parents, Jeff and Cathy Churchill, the rest of my family and Emily Jones for putting up with me going to school and living at home for so long, it would not have been possible without you guys. I'd also like to thank the rest of the Earth Science grad students at Brock for giving me advice, bouncing ideas around and letting me distract you guys.

This work is supported by a Canadian Space Agency Participating Scientist Grant to Schmidt, a Queen Elizabeth II Graduate Scholarship in Science and Technology to Churchill and Brock University Graduate Studies Grants to Churchill.

Table of Contents

List of Tables

List of Figures

List of Abbreviations

APXS	Alpha Particle X-Ray Spectrometer
AVA	Augmented Visualization of Attitude
ChemCam	Chemistry & Camera
CheMin	Chemistry & Mineralogy X-Ray Diffraction
CTX	Context Camera
DEM	Digital Elevation Model
FC	Fractional Crystallization
FWHM	Full width at half maximum
HiRISE	High Resolution Imaging Science Experiment
HRSC	High Resolution Stereo Camera
H/W	Height to width ratio
IR	Infrared
Kd	Partition Coefficient
MA	Mineral Accumulation
MER	Mars Exploration Rover
MOLA	Mars Orbital Laser Altimeter
MSL	Mars Science Laboratory
NGL	North Gale Landform
PIXE	Particle-Induced X-Ray Emission
SAM	Sample Analysis at Mars
TAS	Total Alkali-Silica
THEMIS	Thermal Emission Imaging System
Wt%	Weight percentage
XRF	X-Ray Fluorescence

Chapter 1: Introduction

1.1 Space Exploration

Since the end of the Apollo missions in the 1970s, all exploration of the solar system has been conducted by orbiters and robotic probes. Mars has long been a target of our exploration of space. It is a terrestrial planet in the habitable zone (a region in space surrounding a star where liquid water may be found on the surface with sufficient atmospheric pressure) and, unlike Venus, it is possible for long term surface exploration. Numerous missions have been flown to Mars over that time, from the first successful mission Mariner 4 (1965) to the complex current missions such as Mars Reconnaissance Orbiter (2005) and Mars Science Laboratory (2012) (Anderson H. R., 1965; Graf, et al., 2005; Grotzinger J. P., et al., 2012). The study of Mars and our understanding of the planet has come a long way with new generations of orbiters, landers, and rovers providing more detail at higher resolution with better instruments. Some advantages of the newer technology include: cameras in orbit have been able to image the almost the whole planet in up to 5 m/pixel resolution, smaller sections of the planet have imagery with resolution as high as 0.3 m/pixel, and hyperspectral images for surface composition over key areas as well (Figure 1-1) (Graf, et al., 2005). Rovers have also been able to investigate the Mars surface with instruments that measure mineralogy and composition with remote, contact and analytical laboratories as well as image features in high detail (e.g. MSL Curiosity (Grotzinger J. P., et al., 2012) and MER Opportunity/Spirit (Crisp, et al., 2003)).

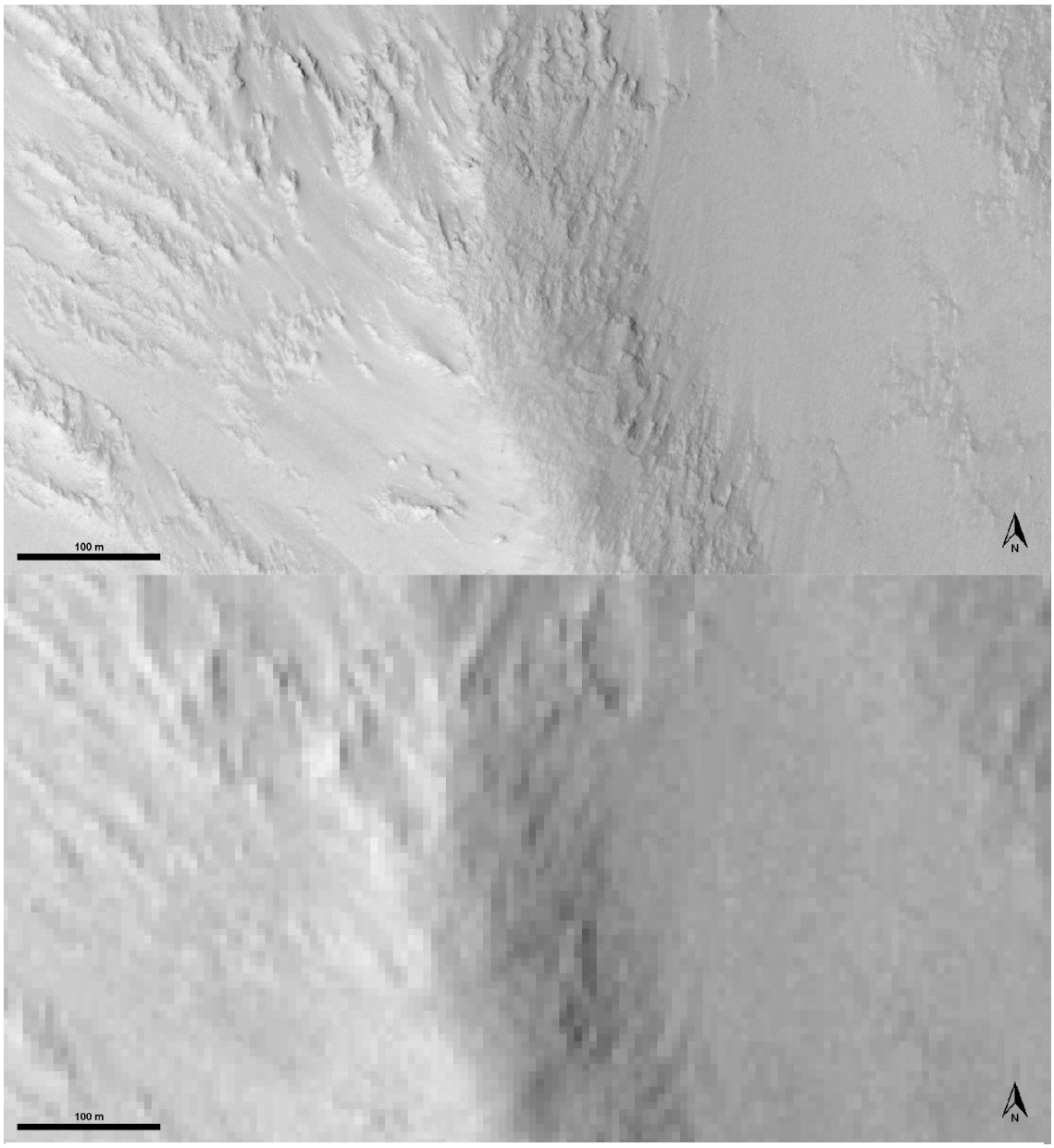

Figure 1-1: Comparison of the resolution for orbital images available currently. Top is an image taken by HiRISE (max: 0.3 m/pixel, pictured: 0.55 m/pixel) and on bottom is an image taken by CTX (max: 5 m/pixel, pictured: 5.39 m/pixel). HiRISE and CTX are instruments on the Mars Reconnaissance Orbiter (launched Aug. 2005). Images: ESP_050396_1770 and B19_017219_1763_XN_03S223W.

1.2 Mars Science Laboratory Rover *Curiosity*

The Mars Science Laboratory (MSL) rover *Curiosity* is the most advanced rover currently exploring Mars (as of 2019) (Figure 1-2). Curiosity was designed to be a mobile science laboratory to conduct advanced experiments on Mars with the goal of

determining the current and past habitability of Mars (Grotzinger J. P., et al., 2012). Curiosity is equipped with ten scientific instruments designed to help it accomplish those goals. The Alpha Particle X-Ray Spectrometer (APXS) located on the rover's arm is used to investigate the elemental composition of surface targets near the rover (Grotzinger J. P., et al., 2012). ChemCam is used to remotely get elemental composition of surface targets within 7 m and take images of the targets (Grotzinger J. P., et al., 2012). CheMin is used to determine mineralogy of rock and soil samples collected by the rover (Grotzinger J. P., et al., 2012). Mars Hand Lens Imager (MAHLI) is used to acquire close up and far away images to aid in interpretation of targets (Grotzinger J. P., et al., 2012). Mars Descent Imager was used to capture images of the original descent to the surface and now captures images below the rover (Grotzinger J. P., et al., 2012). Mastcam is used for imaging experiments during the mission (Grotzinger J. P., et al., 2012). Sample Analysis at Mars (SAM) is a combination of three instruments (Quadrupole Mass Spectrometer, Gas Chromatograph and Tunable Laser Spectrometer) used to investigate Mars for chemistry (molecular and elemental) related to life and the habitability of the present and past in Gale Crater (Grotzinger J. P., et al., 2012).

APXS is of particular interest in this study for its ability to give geological context to the samples delivered to CheMin and SAM instruments of the rover and investigation into the formation of rocks and soils of Gale Crater (Grotzinger J. P., et al., 2012). The measurements taken by APXS combined with context images from MAHLI help to classify rock/soil targets by rock type and potential origin.

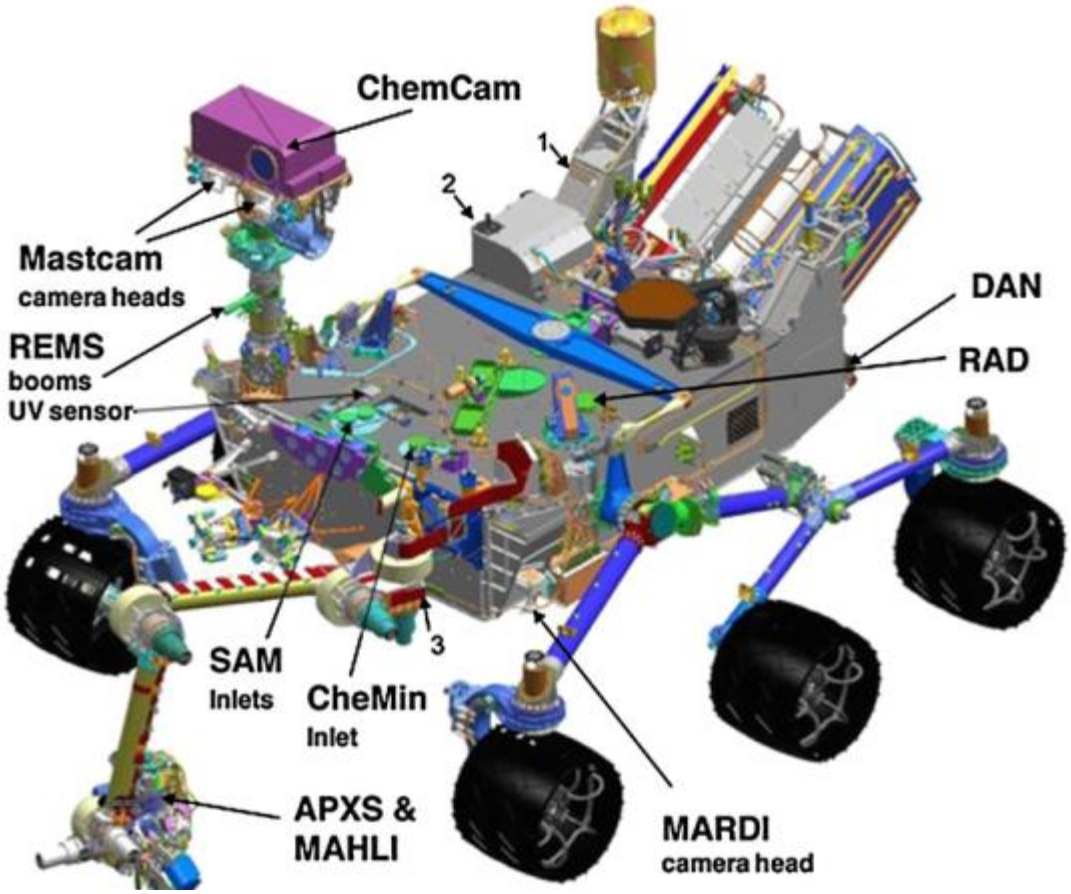

Figure 1-2: An artistic impression of the MSL rover Curiosity with the locations of its primary instruments indicated. Numbered targets indicate the location of calibration targets for some of the instruments. Source: (Grotzinger J. P., et al., 2012)

1.3 Mars History

Mars was formed at approximately the same time as the Earth at ~4.5 Ga (Carr & Head III, 2010). It had a relatively quick accretion and differentiation period which lasted a few tens of millions of years, while at least 70% of the crust had formed by ~4 Ga (Carr & Head III, 2010). Mars' history is divided into four time periods: Pre-Noachian, Noachian, Hesperian, Amazonian (Carr & Head III, 2010). The Pre-Noachian is defined as the time from formation (4.5 Ga) up until the formation of Hellas Basin (Figure 1-3; estimates range from 4.1 to 3.8 Ga) (Carr & Head III, 2010). The Pre-Noachian is characterized by impacts that formed large basins, formation of the global dichotomy

(Figure 1-3), a planetary magnetic field and the start of the accumulation of Tharsis (Figure 1-3) (Carr & Head III, 2010). The Noachian period (4.1-3.8 to 3.7 Ga) is characterized by a relatively high rate (for Mars) of cratering, erosion, volcanism and valley formation (Carr & Head III, 2010). There were occasional warm, wet periods which resulted in phyllosilicate and sulfate production (Carr & Head III, 2010). The Hesperian period (3.7 to 3.0 Ga) is characterized by continued volcanism, flooding, lower erosion rates, and ice activity (Carr & Head III, 2010). The Amazonian period (3.0 Ga to present) is characterized by slowing geological activity (volcanism, floods), extremely low erosion rates, landslides and ice activity (Carr & Head III, 2010).

In the early part of the history of Mars (within 500 million years of formation), it developed an asymmetry in its crust known as the global dichotomy (Figure 1-3) (Golabek, et al., 2011; Carr & Head III, 2010; Šrámek & Zhong, 2012; Andrews-Hanna, et al., 2008). The dichotomy divides Mars into two parts: the southern highlands and the northern lowlands. The two parts of the crust have three distinctive differences between them. (1) There is an average difference of 5.5 km in overall elevation between the northern and southern hemispheres of Mars (Carr & Head III, 2010). The northern portion has a lower average elevation which the southern portion has a higher average elevation (Šrámek & Zhong, 2012). (2) There is a large difference in the crustal thickness between the hemispheres; the thicker southern hemisphere crust is ~60 km and the thinner northern crust is ~30 km thick (Carr & Head III, 2010). And (3), there is a difference in the density of cratering between hemispheres; the southern highlands are more visibly cratered than the northern lowlands, which may have been buried by

younger deposits, resurfaced by geologic processes or protected by an ocean (Carr & Head III, 2010; Citron, et al., 2018). Along the dichotomy boundary, is a unit which transitions from the heavily cratered highlands to the smoother plains of the lowlands (Tanaka, et al., 2014). This transition unit has a variety of landforms associated with it, such as mesas, buttes, knobs, scarps and fretted terrains. Hypotheses for the formation of the dichotomy include a giant impact (Andrews-Hanna, et al., 2008), mantle plume upwelling (Šrámek & Zhong, 2012) or a combination of those (Golabek, et al., 2011). The northern lowlands have a lower average elevation, the crust is thinner, the structure/composition is different, and the surface is younger on average than the southern highlands (Bandfield, et al., 2013).

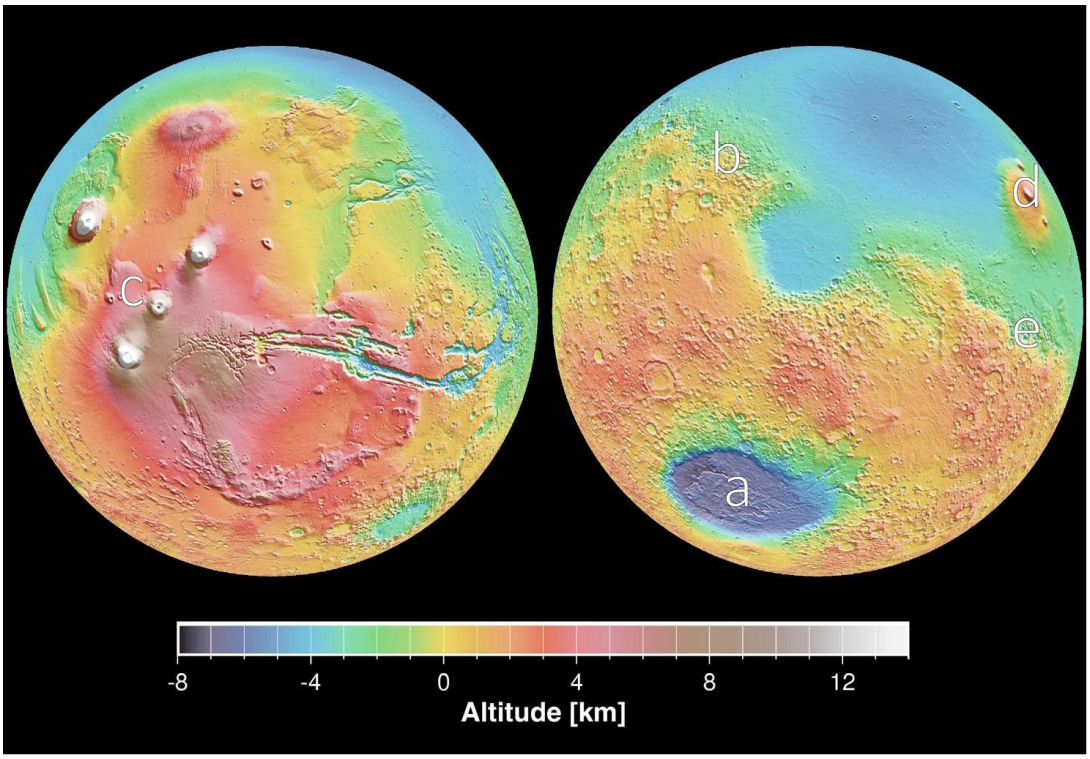

Figure 1-3: Map of Mars surface with MOLA elevation data. White/brown/red are the highest elevation and purple/blue are the lowest elevation. (a) Hellas Basin is the low elevation ellipse in the lower left hand corner of the map. (b) The dichotomy can be seen as there is a distinct change in elevation between the southern and northern hemisphere. (c) Tharsis region is the red area with white spots on the right side of the map. (d) Elysium rise is the high point located to the left of center of the map. (e) Gale Crater, location of the MSL Curiosity mission. Source: https://www.jpl.nasa.gov/spaceimages/details.php?id=PIA02820

Mars has a varied and active surface, evidence of impact cratering as well as fluvial, aeolian, glacial and volcanic activity has been observed on the surface. Over its history, volcanic processes and impact events have had the largest impact on surface and crustal modification. Mars was much more active in its early history; much of this activity has slowed down greatly (or stopped) since near the end of the Hesperian period (Carr & Head III, 2010). The reduction in surface activity helps to better preserve ancient landforms than on the Earth.

1.4 Martian Volcanism

It has been estimated that between 40 and 60% of the Mars surface has a volcanic origin (Parfitt & Wilson, 2011; Tanaka, et al., 2014). Volcanism has been active for most if not all Martian history with evidence of volcanic activity as recent as ~2 Ma (Werner, 2009). Volcanic activity is associated with heat flow from the planet. There was a high amount of heat flow from the formation of Mars (up to 70 mW/m^2) which has steadily declined since then (less than 20 mW/m^2) (Carr & Head III, 2010). Volcanic activity was likely spread over most of the globe before the end of the Noachian period and then became more localized to Tharsis, Elysium and Circum-Hellas provinces (Figure 1-3) (Werner, 2009). Over time, activity at Circum-Hellas and then Elysium also ceased leaving only Tharsis active (possibly currently active) (Werner, 2009). The formation of major volcanic features was likely started before 4.0 Ga due to their completion of growth to their current size around 3.6 Ga (Werner, 2009).

Diverse volcanic features have been identified on Mars. There is evidence of both monogenetic and polygenetic landforms, conventional and phreatomagmatic eruptions, as well as explosive and effusive eruption styles (Platz, et al., 2015; Broz & Hauber, 2013). A change in the dominant eruption style from explosive to effusive in the Hesperian period has been proposed (Robbins, et al., 2011). The change may have been due to a decrease in near surface water so there were less magma-water interactions or possibly a decrease in the actual volatile content in the magma itself (Robbins, et al., 2011). There is a difference observed in the volcanic activity on either side of the dichotomy boundary as well; effusive volcanism dominates the northern lowlands of

Mars and in the southern highlands, the primary eruptive style was apparently explosive (Wilson & Head III, 1994).

Volcanic landforms can be directly related to the eruption of a volcano or tangentially related through the conditions that volcanoes create and influence on the surrounding environment. The landforms can be built up over time gradually or created more rapidly during a single event. They may be the results of explosive or effusive eruptions; they may be the result of conventional or phreatomagmatic eruptions. There are a variety of volcanic landforms found on Mars, demonstrating the varied processes and environments experienced in the past. There are a variety of volcanoes including the enormous shields of Tharsis (Sigurdsson, et al., 2000), potential supervolcanoes in Arabia Terra (Michalski & Bleacher, 2013), and smaller pyroclastic cones all over the planet (Broz & Hauber, 2012). There are a variety of volcanic deposits that range from relatively small features such as lava flows and tubes to enormous ones, such as the Tharsis bulge and Medusa Fossae Formation. Other volcanic features show interactions with the hydro/cryosphere such as tuff cones (Broz & Hauber, 2013), rootless cones (Lanagan, et al., 2001), tuya (Cousin & Crawford, 2011) and chaotic terrain (Chapman & Tanaka, 2002; Meresse, et al., 2008).

1.4.1 Redistribution of Volcanic Materials

Landslides have been observed to be fairly common on terrestrial planets such as Mars (Crosta, et al., 2018) and can occur on different landforms including craters, canyons and volcanoes. A large number of landslides have been observed in Valles Marineris and they are relatively widespread over the planet. Landslides can be

triggered by a variety of environmental factors including precipitation, tectonic activity, volcanic activity, temperature change, and slope change (Crosta, et al., 2018). The largest landslides observed on Mars have occurred on Olympus Mons, the largest volcano in the solar system (Crosta, et al., 2018). The instability in the composition of volcanic edifices (intermixed layers of tephra and lava flows) allows for the collapse and dispersal of debris in massive debris avalanches (Crosta, et al., 2018; Siebert, 1984). Terrestrial volcanoes have been known to generate landslides which remove a significant portion of the edifice and deposit it nearby and there are many examples such as the volcanoes Mount St Helens, Bezymianny and Bandai (Siebert, 1984). Collapses of volcanic edifices often have large landslides associated with them: up to 40 km^3 removed from the volcano, up to 100 km long runout for the landslide and cover a large area (up to 1500 km^2) (Crosta, et al., 2018). Those landslides have distinctive morphologies they are associated with such as horseshoe shaped depression in the edifice, increasing size of opening away from the center of the volcano, hummocky topography extending from the depression, and large blocks present in the deposit (Siebert, 1984).

Clastic sediments are fragments/grains of pre-existing rocks or minerals broken off from their parent rock through physical weathering and transported into sedimentary deposits (Marshak, 2008). On Mars, erosion by wind, ice, water or cratering can remove fragments/grains from a source area before transporting those materials into depositional areas (such as craters or deltas) where they then lithify. The fragments may retain the mineralogy/composition of the source area (if they undergo little/no

alteration). Some of the clastic sediments on the surface of Mars have a volcanic composition due to the source rocks and these are referred to as volcaniclastic (Schmidt, et al., 2014). Volcaniclastic sediments have been suggested to be a part of Martian rocks as early as the Pathfinder mission on Ares Vallis (McSween, et al., 1999) up to the current MSL Curiosity mission in Gale Crater (Schmidt M. , et al., 2017). Pathfinder examined rocks with compositions similar to igneous rocks but were texturally similar to sedimentary rocks which suggested the possibility that those rocks were clastic rocks largely made of volcanic fragments (McSween, et al., 1999). Curiosity examined several targets near an ancient delta known as the Bradbury assemblage which had a volcanic composition (Schmidt, et al., 2014). The Bradbury assemblage is thought to have been eroded from its original source (eroded from the rim of Gale Crater or transported by Peace Vallis drainage) before deposition near Peace Vallis alluvial fan (Schmidt, et al., 2014).

Dust is widespread on the surface and in the atmosphere of Mars, the dust covers most of the surface discontinuously and can build up into a rind on rock surfaces (Berger, et al., 2016; Schmidt, et al., 2018). The dust has a composition similar to the global soil unit as well as the bulk crust of Mars; it is a basaltic composition and the dust is further enriched in S and Cl compared to soil and crust (Berger, et al., 2016). The dust maintains a global uniformity in composition through periodic global dust storms which mix and distribute the dust over the surface (Schmidt, et al., 2018). Theories on the origin of the Martian dust involve wind erosion of altered Martian Crust (Bell III, et al.,

2000) or the Medusa Fossae Formation (Ojha, et al., 2018) which are both considered volcanic sources.

1.4.2 Collapse Features

Chaotic terrain is a landform found on Mars that resembles a collection of large blocks with interconnected valleys between them which are below the surrounding terrain (Figure 1-4). The boundaries of the landform are often elliptical and associated with a large outflow channel (Chapman & Tanaka, 2002). It is possible that the chaotic terrain is confined to ancient impact craters that were later buried by sediment (Chapman & Tanaka, 2002). The interior is a collection of blocks, mesas, buttes, and hills with interconnected valleys between them (Chapman & Tanaka, 2002; Meresse, et al., 2008). Chaotic terrain can be hundreds of km wide with the size of the interior blocks up to 50 km in diameter but can also be much smaller (Meresse, et al., 2008). Chaotic terrain can be explained as collapsed highland terrain into low areas, it appears commonly near the dichotomy boundary and it prevalent in Valles Marineris where the chaotic terrain is up to 7 km below the nearby highland material (Meresse, et al., 2008). Zegers, et al. (2010) proposed a model that the heat forming chaotic terrain would come from the heat flux of Mars and be insulated from the overburden sediments on top of the ice layer. This would cause a change in the isotherm resulting in the melting of the ice layer and formation of subsurface lakes (Zegers, et al., 2010). The overburden would collapse into the lake as the water is catastrophically discharged (Zegers, et al., 2010). This model requires substantial ice layers and overburden (1-2 km each) forming inside of a pre-existing depression (e.g. crater) and results in > 1 km relief differences between

blocks and channels (Zegers, et al., 2010). Smaller chaotic terrain examples (<100 m relief difference) do not fit the same model and would require a different heat source to form. Another hypothesis suggest that chaotic terrain is the result of magma interacting with the subsurface water-ice rich layer and as a result are related to nearby volcanic activity (Meresse, et al., 2008). Meresse, et al. (2008) suggests that a sill intrusion started the formation of the chaotic terrain although other hypothesis do exist (releasing liquid CO_2 from gas hydrates or breach of confined subterranean aquifers). A study of Hydraotes Chaos by Meresse, et al. (2008) indicates that the sill would melt ice contained in the ground causing collapse of the overlying terrain, the water discharge through cracks formed during subsidence of the surface and finally volcanic cones forming on the surface from further rising magma.

Figure 1-4: An example of chaotic terrain on Mars. Hydraotes Chaos is the collection of blocks in the center of the image. To the north of Hydraotes Chaos there are outflow channels were water is said to have flowed out when creating the landform (Meresse, et al., 2008).

Pit crater chains are a chain of depressions that can be linked together into linear channel (Wyrick, et al., 2004). The origin of pit crater chains is associated with the

collapse of the surface into a void space below (Wyrick, et al., 2004). There are several hypotheses for the formation of the void space: tectonic activity (faulting, fissuring), subsurface dissolution and volcanic (collapsed lava tubes, dike swarms, collapsed magma chambers) (Scott & Wilson, 2002; Wyrick, et al., 2004). Scott & Wilson (2002) suggest that pit chain craters are related to and the result of volcanic activity. Degassing of dikes through surface cracks creates a void space for the surface to collapse into creates small crater chains (Scott & Wilson, 2002). Explosive Plinian eruptions creates void spaces along the feeder dikes which then collapse creates larger crater chains (Scott & Wilson, 2002). Wyrick, et al. (2004) suggests that pit crater chains are associated with regional extension and local fissuring.

1.5 Gale Crater

Gale Crater (~155 km) (Figure 1-3, Figure 1-5) is a Noachian (~3.5-3.8 Ga) crater located along the dichotomy boundary. According to Tanaka, et al. (2014), Gale Crater is surrounded by an impact unit which covers the older terrain. It contains the crater rim and ejecta blanket which cover the Hesperian and Noachian transition unit present along the dichotomy boundary (Tanaka, et al., 2014). The transition unit commonly contains knobs, mesas, debris aprons, plains, impact breccias, sedimentary and volcanic deposits (Tanaka, et al., 2014). The older Noachian age landforms may be covered by Hesperian age mass wasting deposits (Tanaka, et al., 2014). To the south of Gale Crater are the heavily cratered southern highlands. They are middle Noachian aged, can be heavily degraded and composed of impact, volcanic, fluvial and basin materials (Tanaka, et al., 2014). Amazonian to Hesperian aged volcanic units probably sourced from the

Elysium volcanoes covers the areas to the north of Gale Crater along with a unit with a number of large plateaus (Tanaka, et al., 2014).

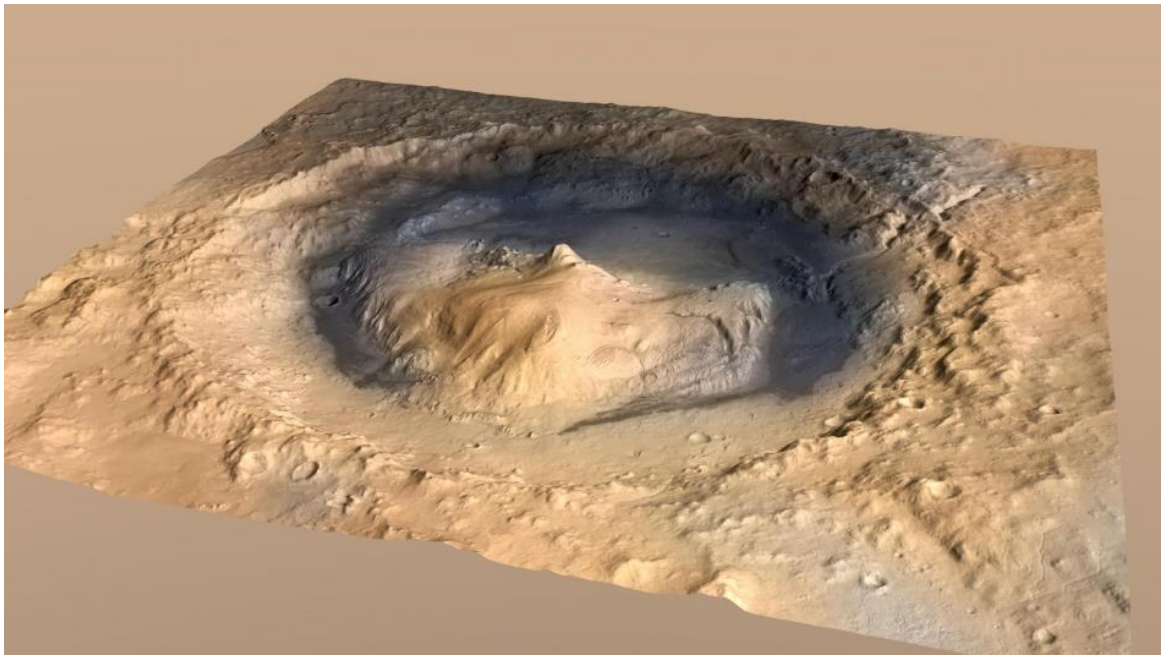

Figure 1-5: Image of Gale Crater on Mars looking southeast. The image is an artistic impression combining elevation data from HRSC and image data from CTX at two times vertical exaggeration. Image credit: NASA/JPL-Caltech/ESA/DLR/FU Berlin/MSSS

Gale Crater was likely filled with sedimentary deposits before erosion removed much of the infill (Grotzinger & Milliken, 2012; Le Deit, et al., 2013; Thomson, et al., 2011). Exhumation and erosion of the sediments filling the crater sculpted a ~6 km tall mountain made of stratified sedimentary units inside of the crater called Aeolis Mons (Thomson, et al., 2011). The upper sedimentary packages of Aeolis Mons appear to consist of dust, volcanic ash, impactor debris and aeolian sand, while the lowermost sedimentary packages appear have formed from lacustrine sediments (Le Deit, et al., 2013). Sediments on the crater's floor and walls appears to be alluvium and colluvium sourced from the crater walls (and possibly outside the crater) (Le Deit, et al., 2013; Palucis, et al., 2014). Outcrops on the crater floor and lowermost Aeolis Mons

encountered by the Curiosity rover are consistent with deposition in fluvial, deltaic and lacustrine environments (Grotzinger, et al., 2015b).

In northern Gale Crater, the Peace Vallis channels system and alluvial fan provides evidence for past water flow into Gale Crater and represents a potential source for sediments in along Curiosity's traverse of the crater floor (Palucis, et al., 2014). The Peace Vallis catchment lies to the north of Gale Crater; it is an irregular terrain with irregular hills (up to 350 m relief) mantled in debris (Palucis, et al., 2014). There is limited exposed bedrock in the area as the mantling debris covers a lot of the ground/hills (Palucis, et al., 2014). The plains between the hills have been hypothesized to be composed of mixtures of colluvium, fluvial, aeolian sediments and possibly volcanic ash (Palucis, et al., 2014). Valleys cut through these plains where surface water may have transported local sediments toward Gale Crater and the Peace Vallis fan system (Palucis, et al., 2014).

Further north of Gale Crater, there is an interesting landform that will be referred to as North Gale Landform (NGL) (Figure 1-6) which is the subject of investigation in Chapter 2. This landform has a distinct half-moon shape with a sloped debris pile in the convex opening. Its high relief (3.2 km) relative to nearby landforms and the distinct shape suggest that it may be different from the nearby mesas and hills and deserves a closer look. The terrain of irregular hills and depressions between NGL and the rim of Gale Crater also appears different from the surrounding terrain. NGL appears to have collapsed and produced a landslide deposit directed towards Gale

Crater and Peace Vallis. The landslide appears to have entered the catchment area of Peace Vallis and could represent an important sediment source for Gale Crater.

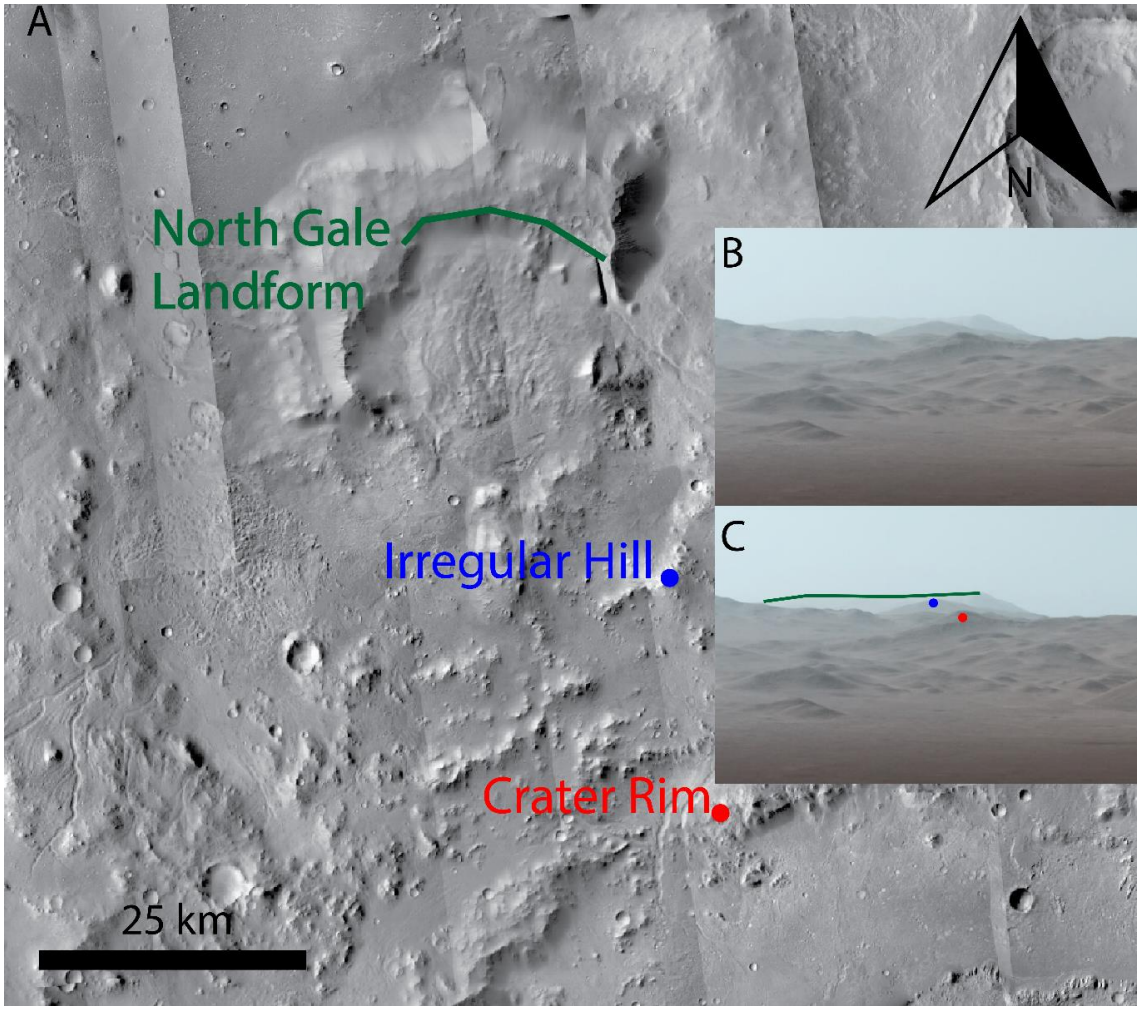

Figure 1-6: Images of North Gale Landform. (A) Map showing the location of North Gale Landform relative to the rim of Gale Crater. The Curiosity rover mission location is located just south of the bottom edge of the map. The map is a mosaic of CTX images (Malin, et al., 2007) from USGS Gale Mosaic (B) View of North Gale Landform from the MSL Curiosity rover on sol 1856 taken by MASTCAM. North Gale Landform is approximately 85 km away from the rover. Image from Fred Calef III. MASTCAM seqid 9703. (C) North Gale Landform, crater rim and irregular hill marked on the image to give context.

1.6 Curiosity in Gale Crater

In 2012, the MSL rover *Curiosity* (Figure 1-2) landed in Gale Crater on a mission to investigate the crater for signs of life and past habitable environments on Mars (Grotzinger J. P., et al., 2012). Over the course of the mission, Curiosity has taken many

measurements of rock, soil and drill tailings. Much of the rock has been interpreted as sediments composed of crushed up volcanic rocks (volcaniclastic) as igneous minerals were identified (pyroxene, quartz, feldspars, olivine, etc.) (Bish, et al., 2013; Downs & MSLScienceTeam, 2015; Vaniman, et al., 2014; Treiman, et al., 2015) and the composition of the targets are igneous-like (Cousin, et al., 2017; Schmidt, et al., 2014). It was discovered early on in the mission that there are targets which may represent least altered igneous endmembers. Evidence of these least altered endmember igneous contributions to the sediments of the Bradbury Group in Aeolis Palus has been uncovered by both the APXS and ChemCam instruments on the rover (Cousin, et al., 2017; Mangold, et al., 2017; McLennan, et al., 2014; Sautter, et al., 2014; Schmidt, et al., 2014; Schmidt M. E., et al., 2017; Siebach, et al., 2017; Stolper, et al., 2013).

Igneous compositions were detected in some APXS targets examined from the first (Jake_Matijevic on sol 46) until it the last target before Pahrump Hills (Homewood_rp on sol 742) and then again in Pogy (sol 1606). The targets with igneous compositions can be separated into four classes of different compositions named after the original target: basaltic sediments of the Bathurst_Inlet class, igneous float blocks and cobbles of the Jake_M class (includes subclasses Matthew and Clinton), possibly igneous float rock Nova and cap rock Pogy (Schmidt M. , et al., 2017). Nova and Pogy classes contain only one target each while the Bathurst Inlet and Jake M class compositions have been observed in several different samples. Jake M class targets have an evolved composition similar to a terrestrial mugearite, there are elevated Al and

alkalis with low Mg (Schmidt, et al., 2014; Stolper, et al., 2013). Bathurst Inlet has a mafic composition with low Al and high K and Fe (Schmidt, et al., 2014).

1.7 Study Purpose

The purpose of this study is to examine the volcaniclastic sediments found in Gale Crater by the MSL *Curiosity* rover, determine how many distinct volcanic sources are required and suggest a possible external source. Chapter 1 provides background information for Mars, Martian volcanology, Gale Crater, and Curiosity. In chapter 2, an interesting landform near Gale Crater will be examined to determine its origin and effect on the surrounding area. In chapter 3, the classes of volcanic sediment will be examined to determine if there is any petrogenetic link between them and the minimum number of volcanic sources to generate them. In chapter 4, the link between the landform and the volcanic sediment will be examined in further detail.

Chapter 2: Volcano and Debris Avalanche Deposit North of Gale Crater, Mars

2.1 Introduction

Since 2012, the MSL rover Curiosity has been exploring the sedimentary rocks of mixed provenance exposed in Gale Crater (3.6 – 3.8 Ga) (Grotzinger, et al., 2015b). The crystalline component of sediments inside Gale Crater are 4.21 ± 0.35 Ga (K-Ar dating on Cumberland drill sample of the Sheepbed mudstone unit) and the exposed surface of the crater floor is 78 ± 30 million years (Farley, et al., 2014). The sediments have been proposed to have originated as the crystalline basement and impact ejecta (Grotzinger J. P., et al., 2015) and to largely derive from the northern rim of Gale Crater as well as the catchment area for Peace Vallis (Figure 2-1) (Palucis, et al., 2014; Grotzinger J. P., et al., 2015). However, it is possible that some of the sediments derive from sources beyond the present-day catchment. There is a need to identify other potential sources for the volcaniclastic sediments found in Gale Crater as there is evidence that the range of volcanic compositions requires several igneous sediment sources (Chapter 3) (Schmidt M. , et al., 2017). North Gale Landform (NGL) is a potential source for some of the volcaniclastic sediments in Gale Crater (Figure 2-1).

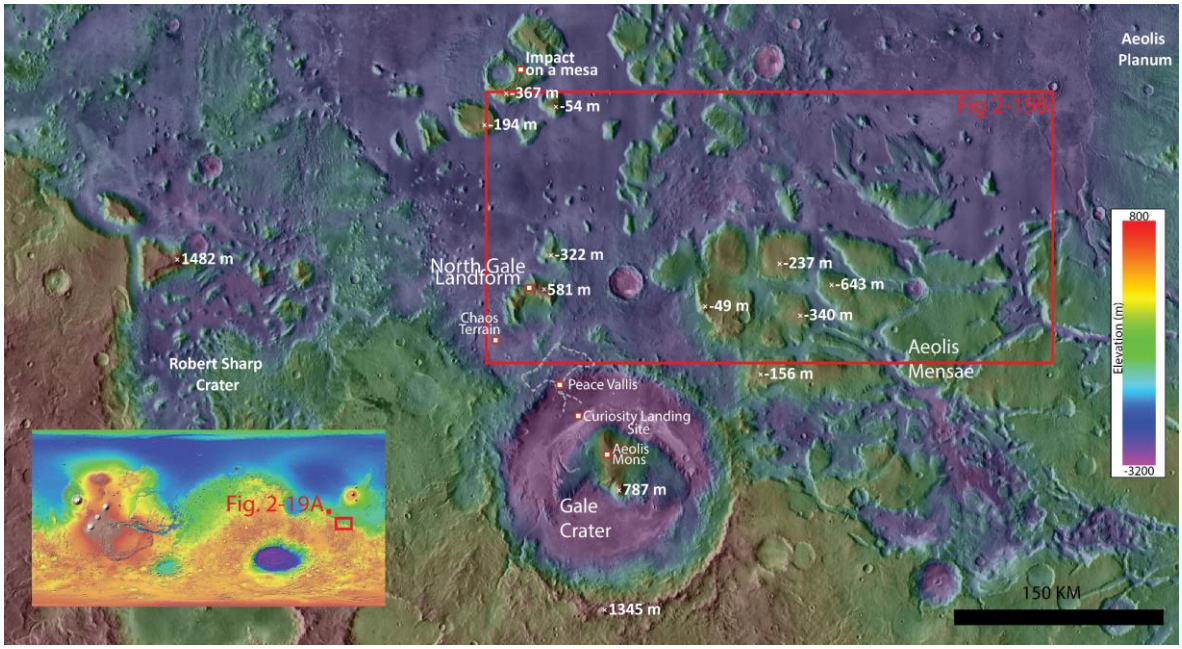

Figure 2-1: Regional map (THEMIS Day IR imagery (Edwards, et al., 2011), MOLA (Smith, et al., 1999) elevation) of the area surrounding North Gale Crater. Labels have been given to important landforms or landmarks in the area, high points in the terrain were also marked to give an idea of the elevation of features in this region. The coloured elevation scale goes from -3200 m (purple) to 800 m (red). Peace Vallis' current catchment is outlined in grey (Palucis, et al., 2014). The landing site of MSL Curiosity is also indicated. The mesas of Aeolis Mensae lie to the east and scattered mesas are also north of North Gale Landform. The Martian dichotomy crosses east-west through the map; a sharp change from the southern highlands to the northern lowlands is clearly visible. The dichotomy is interrupted by Gale Crater and Robert Sharp Crater which both intersect the boundary. Image created in JMARS (Christensen, et al., 2009). Inset shows location on Mars. Image of MGS MOLA Colorized Hillshade.

2.1.1 Volcaniclastic Sediments in Gale Crater

So far, Curiosity has examined two main units in Gale Crater: the Bradbury Group and Mt. Sharp Group (Grotzinger J. P., et al., 2015). The Bradbury Group (bedrock targets before sol 755), which includes mudstones, sandstones, and conglomerates (Grotzinger J. P., et al., 2015), is thought to be isochemically altered from their original state and their compositions are thought to largely reflect their igneous provenance (McLennan, et al., 2014; Sautter, et al., 2014; Schmidt, et al., 2014; Hurowitz, et al., 2017; Grotzinger J. P., et al., 2015). Evidence of these least altered endmember igneous contributions to the sediments of the Bradbury Group in Aeolis Palus has been uncovered by both the APXS and ChemCam instruments on the rover (Cousin, et al.,

2017; Mangold, et al., 2017; McLennan, et al., 2014; Sautter, et al., 2014; Schmidt, et al., 2014; Schmidt M. E., et al., 2017; Siebach, et al., 2017; Stolper, et al., 2013). Igneous compositions were detected in some APXS targets examined from the first (Jake_Matijevic on sol 46) until it the last target before Pahrump Hills (Homewood_rp on sol 742) and then again in Pogy (sol 1606).

Evidence for volcanic activity in/around Gale Crater is indicated by zinc and germanium enrichment (hydrothermal alteration providing secondary enrichment) (Berger, et al., 2017). Berger, et al. (2017) suggests that the enrichment did not take place in situ, rather a source region was enriched before sediments were transported into Gale Crater. In addition, the silica polymorph tridymite was identified by CheMin as 14 wt.% of the Buckskin drill sample (Murray mudstone) (Morris, et al., 2016). Morris, et al. (2016) suggests that the tridymite indicates that there was a low pressure, high temperature silicic volcanic process that produced rocks at a volcanic source area that were then eroded and deposited as detrital sediment in the former Lake Gale.

2.1.2 North Gale Landform

NGL is a previously unclassified landform located ~45 km to the north of Gale Crater (Figure 2-2) in the Hesperian and Noachian transition unit (Tanaka, et al., 2014). It is ~44 km wide, has a relief up to 3.2 km and has an arcuate shape. It has a solid cap and is surrounded by talus slopes which cover the sides of NGL. The most striking feature is a 25-km wide amphitheatre-shaped >1 km deep depression in the southern flank. The floor of the depression is covered in sediments and dissected by channels.

At the southern edge of NGL's amphitheatre is an area of irregular hills and depressions (here dubbed hummocky terrain) up to 40 km wide and 43 km long extends up to the edge of Gale Crater (Figure 2-3). The largest of these irregular hills have up to 1 km relief above the surrounding terrain. The hummocky terrain extends into (and composes the boundaries for) the proposed catchment area of Peace Vallis (Palucis, et al., 2014) and possibly into Gale Crater (near Peace Vallis). NGL has a shape, relief and morphology that is unique among dichotomy boundary landforms as well as modified impact craters (common in the Hesperian and Noachian transition unit).

The aim of this study is to demonstrate that NGL is not a common dichotomy boundary landforms and modified impact craters as well as establish NGL as a volcanic feature. The potentially volcanic nature of NGL, close proximity to Gale Crater and connection to the hummocky terrain represents a source and transportation method for the volcaniclastic sediments discovered in Gale Crater.

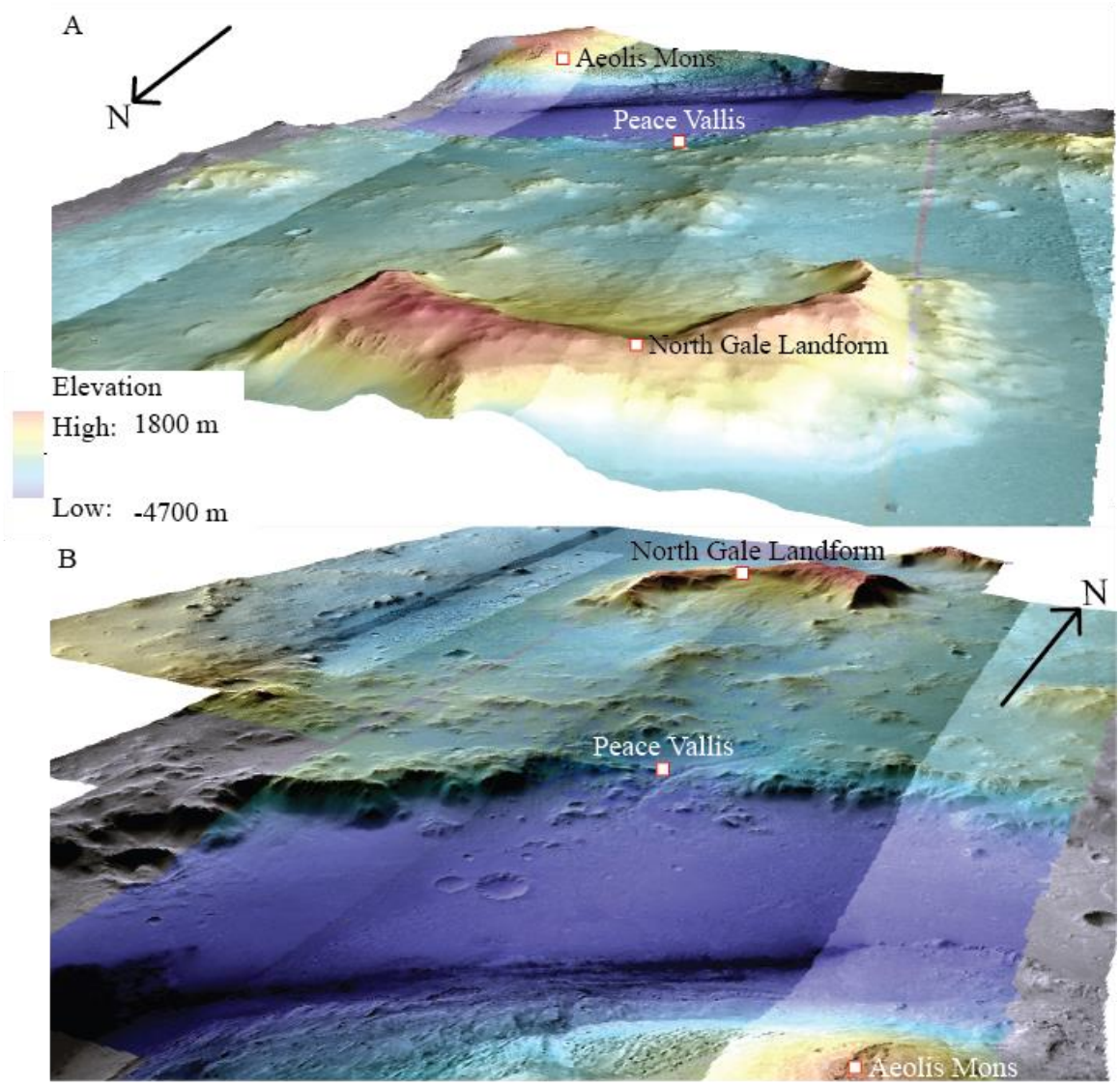

Figure 2-2: 3-D representation of the northern region of Gale Crater created using CTX (Hare, et al., 2016) images overlaying HRSC (Neukum & Jaumann, 2004) DEM. Hummocky terrain comprising mounds and depressions occurs between Peace Vallis and North Gale Landform. North Gale Landform has the highest elevation of any feature north of the dichotomy in the surrounding 100+ km. The HRSC DEMs are coloured to represent the elevation at each point; purple is the lowest elevations and red is the highest elevations Perspective view: A. North Gale Landform toward Gale Crater, and B. Aeolis Mons toward North Gale Landform.

2.1.3 Dichotomy Boundary Landforms

NGL is located in the Hesperian and Noachian transition unit on the north side of the dichotomy boundary. There are several landforms common to this unit (along the dichotomy boundary) which are important to note for this study: colles (knobs, hills, buttes) and mesas (Tanaka, et al., 2014). NGL and associated landforms resemble some

dichotomy boundary landforms, but closer examinations will show that they are distinct features.

Aeolis Mensae (Figure 2-1) to the east of Gale Crater is composed of a group of very large mesas (30 – 70 km wide, <2 km relief) that are all similar in relief and morphology. These mesas do not have extensive debris aprons around their base which are present in other areas (such as Arabia Terra), the talus materials appear to be transported away when they reach the ground (Irwin III, et al., 2004). Smaller mesas occur further north of Gale Crater (20 – 30 km wide, up to 2.3 km relief) which appear in smaller groups with large areas of plains between the groups. Isolated mesas are present in Nepenthes Mensae (~1400 km northwest of Gale Crater) along the dichotomy boundary (also in Hesperian and Noachian transition unit). Mesas have a rounded shape, a resistant cap unit with 3-10 km diameter and are 100s of m in relief at Nepenthes Mensae.

Knobs, hills and buttes (together called colles) are all smaller features than mesas, often 10s-100s of m in diameter with a similar relief. They have a rounded appearance, some have a spur-like features on the top and are surrounded by talus slopes.

2.1.4 Impact Craters on Mars

Impact craters are a common feature on the surface of Mars. Its thin atmosphere, ancient terrain and slow erosion rates (compared to Earth) contribute to the amount of impacts currently visible on the surface (Carr & Head III, 2010). In

general, an impact crater is expected to have a circular to oval shape, elevated rim, depressed floor and (if diameter >3-5 km) a central peak in the center (Hargitai & Kereszturi, 2015). However, there are crater types with variations on each of those attributes. The type of crater depends on the size of the impactor, the surface composition and surface features (Hargitai & Kereszturi, 2015). The morphology of NGL resembles an impact crater (pedestal craters, perched craters, excess ejecta craters, eroded/degraded craters and mesa impacts) but examinations of a variety of impact crater landforms will show that they are distinct features.

Eroded or degraded craters have been altered from their original morphology in some way (Hargitai & Kereszturi, 2015). Erosional processes may remove the ejecta blanket, alter the rim of the crater and/or change the appearance/tilt of the crater floor. The rim may collapse inwards during mass wasting events which causes the rim to lower and move away from the center of the crater. The crater rim can become indistinguishable from surrounding terrain. Fluvial erosion can erode valleys through and remove evidence of the rim. Sediment fill can cover a central peak or bury a crater entirely. Crater ejecta blankets may be eroded easily (Hargitai & Kereszturi, 2015).

Crater types with an elevated floor (compared to surrounding terrain) are pedestal, perched and excess ejecta craters. Pedestal Craters are small (up to 5 km diameter, 100 m relief) craters that sit on top of a plateau due to their ejecta blanket preventing sublimation of ground ice (Hargitai & Kereszturi, 2015). Perched craters (6-23 km diameter, up to 250 m height) are infilled higher than the surrounding terrain after impact which keeps their crater floor above the surrounding terrain (Hargitai &

Kereszturi, 2015). An excess ejecta crater (5-18 km diameter) has extreme amounts of ejecta (250% of crater volume) surrounding the crater which leaves it elevated above the surrounding terrain (100-200 m) but the floor of the crater is left below the surrounding terrain (Hargitai & Kereszturi, 2015). These crater types all rely on the ejecta produced during an impact to protect the subsurface ice layer from sublimation which leaves all or part of the crater above the surrounding terrain.

Impacts into a landform can alter the way the crater appears. If the landform is not totally destroyed by the impact, the crater may be elevated above the regular terrain, it may not have a continuous rim, and the crater floor may be tilted from horizontal. The overall shape of the impact may be distorted from circular. An ejecta blanket may be partially or wholly obscured by the landform.

The unique landform NGL represents a potential sediment source for the volcaniclastic sediments discovered in Gale Crater (Figure 2-3). This landform appears to be distinct from other landforms located in this area as well as distinct from a crater. Between NGL and the northern rim of Gale Crater, there is an area of irregular hills and depressions that is also distinct from other regions near the rim of Gale Crater. This study utilizes orbital imagery/datasets to identify landforms, examine the geomorphology and tectonic environment to determine the origin of each of these features and establish a link between NGL, hummocky terrain and the sediments within Gale Crater.

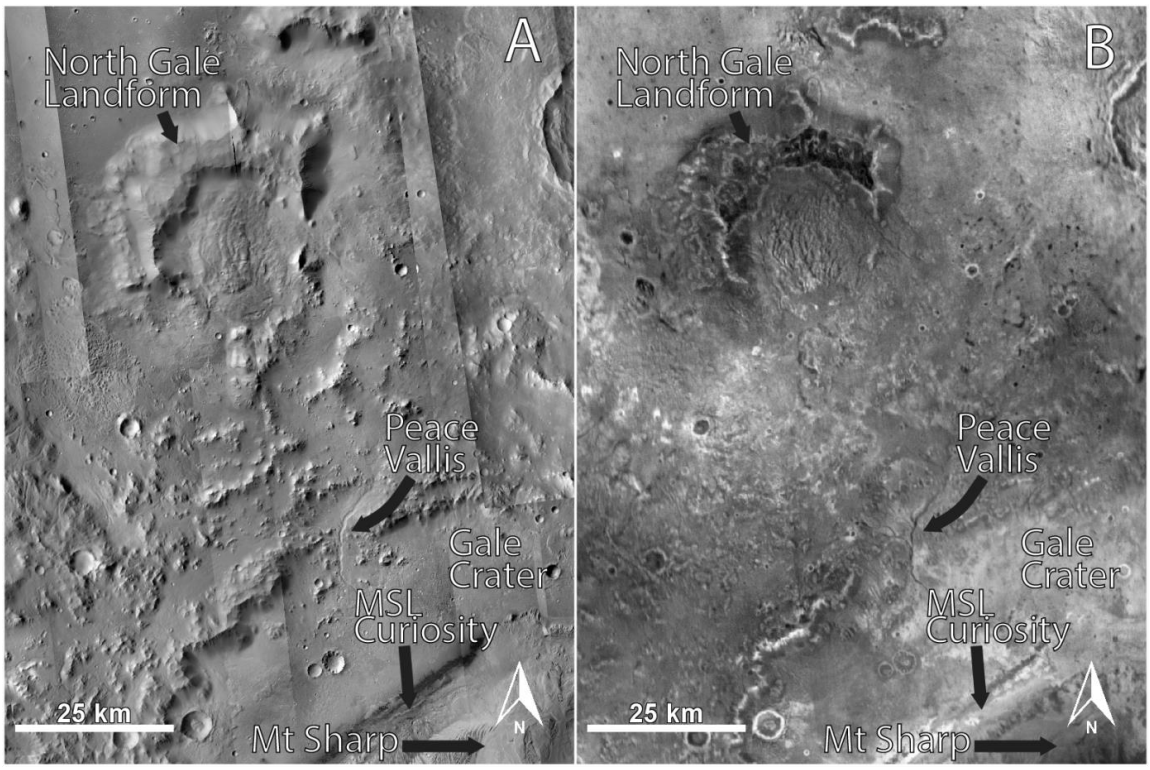

Figure 2-3: Context map for North Gale Landform and Gale Crater in visible (A) and infrared (B) using CTX images and the USGS Gale Mosaic (Malin, et al., 2007) as well as THEMIS Night IR (Edwards, et al., 2011).

2.2 Methods

Mars surface morphological data were provided by several imaging instruments onboard Mars orbiters (Table 2-1). They include digital elevation models (DEM) computed from Context Camera (CTX) (Hare, et al., 2016), the High Resolution Stereo Camera (HRSC) (Neukum & Jaumann, 2004) data from the Mars Orbital Laser Altimeter (MOLA) (Smith, et al., 1999). High resolution images are from the CTX and High Resolution Imaging Science Experiment (HiRISE) (McEwen, et al., 2007) datasets. Medium resolution images are from the Thermal Emission Imaging System (THEMIS) (Edwards, et al., 2011) datasets. Digital Elevation Models of NGL to Mount Sharp in Gale Crater were created with CTX and HRSC orbital images using the ArcGIS programs

ArcScene and ArcMap. Elevation profiles were acquired using JMARS (Christensen, et al., 2009) from the MOLA and HRSC datasets and Google Earth.

Table 2-1

Instruments used for this study.

Instrument	Images
Context Camera (CTX)	D03_028269_1752_XI04S222W, D03_028335_1754_XI_04S222W, P22_009650_1772XI_02S222W, P22_009716_1773_XI_02S223W, G22_026990_1775_XI_02S224W, G23_027267_1774_XI_02S224W, D17_034005_1766_XI_03S223W, F06_038304_1753_XI_04S223W, F21_043948_1785_XN_01S223W, P12_005787_1779_XN_02S223W, B21_017786_1746_XN_05S222W, F20_043526_1777_XN_02S223W, B17_016230_1762_XI_03S223W, B17_016296_1762_XI_03S223W, B19_017219_1763_XN_03S223W, B21_017786_1746_XN_05S222W, F11_040009_1226_XN_57S316W, P17_007489_2193_XN_39N260W, P16_007344_2195_XN_39N261W, J02_045714_2171_XN_37N200W, B20_017574_2179_XN_37N201W, G22_026989_2176_XI_37N201W, F01_036127_2168_XN_36N200W, B17_016229_2167_XN_36N200W, F21_044093_1818_XN_01N223W, B18_016652_1811_XN_01N224W, P15_007000_1786_XN_01S222W, P22_009650_1772_XI_02S222W, F20_043526_1777_XN_02S223W, D13_032304_1793_XN_00S223W, F01_036272_1280_XN_52S186W, F10_039569_1288_XN_51S185W, P13_006221_1301_XN_49S186W, Gale Mosaic (USGS)
High Resolution Imaging Science Experiment (HIRISE)	ESP_050396_1770
High Resolution Stereo Camera (HRSC)	H4235_0001_ND4, H1938_0000_DA4
Thermal Emissions Imaging System (THEMIS)	Thermal Emission Imaging System (THEMIS) - daytime infrared (IR) 100 meter/pixel mosaic (version 12), Thermal Emission Imaging System (THEMIS) - nighttime infrared (IR) 100 meter/pixel mosaic (version 14)
Mars Orbital Laser Altimeter (MOLA)	Mission Experiment Gridded Data Records (MEGDRs)
Google Earth	Google Earth Elevation Data

2.3 Results

2.3.1 NGL Physical Description

NGL (Figure 2-4) is an arcuate, quasi circular landform with a 44 km diameter and a maximum relief of 3.2 km and stands above the surrounding terrain (NGL elevation is

581 m, terrain is approximately -2700 m). Some of the other features in the region with comparable elevations are in Figure 2-1: Aeolis Mons (787 m), south rim of Gale Crater (1345 m), dichotomy boundary near Robert Sharp Crater (1482 m). Notably, NGL is higher in elevation than standalone mesas (-367 to -54 m) and platform mesas of Aeolis Mensae (-643 to -49 m). NGL includes the capping unit, spur unit, talus slope unit, knobby unit, sediment gravity flow unit and dissected surface unit. These units are defined/characterized in a morphological map (Appendix A).

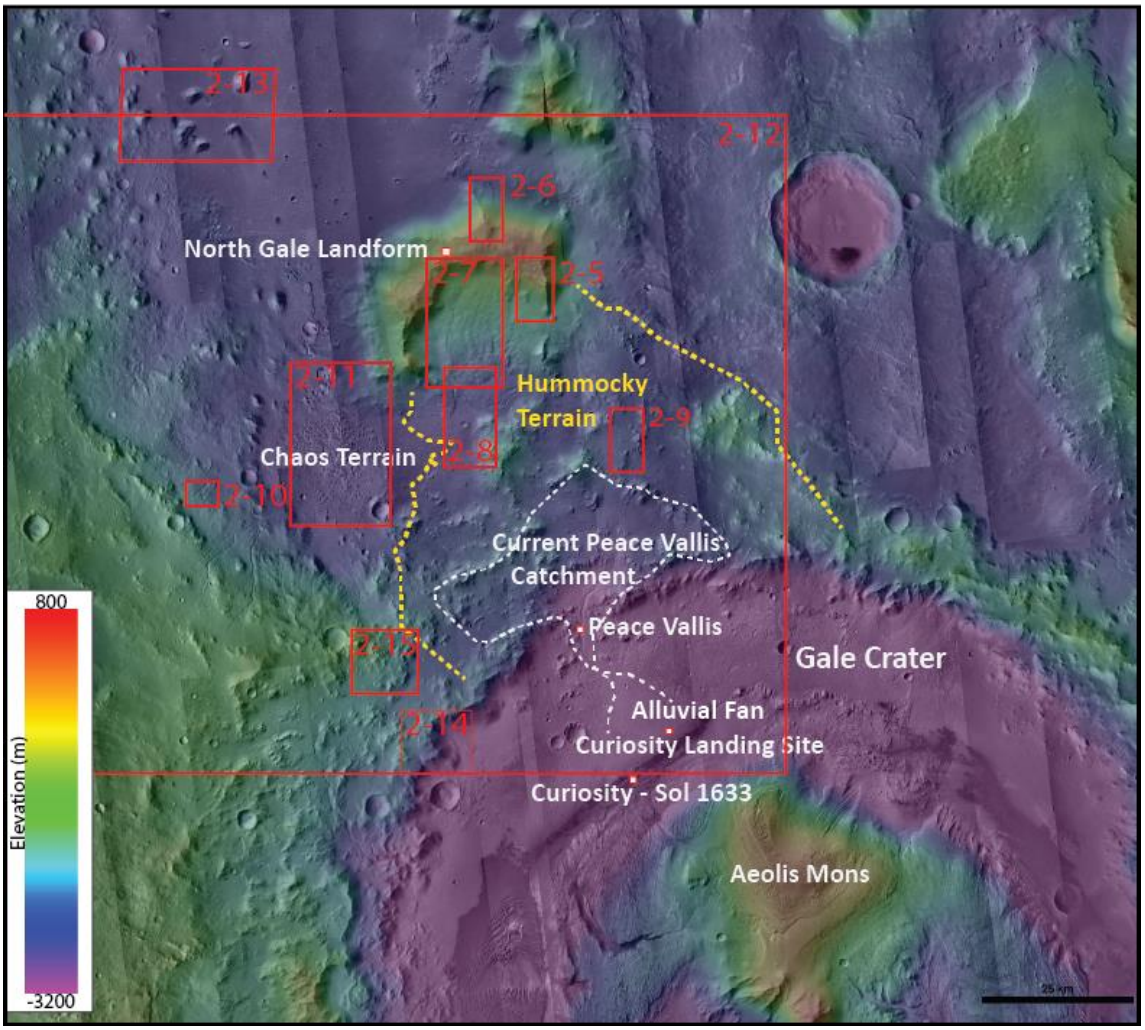

Figure 2-4: Local map (CTX (Hare, et al., 2016; Malin, et al., 2007) imagery, MOLA (Smith, et al., 1999) elevation) of the area surrounding North Gale Crater. North Gale Landform is located near the top of the map. Hummocky terrain and the present Peace Vallis catchment, and nearby chaos are indicated.

There is a resistant capping unit on top of NGL (Figure 2-5, Figure 2-6) with smooth and mottled textures. It is sparsely cratered and has depressions and rises (small hills, platforms, and ridges). The capping unit appears dark with bright areas on the edges of internal features in THEMIS Night IR images, indicating an unconsolidated surface (dust, sediments, etc.) covering an indurated material underneath. The center of the capping unit has a higher relief than near the edges and slopes towards the spur unit that lines the exterior of the capping unit. The eastern side of the capping unit is higher than the western side. The elevation ranges from 581 m in the east to -1481 m in the northwest, where it appears the capping unit has slumped downslope.

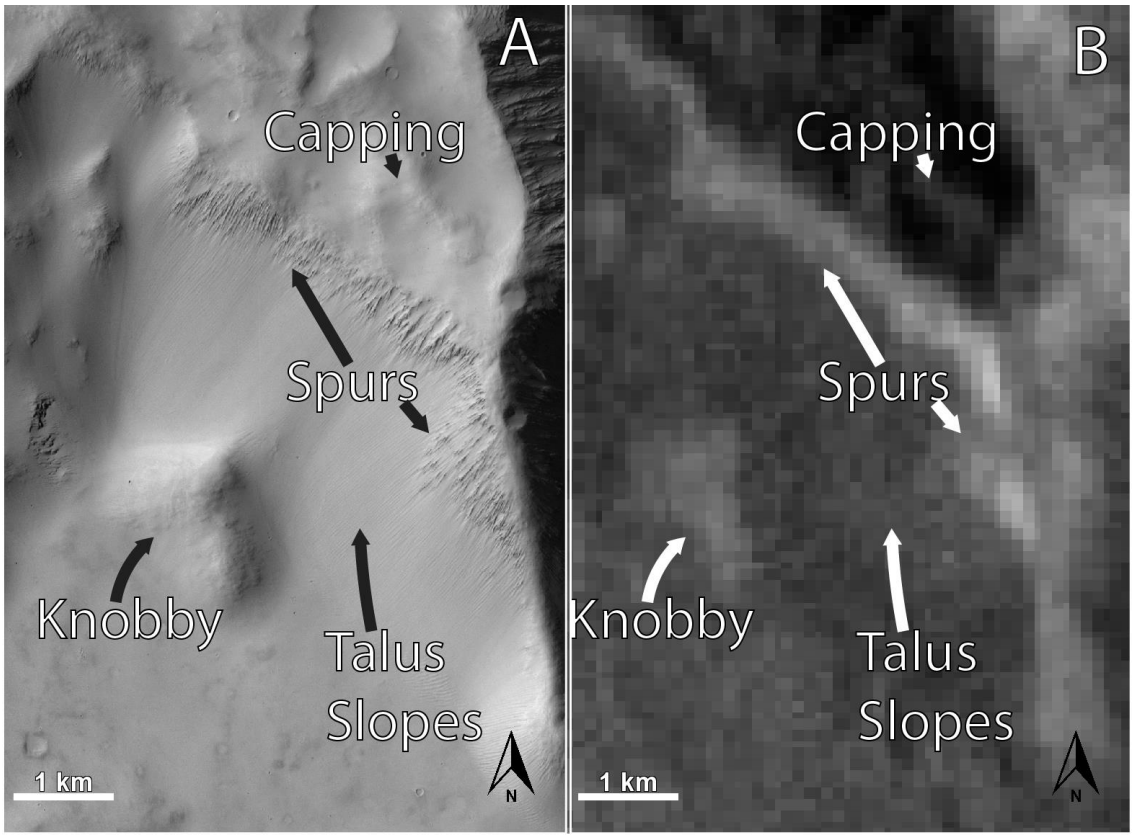

Figure 2-5: The capping unit, talus slope unit, knobby unit and spur unit of North Gale Landform in visible (A, CTX) and infrared (B, THEMIS). The capping unit covers the entire top of NGL, terminates at rocky outcrops of the spurs unit along the top edges. Has both smooth and mottled textures, is lightly cratered with bumps and depressions. Talus slopes unit appear to originate at the spurs unit surrounding the upper edge of the capping unit. Talus slopes have a linear pattern downslope from the spurs unit to the surrounding terrain. Radial spurs that extend away from the capping unit still have talus slopes associated with them. The knobby unit appears downslope of the spur and talus slopes units and appears to be consolidated with talus slopes surrounding them.

The rocky outcrops surrounding the capping unit extend radially outward as branching spurs (spur unit) around portions of the NGL (Figure 2-5, Figure 2-6). The spur unit appears bright under THEMIS Night IR, indicating indurated material not covered in dust/sediments. There are several radial spurs on NGL that extend up to 10 km from the capping unit and range in relief from level with the capping unit (~35m) to within a couple hundred meters of the surrounding terrain's elevation (~-2300m). The lower terminus of the spurs may be buried in talus or other sediment deposits.

While the capping unit and spur unit appear consolidated (or consolidated under dust/sediment cover), the NGL is surrounded by steep talus slopes (up to 25°) (Figure 2-5, Figure 2-6) and other materials associated with mass movement and collapse. The talus slopes surrounding NGL occur downslope from the spur unit and capping unit. The talus slopes often have linear streaks (bright on mid tone in CTX images) that point downslope. In THEMIS Night IR, the talus slopes are slightly lighter than the capping unit but are darker than the spurs, indicating a friable, unconsolidated surface with a larger grain size than the dust/sediment covering the capping unit. There are no boulders observed in the talus slopes in HiRISE images (up to 30 cm/pixel). There are few elliptical craters in the talus slopes of the amphitheatre interior and none on the exterior slopes, indicating poor crater retention.

A knobby unit occurs below the talus slopes on the western exterior and northeastern interior of NGL (Figure 2-5, Figure 2-7). They have a knobby appearance with indurated spurs (bright THEMIS Night IR with a softer, darker, eroded appearance compared to spur unit) on top of friable debris aprons (dark THEMIS Night IR with sporadic craters and dunes compared to talus slope unit) and are either at the base of the talus slopes (exterior) or on the slope itself (interior). Knobs appears mottled and consolidated. They are also brighter than the talus slopes in THEMIS Night IR but darker than the spurs so we interpret the knobby unit to represent an accumulated debris apron with large slump blocks that originated from the capping unit suggesting the knobby unit may have been part of the capping/spur unit before being transported downslope. Where in association with the knobby unit, the talus slopes are interpreted

to represent scarps of mass movement. A leveed sediment gravity flow (Figure 2-6) (~2 x 5 km, possibly a slump or debris flow) occurs at the north side of NGL. The sediment gravity flow has a large lip (approximately 25 m higher relief than material in the flow) at the end of the flow. The edges of the flow are also elevated above the interior portion. To the west and north of NGL, the talus slopes and knobby unit terminate abruptly at the bottom of the slope, and the surrounding plains do not appear to be covered by talus material. The northeast, east and south sides of NGL may have a skirting unit, hummocky terrain or crater ejecta covering the surrounding plains.

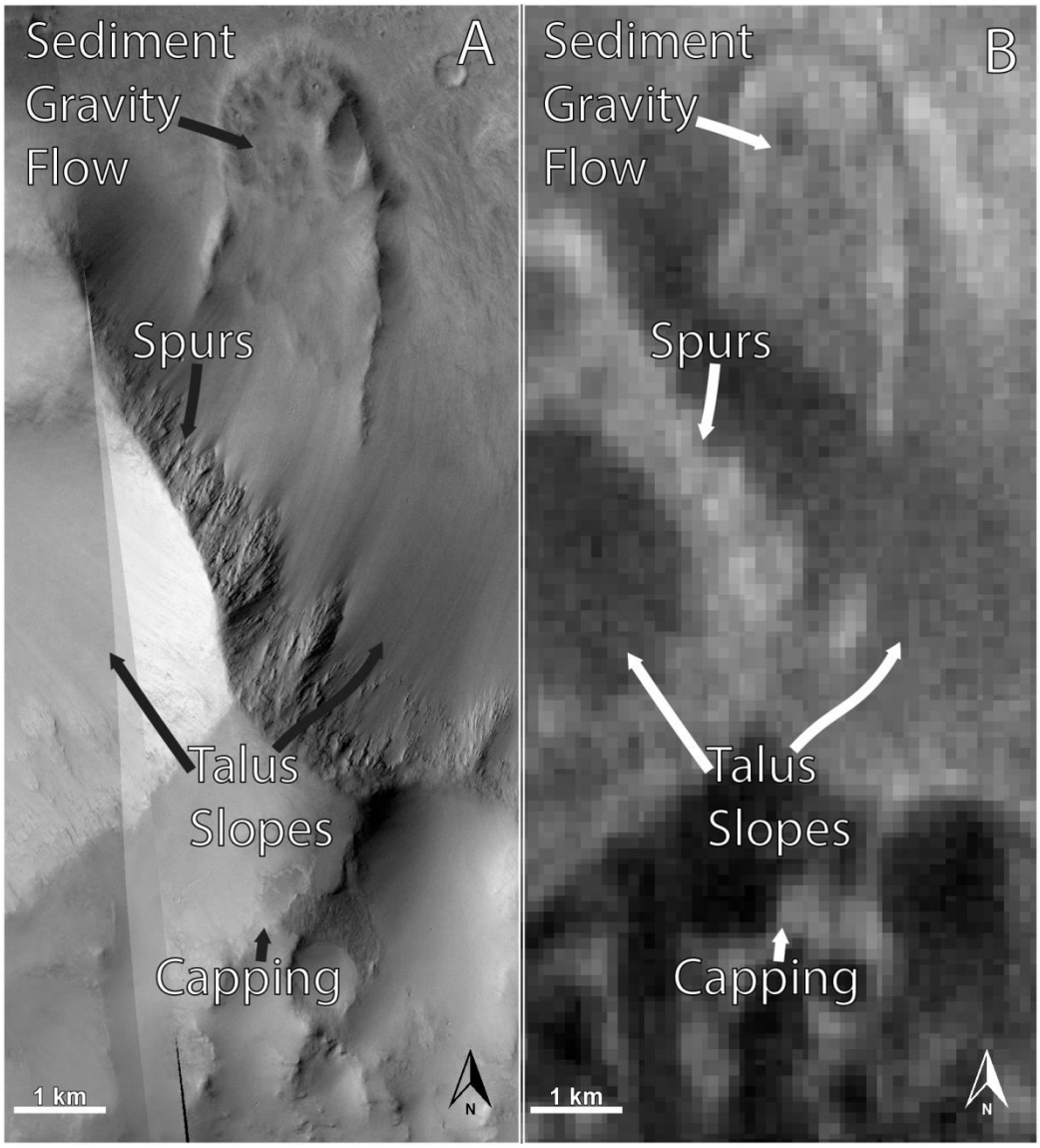

Figure 2-6: Sediment gravity flow from the northern flank of North Gale Landform in visible (A, CTX) and infrared (B, THEMIS). It has steep sides and depressed interior. The origin point is covered in talus.

NGL features a large (~25x20 km) depression (amphitheatre) that opens to the south-southeast (Figure 2-7). The dissected surface unit inside the amphitheatre is 700 to 1500 m below the capping unit where the sidewalls (talus slope unit) meet the floor of the amphitheatre (dissected surface unit). The floor of the amphitheatre slopes 5˚ to the south, dropping ~1500 m in elevation over the ~17 km length, and has a dissected surface morphology (covered in channels that may have been created by flowing water)

over the entire floor. The floor is light to mid tone, has small craters (fresh to very eroded), and the dissections are spread over the entire surface. The floor has a dark to light-medium appearance in THEMIS Night IR. The surface is brighter on channel banks, the center of the larger channels is dark, and the surface has medium brightness away from the channels/banks. This suggests there are fine sediments in the interior of the channels, less sediment coverage on the banks of the channel (possibly indurated material) and friable material covering the surface away from the channels. The THEMIS Night IR surface brightness is higher towards the bottom of the sloped amphitheatre floor near the center. This could suggest that there is less sediment coverage on the banks where the channels start to converge. The amphitheatre floor (dissected surface unit) terminates into an erosion resistant unit and hummocky terrain unit to the south.

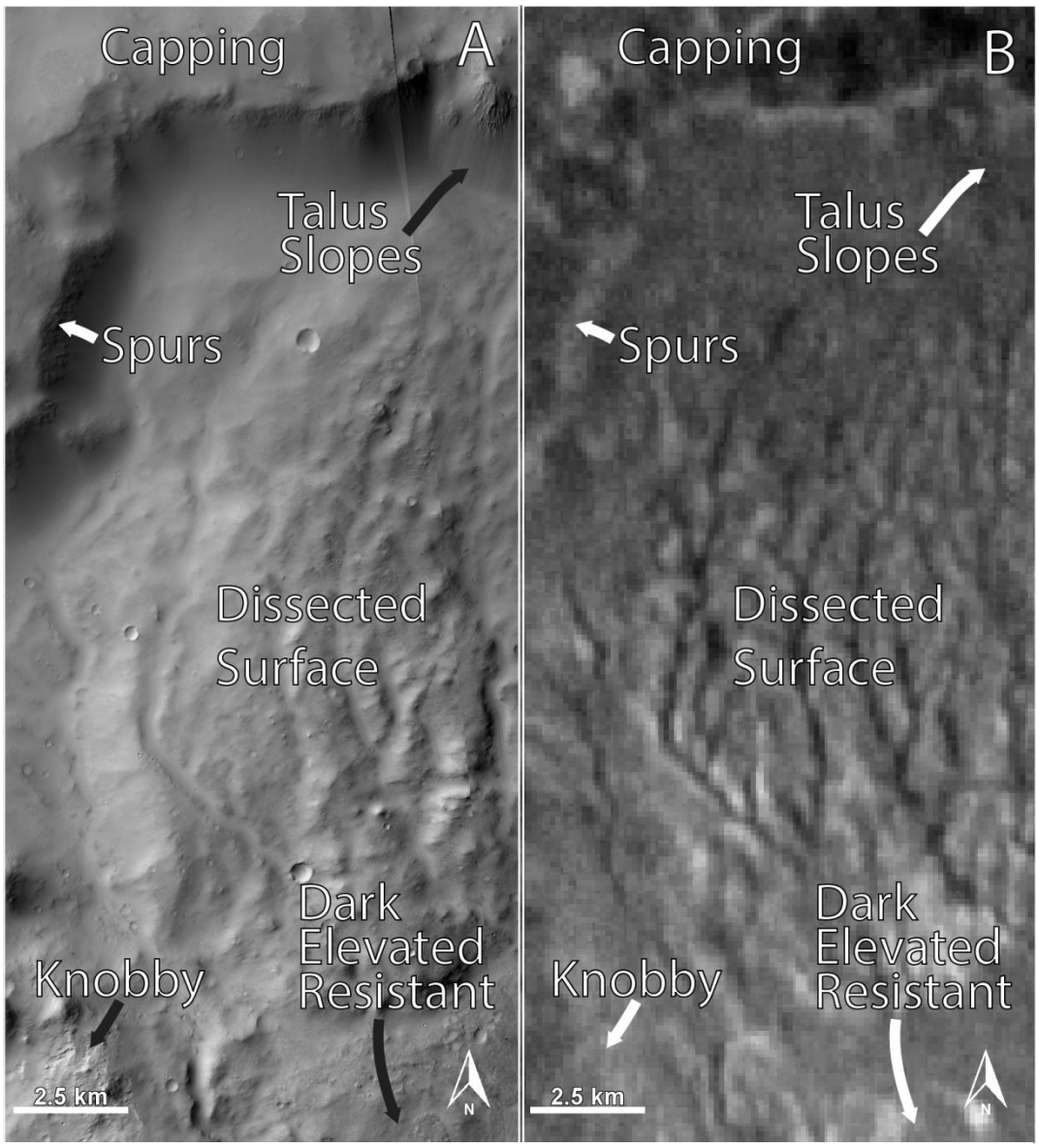

Figure 2-7: The dissected surface of the amphitheatre of North Gale Landform in visible (A, CTX) and infrared (B, THEMIS). It appears that channels were carved into the soft surface of the amphitheatre floor, likely by flowing water. the channels appear to all flow roughly south. The amphitheatre is surrounded by talus slope unit originating at the spur unit.

2.3.2 NGL Related Features

Surrounding NGL there are some related features including hummocks unit, cratered, mottled plains unit, dark elevated resistant unit, dissected surface unit, pit crater chain unit and chaotic terrain unit. These units are defined/characterized in a morphological map (Appendix A).

The area between NGL and the rim of Gale Crater to the south contains groups of large, irregularly shaped hills, called hummocks that are separated by depressions (Figure 2-8). We refer to the hummocks unit and units in the depressions collectively as hummocky terrain. The depressions contain the cratered, mottled plains unit (Figure 2-9), dark elevated resistant unit (Figure 2-8), and more of the dissected surface unit (Figure 2-7).

The hummocks unit only appears in the area between NGL and the northern rim of Gale Crater in a fan shape about 40 km long (Figure 2-4). This fan of hummocks extends from the amphitheatre on the south side of NGL to the edge of the crater rim on the north side of Gale Crater. This area is not continuously covered by the hummocks as there are depressions, eroded channels and plains in between them. The larger hummocks (up to 1 km relief and 8 km wide) are concentrated along the central axis of the debris avalanche; smaller hummocks are more likely present off axis to the edges of the hummocky terrain. The hummocks appear in clusters most often, sometimes the groups of hummocks form a linear, longitudinal ridge rising above the dissected, cratered plains surrounding it. Some of the hummocks have visible spurs however they are not as prominent as the spurs on the rim of Gale Crater or on NGL. Hummocks of all sizes have some talus on the steeper slopes and possibly unconsolidated debris piled up between the blocks.

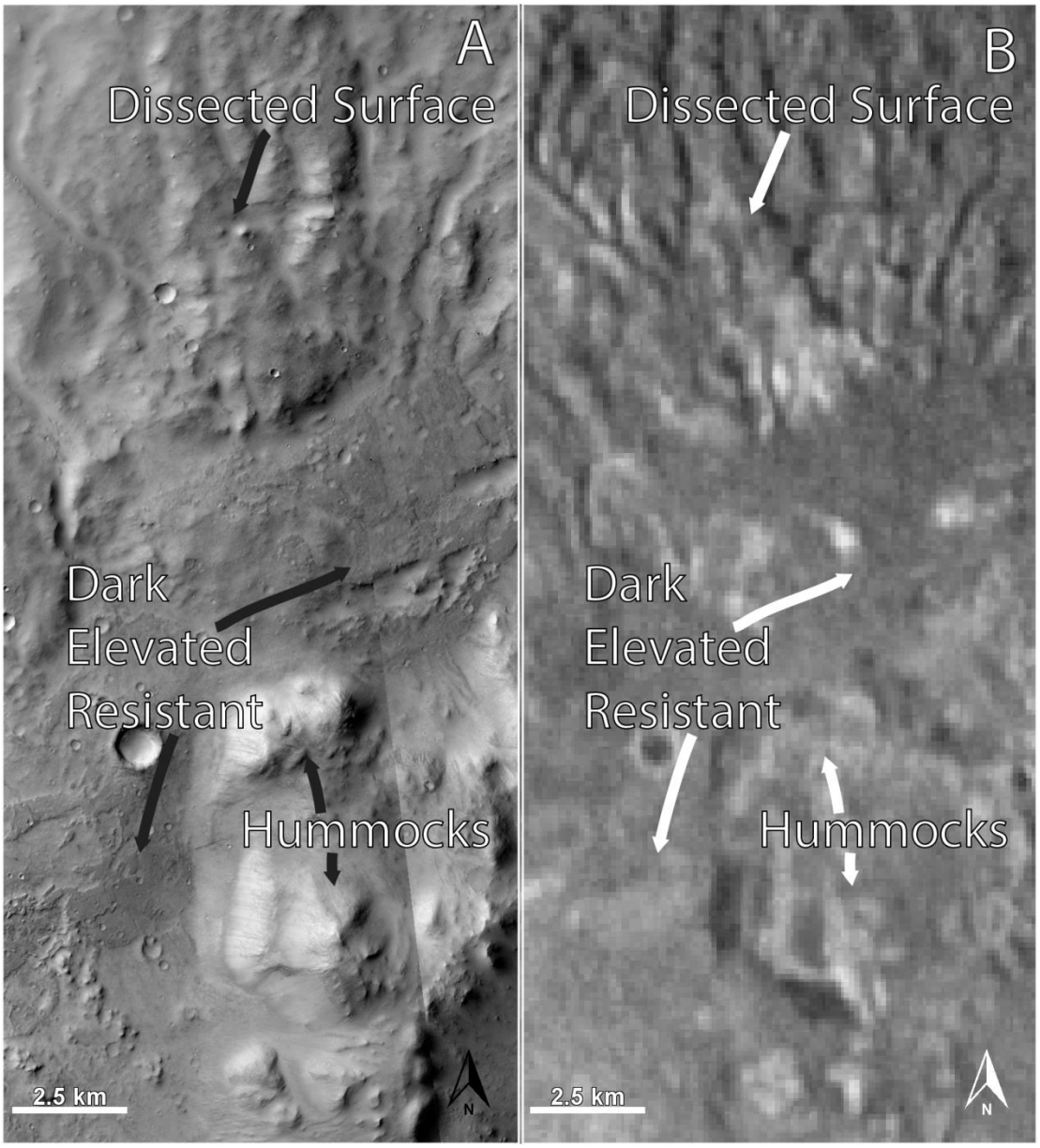

Figure 2-8: An example of hummocks between North Gale Landform and the northern rim of Gale Crater in visible (A, CTX) and infrared (B, THEMIS). The hummocks unit starts near (<5 km) the base of the dissected unit in the amphitheatre of NGL. The hummocks and depressions between them make up the hummocky terrain which was deposited during a debris avalanche. The debris avalanche originated from the southern flank of North Gale Landform. Dark elevated resistant unit appears between hummocks in the depressions.

Cratered, mottled plains unit appears in between the hummocks and is visible between NGL and the rim of Gale Crater (Figure 2-9). The unit has a moderately cratered and mottled surface. It is mid toned in visible images and medium to dark in THEMIS

Night IR. Mottling of the surface may be due to a recent (<1 Ga) mobilization of fines due to a fluvial event (Newsom, et al., 2019).

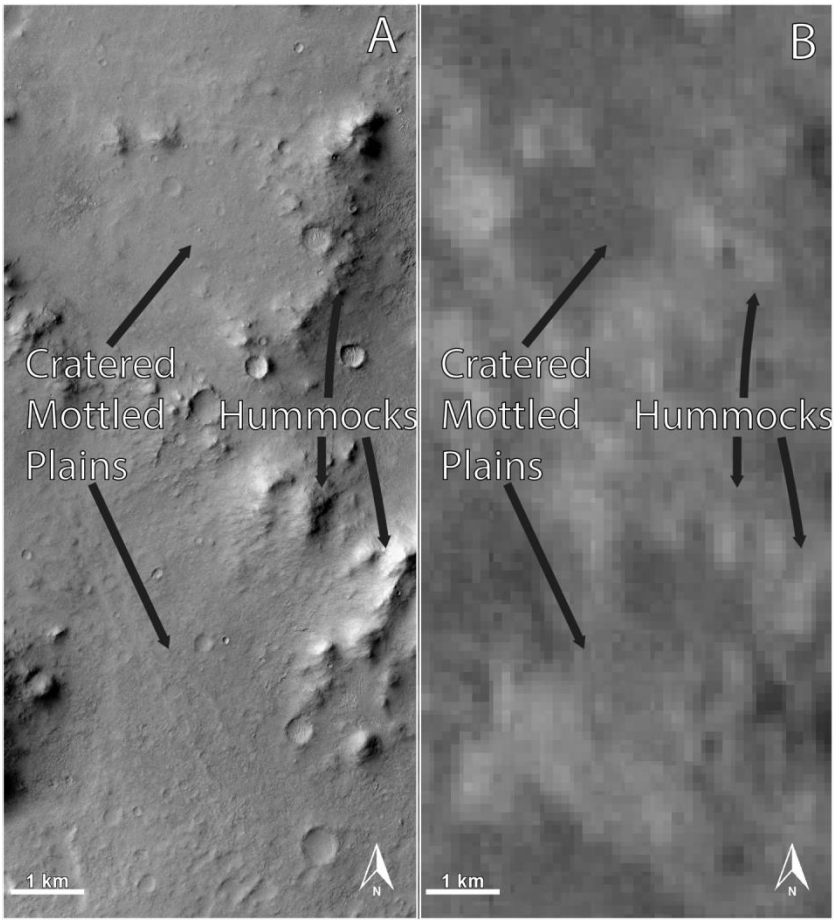

Figure 2-9: An example of the cratered, mottled plains between NGL and the northern rim of Gale Crater in visible (A, CTX) and infrared (B, THEMIS). This unit appears in the depressions between the hummocks, it shows signs of cratering on the surface. The lack of significant channels on the surface distinguish it from the dissected surface unit near Peace Vallis.

The dark elevated resistant unit (Figure 2-8) is raised relative to the cratered, mottled plains (Figure 2-9) as indicated by shadows in CTX images; the elevation difference too small for MOLA interpretation. It has a higher relief than the cratered, mottled plains unit however it may be more resistant to deflation instead. It is darker tone than the other units as well. There are small craters covering the surface and it has irregular edges. There are large portions of this unit near the base of NGL and some

other portions near Gale Crater. There are sections in the cratered, mottled plains between NGL and Gale Crater as well as in the cratered lowlands plains north of Gale Landform.

A pit crater chain (pit crater chain unit) is ~40 km west-southwest of NGL. It is a linear series of craters that are connected together (Figure 2-10). Pit crater chains are features formed by the collapse of the surface into a significant void space below the surface (Wyrick, et al., 2004). The void spaces are thought to have several different methods of formation; several hypotheses include volcanic or tectonic processes: collapsing of a lava tube or magma chamber, dike swarms, and fissuring beneath a loose surface (Scott & Wilson, 2002; Wyrick, et al., 2004). The pit crater chain near NGL is oriented NE-SW; the same orientation as the regional fabric and perpendicular to the amphitheatre opening suggesting there may be some tectonic relationship with NGL.

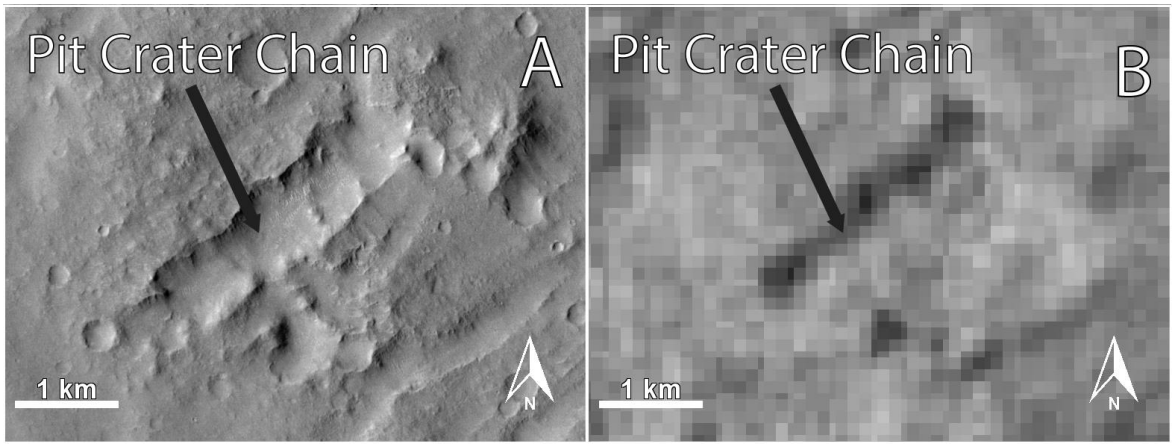

Figure 2-10: Pit crater chain located to the southwest of NGL in visible (A, CTX) and infrared (B, THEMIS). A series of connected depressions that may have a volcanic origin. The pit crater chain is oriented consistently with the fabric of the region surrounding Gale Crater (NE-SW).

Chaotic terrain (Chaotic terrain unit) is ~10 km southwest of NGL. It is a rounded rectangular area (15-km by 14 km) that has a surface broken into many polygonal blocks

with quasi-linear depressions between them (Figure 2-11). The blocks are up to 1 km and there are a wide range of block sizes present (10s of m to ~1 km). The depressions are up to several 10s of meters below the blocks and up to 100s of meters wide. Chaotic terrain has been hypothesized to be the result of sublimation of ground ice due to reaction with a magma body, release of liquid CO_2 from gas hydrates or breach of confined subterranean aquifers (Meresse, et al., 2008).

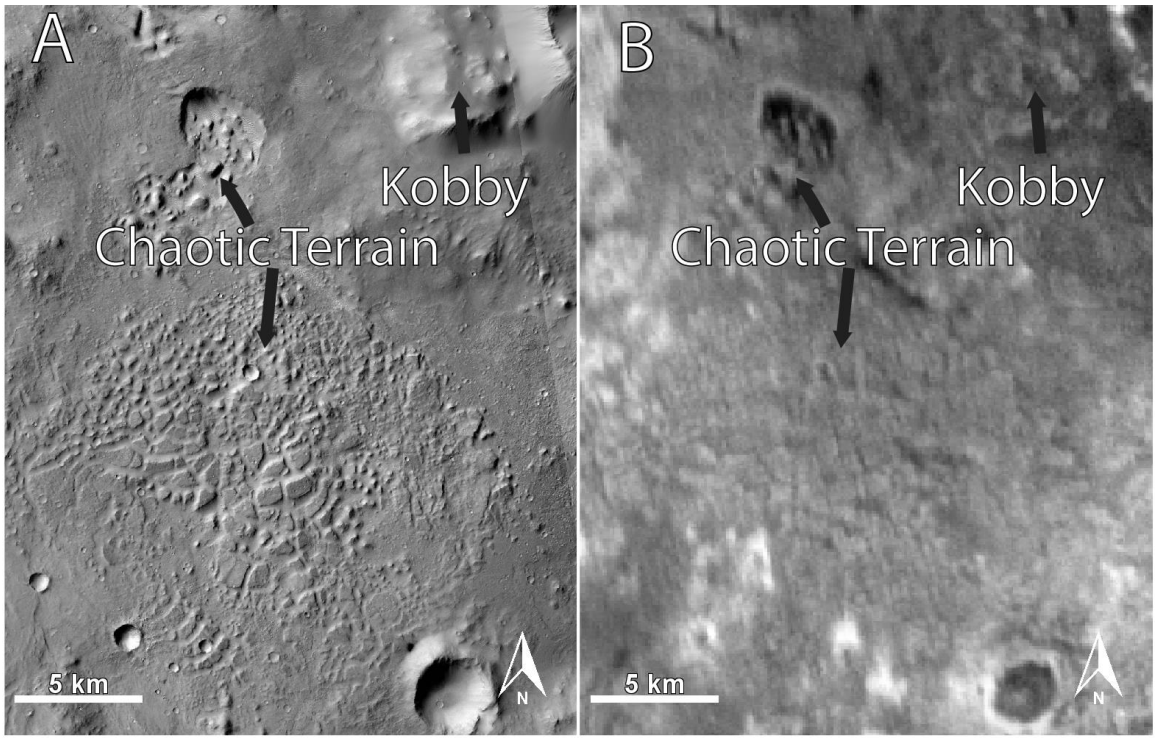

Figure 2-11: Chaotic terrain to the southwest of NGL in visible (A, CTX) and infrared (B, THEMIS). A smaller chaotic terrain appears slightly north of the main unit with an irregular shape. The chaotic terrain has a surface morphology of large blocks with connected depressions, the surface of the blocks resembles the unfractured surface of the dark elevated resistant unit to the east. Knobby unit is at the edge of the western side of NGL.

2.3.3 Other Important Units

Colles are small hills or knobs usually less than 1 km high and may be several km in diameter (Figure 2-12) (Rotto & Tanaka, 1995). The colles often appear in groups but some can be spread out further. The colles can be solitary or very close to others. Colles

appear in shapes ranging from square to circular to elongated. They could be associated with the mesas to the east, possibly as erosional remnants. They appear throughout the rough cratered highlands plains as well as the smoother cratered lowlands plains. They are a common feature in the Hesperian and Noachian transition unit from the USGS Geologic Map of Mars (Tanaka, et al., 2014).

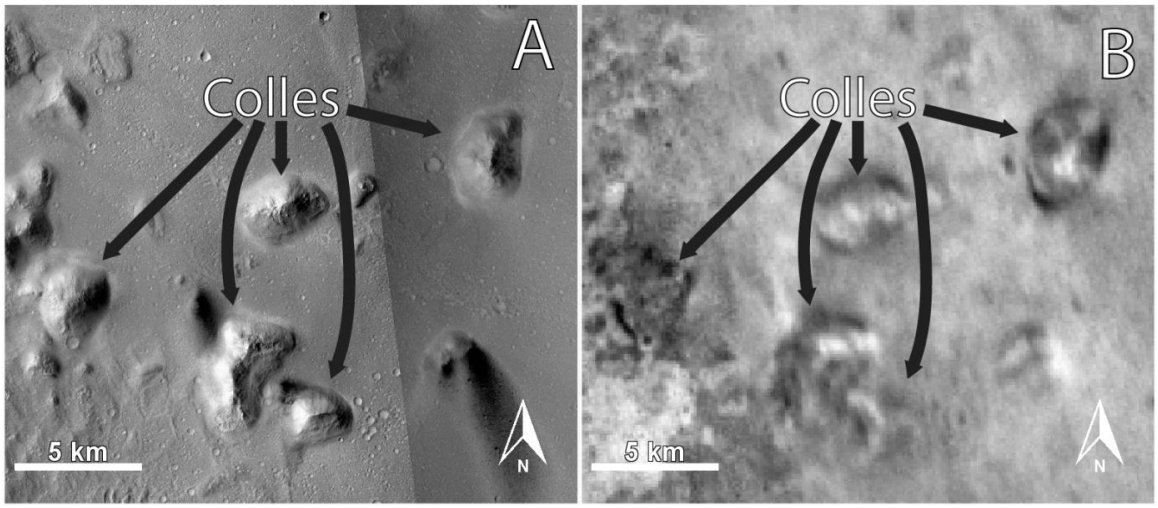

Figure 2-12: An example of the colles found near North Gale Landform in visible (A, CTX) and infrared (B, THEMIS). These small hills and knobs appear north of the dichotomy boundary. They can be solitary or be found in groups.

The Gale Crater Rim unit is composed of the exposed rim of Gale Crater and Gale Crater ejecta directly adjacent to the rim (Figure 2-13). It is characterized by very dark spurs, talus slopes and some hilly ejecta just outside the rim. It has a sharper, more defined appearance than the hummocky terrain which is nearby. This unit is present only on and just outside the rim of Gale Crater in the morphological map area.

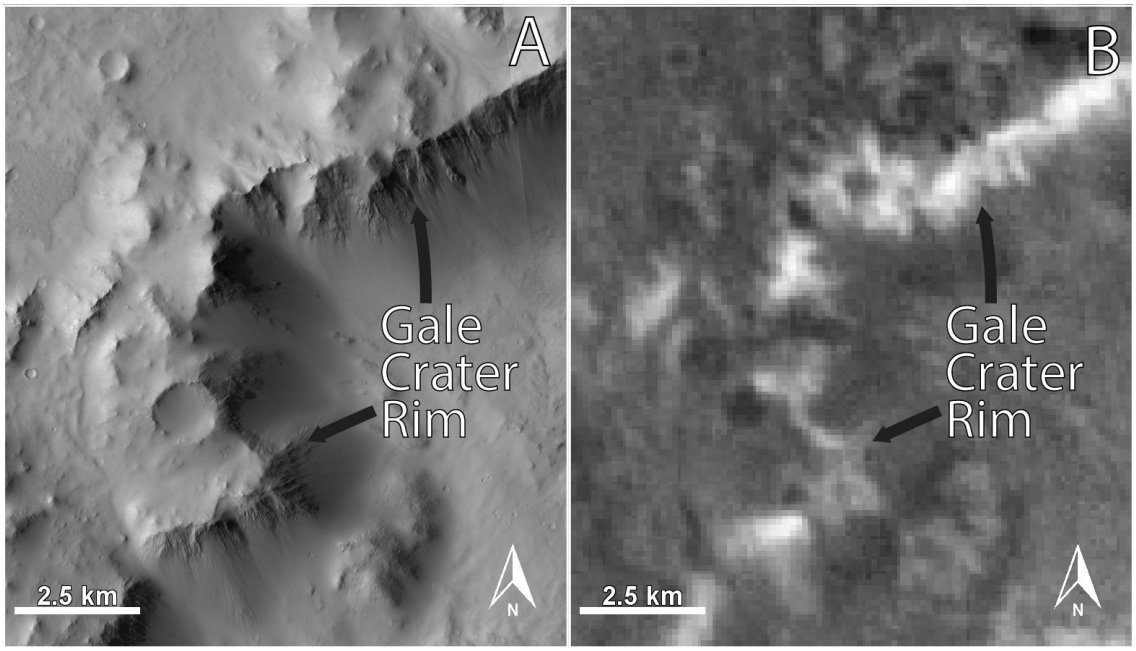

Figure 2-13: A section of the northern rim of Gale Crater in visible (A, CTX) and infrared (B, THEMIS). Dark spurs and extensive talus slopes appear extensively in this portion of the crater rim.

The highland rugged knobby unit is a rough unit that exists on the edge of an elevated section of the cratered plains (Figure 2-14). It has an abundance of knobs and other small hills, in some locations it resembles the hummocky terrain and also has a similar appearance to Gale Crater rim. There are linear ridges of knobs/hills along with more rounded groupings. Ridges can be >10 km long and up to 300 m relief though generally smaller (5 km long, 100 m relief). Troughs between ridges appear smooth or channeled. Troughs and ridges may be related to channeling that appears in the unit. It is possible that some of it is ejecta from Gale Crater, colles or the result of the plains eroding into lower relief plains. It has many small craters and a few relatively large ones. It follows a ridgeline and has a different texture than the higher plains and lower plains.

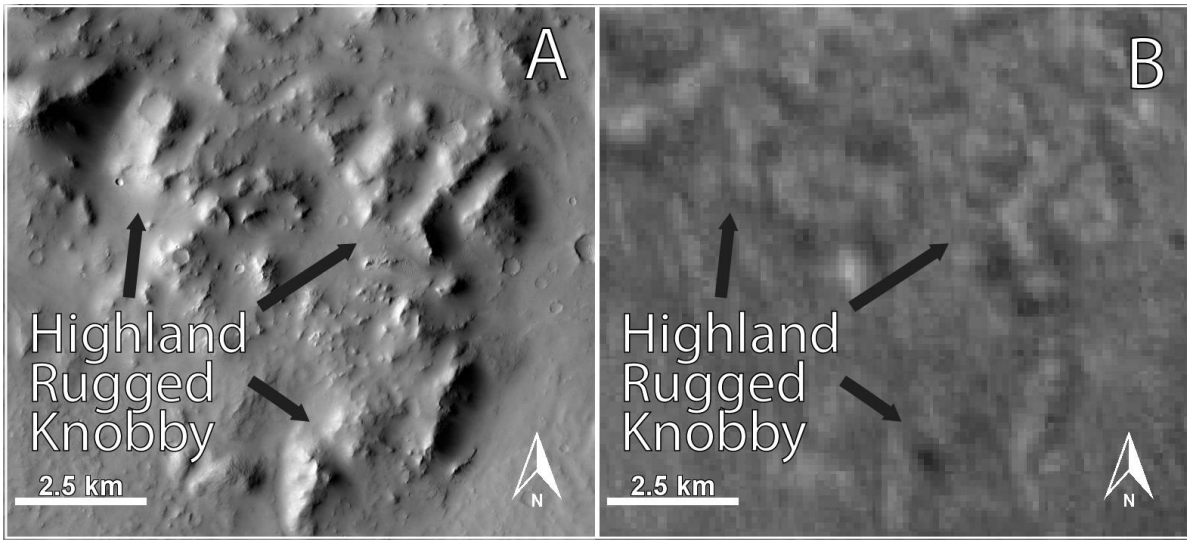

Figure 2-14: An example of the highland rugged knobby unit which features hills and knobs that bear some resemblance to the hummocky terrain to the east in visible (A, CTX) and infrared (B, THEMIS). This unit is extensive along the highland-lowland transition. The hills and knobs extend from near the edge of Gale Crater to further north and west of North Gale Landform.

2.3.4 Morphological Map

A morphological map (Figure 2-15) of the NGL and surrounding area consisting of 13 relevant units classified using visible and thermal infrared orbital images (full description available in Appendix A). A set of CTX images (Table 2-1) was used as a basemap for production of the morphological map (Figure 2-15). The surface was divided into different morphologies using criteria such as tone, texture, crater content, landforms and THEMIS Night IR data. The morphological map was created to provide more detail of the northern Gale Crater region than shown in the current Geological Map of Mars (Tanaka, et al., 2014).

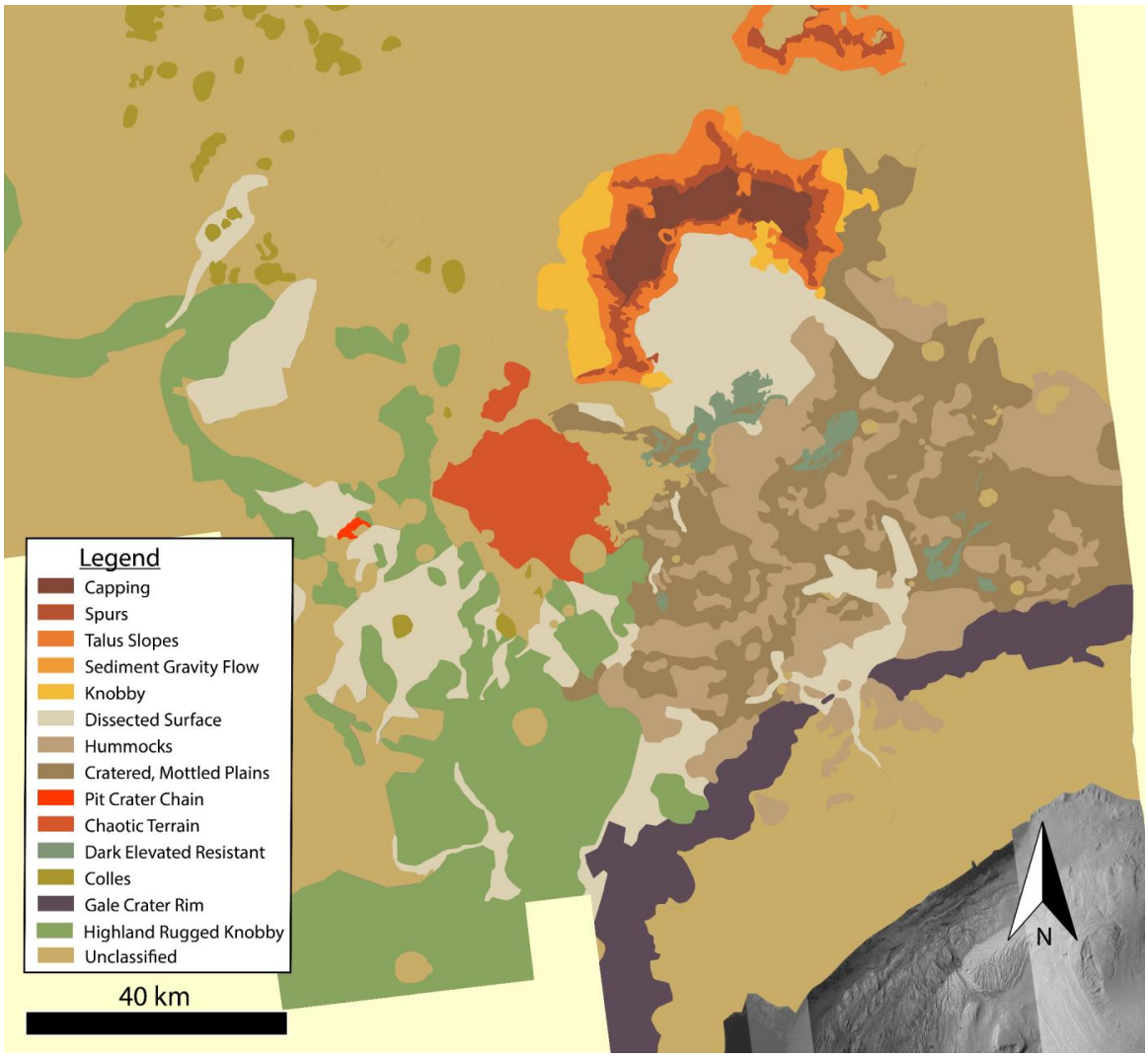

Figure 2-15 : A morphological map of North Gale Landform and the surrounding area. There are 14 relevant units described in this map including 6 on North Gale Landform. CTX basemap images provided by Jon Walmsley. (See Appendix A for full description of area)

The morphological map is used to characterize the morphologies associated with NGL and demonstrate the differences between it and features associated with the dichotomy boundary near Gale Crater. The morphological map is also used to show the difference between hummocky terrain, crater ejecta and small hills and knobs to demonstrate the hummocky terrain as a distinct debris avalanche unit. Cratering, tone,

channels, surface roughness, IR reflectivity and size are some of the criteria used to differentiate the units.

2.3.5 Tectonic Trends

An investigation to the surface dip was conducted to determine if there were any regional tectonic trends apparent that contribute to the volcanic origin hypothesis for NGL. A trend of ~60/240°, parallel to the collapsed side of the NGL, could indicate that the collapse of the southern flank of NGL is related to tectonic activity as this relationship is present with terrestrial sector collapse volcanos.

A map showing the attitude of the Martian surface in the region surrounding Gale Crater was created using ArcMap and the Augmented Visualization of Attitude (AVA) tool (Minin, et al., 2015) (Figure 2-16, Figure 2-17). The Augmented Visualization of Attitude tool is used on the MOLA dataset to show the strike and dip of the Martian surface at 300m/pixel scale. The colours of each pixel on the surface indicate the strike and dip direction calculated from the elevation data of MOLA. The colour of the surface highlights potential lineations present on the Martian surface. Lineations are defined here as any extended feature in the AVA map with a relatively consistent strike and dip direction along the length. These lineations could represent channels, ridges, abrupt edges of features/landforms, fractures, wrinkle ridges or any other linear pattern on the surface. These lineations may indicate signs of stress or weakness which could be evidence of tectonic activity. Lineations that are approximately 65° (±10°) are traced in blue while all other lineations are traced in red.

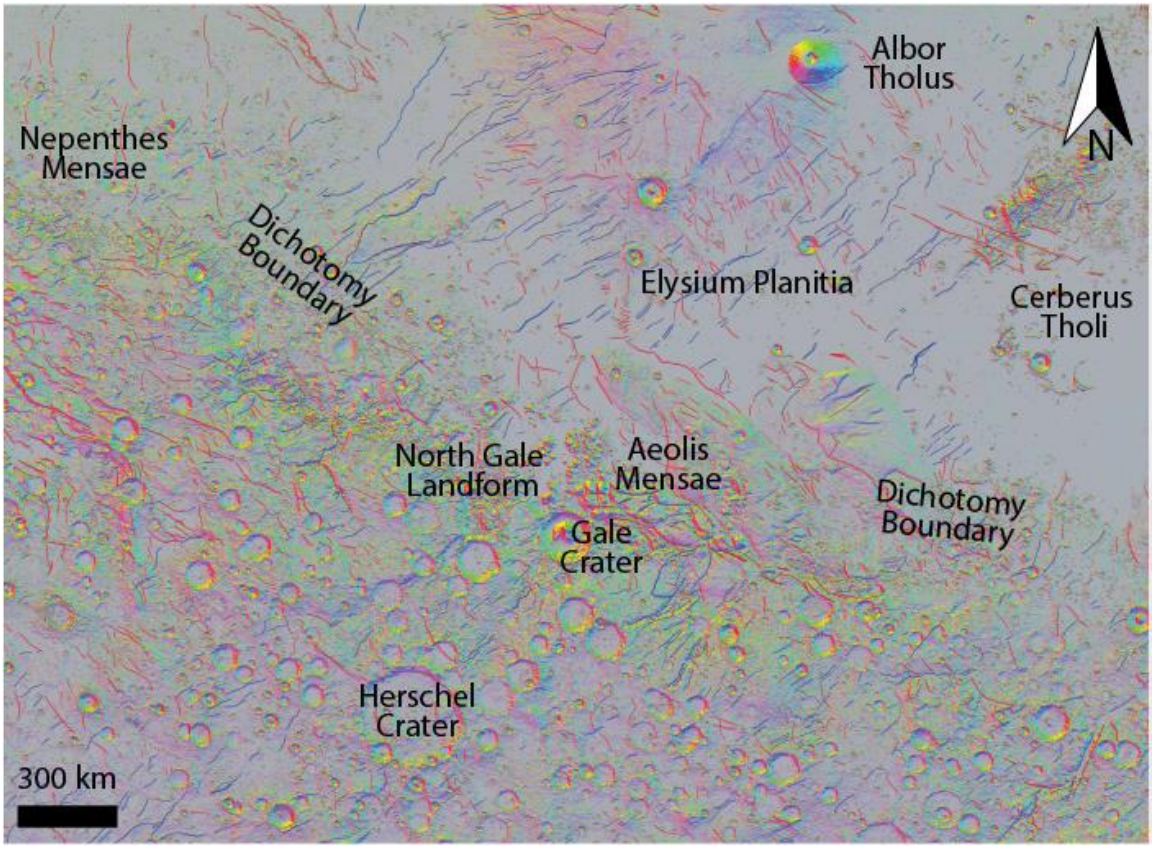

Figure 2-16: Map showing the attitude of the Martian surface in the region surrounding Gale Crater. The AVA (Minin, et al., 2015) tool provides the strike and dip of the surface from a MOLA (Smith, et al., 1999) base map. The strike and dip of the surface are indicated by the colour of the pixels in the image. There are two colours of lines drawn on the map which are used to represent any lineations on the surface. The lineations in blue are roughly oriented NE/SW (approx. ±10°) while the lineations in red are for any other orientation.

2.3.5.1 Regional Trends

The regional AVA map (Figure 2-16) shows the attitude of the Martian surface in the region surrounding Gale Crater (approx. 2000 x 3500 km area) from Cerberus Tholi in the east, Albor Tholus in the north, Herschel crater in the south and Nepenthes Mensae in the west. It shows that there is potentially a lot of tectonic activity in the greater region surrounding NGL and Gale Crater. North of the dichotomy boundary, there are numerous lineations approximately NE/SW (~65°); many are large scale features (10-100s km length) that appear to be wrinkle ridges or grabens (Tanaka, et al.,

2014). In AVA map context, they appear in relatively featureless plains. Some may be related to the Elysium volcanic province located north of NGL. In the top center of AVA map, the southern portion of the Elysium bulge is visible (Alba Tholus is southern most large volcano in Elysium province). It has linear features radiating from its center as well as a predominant NE-SW trend to the lineations overprinting it. Along the dichotomy boundary, numerous lineations run either parallel or perpendicular to the boundary. There are smaller NE/SW trending lineations in this region. South of the dichotomy, there are numerous small NE-SW trending lineations and fewer large lineations running parallel to the boundary.

2.3.5.2 Local Trends

The local AVA map (Figure 2-17) shows the attitude of the Martian surface near NGL and Gale Crater (approx. 1000 x 750 km area) from Aeolis Mensae in the east, Elysium Planitia in the north, Lasswitz crater in the south and beyond Knobel crater in the west. It shows there is a large amount of lineations (and potential tectonic activity) that are trending NE/SW in the local region around Gale Crater and NGL. There are numerous lineations south of the dichotomy with a high percentage of them trending NE/SW with lengths 10 – 100s km. Many of those lineations appear to represent channels, ridges, grabens and potentially wrinkle ridges. The pit crater chain to the southwest of NGL also has this orientation and is lined up with NGL. North of the dichotomy, more of the lineations are not trending NE/SW than to the south. The northern lineations correspond to wrinkle ridges and grabens (Tanaka, et al., 2014) and

less channels than to the south. A concentration of grabens east of Gale Crater separate the mesas of Aeolis Mensae.

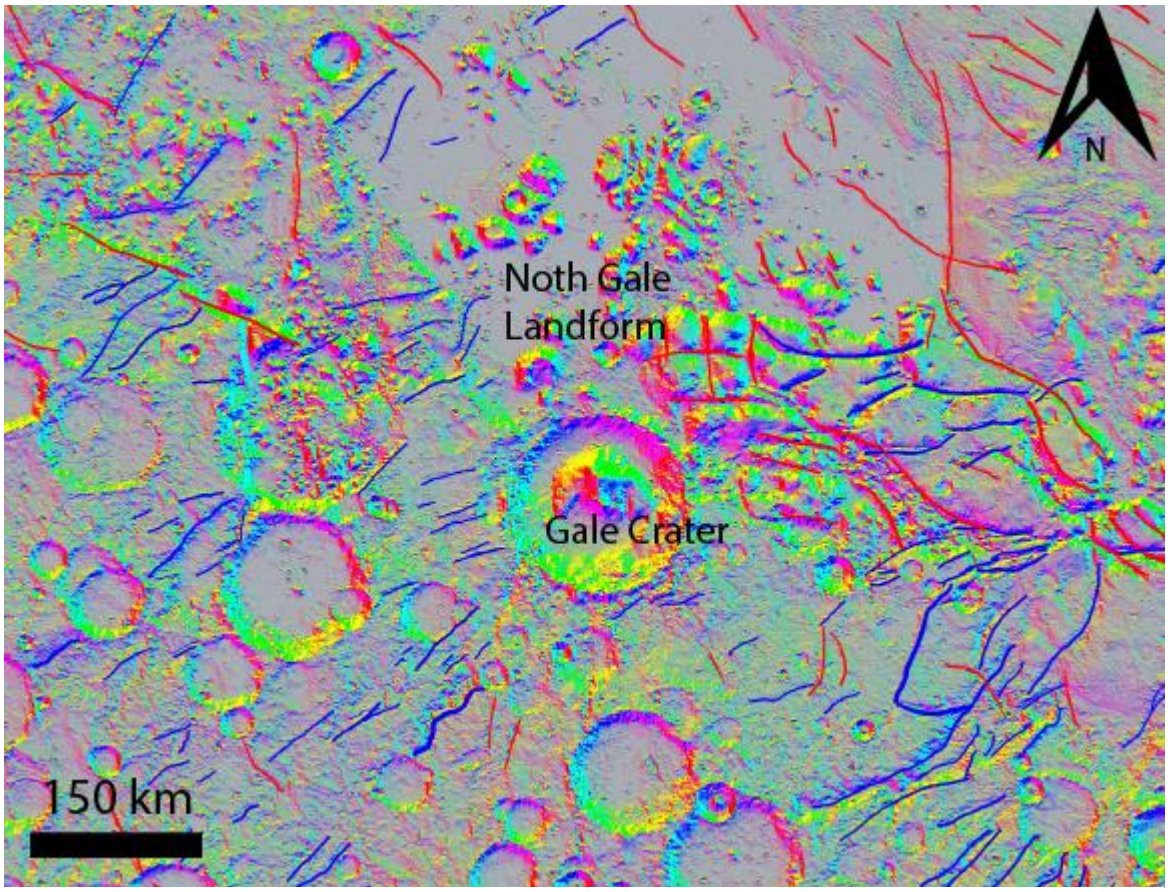

Figure 2-17: Map showing the attitude of the Martian surface in the local area around Gale Crater and North Gale Landform. The Augmented Visualization of Attitude (AVA) (Minin, et al., 2015) tool provides the strike and dip of the surface from a MOLA (Smith, et al., 1999) base map. The strike and dip of the surface are indicated by the colour of the pixels in the image. There are two colours of lines drawn on the map which are used to represent any lineations on the surface. The lineations in blue are roughly oriented NE/SW (approx. ±10°) while the lineations in red are for any other orientation.

2.3.5.3 Data Trends

Over 1400 linear features were manually traced on the map while a smaller subsection closer to NGL had their orientations measured and compiled into a rose diagram (n=584) (Figure 2-18). The resultant vector from this set of lineations has an azimuth 65.8° (Magnitude – 22.0%, circular variance = 0.780, circular standard deviation

= ±99.7°). A Rayleigh test of uniformity for the lineations show there is a preferred trend to the data (R = 22%, Critical Value of R = 7.3%) and the Von Mises model shows that the mean direction of the lineations is 65.8° (K = 0.451, Standard Error of Mean = ±7.5°, 95% Confidence Interval = ±14.9°).

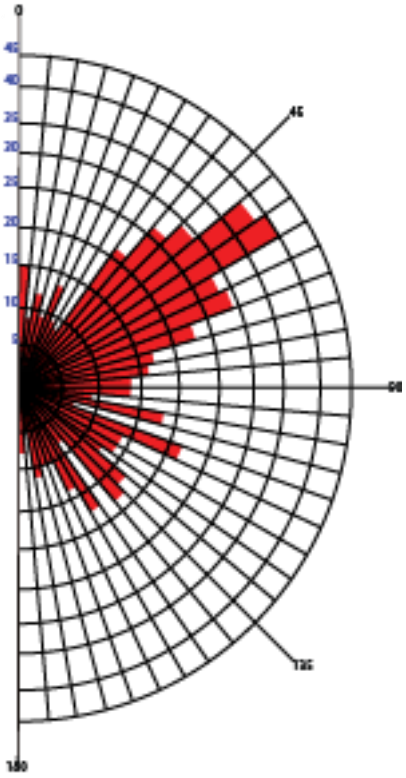

Figure 2-18: Rose diagram compiling orientations within 2000 km of North Gale Landform. The lineations measured were grouped into ranges of 5° and plotted onto the rose diagram. Since it was not important if the lineation was striking to the northeast or the southwest, only that it was striking in one of those directions, all strikes were plotted between 0-180°. A preferred orientation of ~60° is identified that is roughly perpendicular to the amphitheatre.

2.4 Discussion

This section discusses the origin of NGL by examining the morphology of NGL and making comparisons with dichotomy boundary landforms, various types of impact craters, and terrestrial volcanic landforms. The origin of the area of hummocky terrain between NGL and Gale Crater will also be discussed. Further discussion on the

implications for discoveries at Gale Crater in relation to NGL and the hummocky terrain will follow.

2.4.1 Origin of North Gale Landform

We here discuss three potential hypotheses for what the NGL is and how it may have formed to evaluate a most likely scenario. These include:

1) The NGL is a type of dichotomy boundary feature, such as a mesa.
2) The NGL has an impact origin, such as an elevated impact crater or eroded/modified impact crater.
3) The NGL is volcanic and may be the remnants of a collapsed volcanic edifice.

2.4.1.1 Dichotomy Boundary Feature

NGL is located within the Hesperian and Noachian transition unit (and Gale Crater Ejecta unit) and between the platform mesas of Aeolis Mensae to the east (Figure 2-1, Figure 2-3) and colles and isolated mesas of Nepenthes Mensae to the northwest (Figure 2-16) (Tanaka, et al., 2014). In this section, we demonstrate that NGL cannot be classified as a typical dichotomy boundary landform, such as a platform mesa, isolated mesa, or colles.

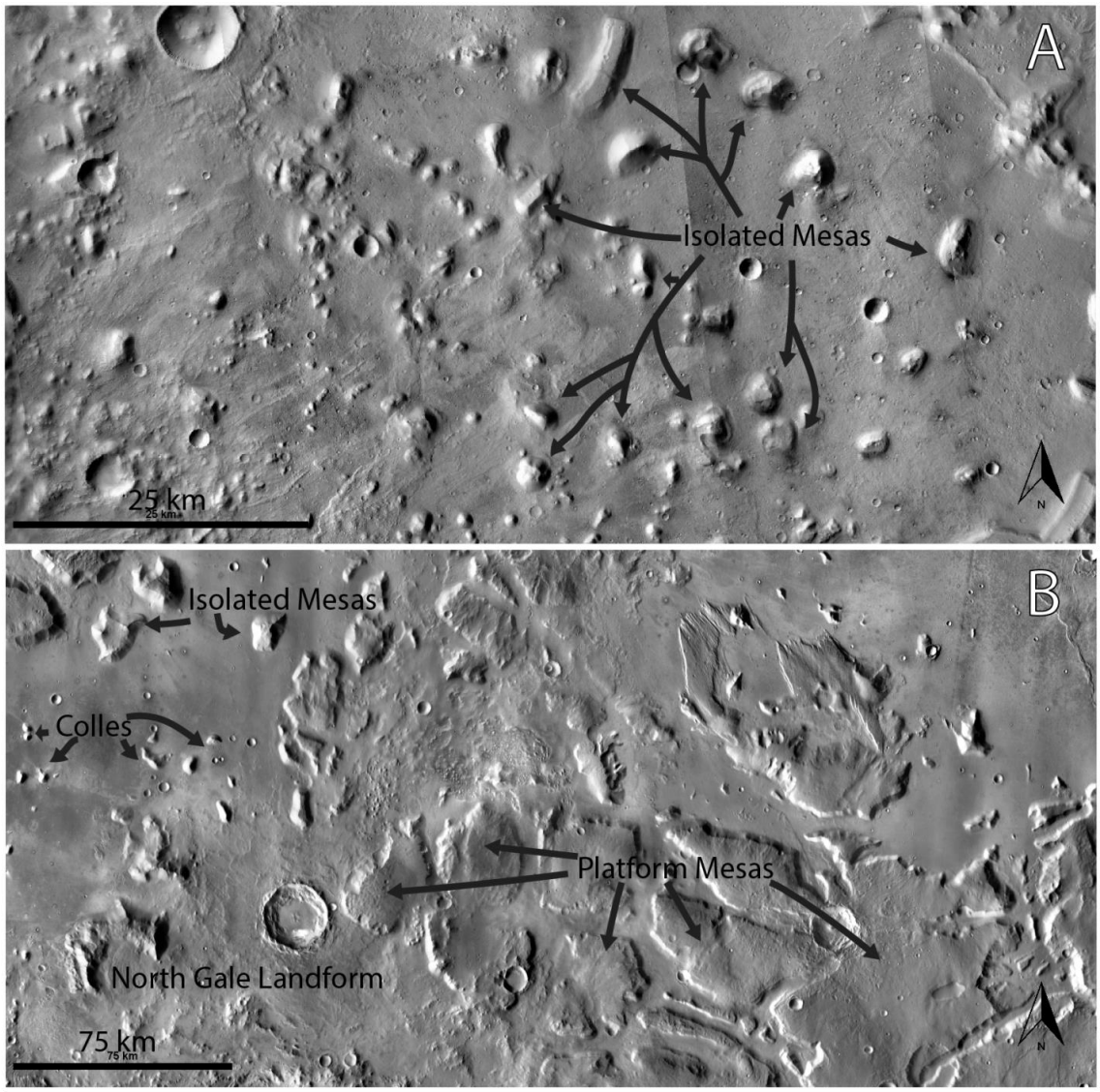

Figure 2-19: Examples of dichotomy boundary landforms (mesas, colles) used for the comparison with North Gale Landform. A: Examples of isolated mesas located in Nepenthes Mensae to the northwest of Gale Crater. They are morphologically distinct from the mesas of Aeolis Mensae. Background images are CTX (Malin, et al., 2007). B: Platform mesas are located in Aeolis Mensae to the east of North Gale Landform. Colles and isolated mesas are north of North Gale Landform. Background map is THEMIS Day IR (Edwards, et al., 2011).

NGL shares some morphological characteristics with the platform mesas such as those at Aeolis Mensae east of NGL (Platform Mesas in Figure 2-19); they can both be high relief, large diameter landforms and surrounded by talus slopes originating from spurs. The diameter of NGL is also within the range observed for platform mesas (44 km vs 30 – 70 km). There are also some striking differences; NGL has a much higher relief

(3.2 km vs ~2 km) than the platform mesas, has only one landform located nearby (smaller hill to the northeast), has no evidence of the internal layering such as in the platform mesas of Aeolis Mensae, and no mesas have the same arcuate shape as NGL. In addition, some of Aeolis Mensae platform mesas lack radial spurs and talus slopes present on all sides of NGL and some mesas have discontinuous spurs and talus.

The formation mechanism of platform mesas (fracturing, dissecting and eroding an aeolian sedimentary wedge) is a plausible formation mechanism for a feature like NGL (Irwin III, et al., 2004). Mesas in the Aeolis Mensae region do not have debris aprons associated with them such as are present in other platform mesa regions (e.g., Arabia Terra), and talus/debris appears to have been transported away when it reached the plains below (Irwin III, et al., 2004). On the northern edge of NGL there appears to be a sharp transition to the plains unit from the talus slope unit that could be evidence of transportation of talus/debris. However, slumps/slides surrounding NGL indicate that not all talus and slump materials are transported away from NGL. Talus slopes and dunes cover the transition from NGL to the plains units so there is currently no way to infer a stratigraphic relationship.

NGL has fewer morphological similarities to isolated mesas than platform mesas (Figure 2-19). While both NGL and isolated mesas can be high-relief, large-diameter isolated landforms, the NGL is more angular than the Nepenthes Mensae mesas and has more morphological similarities to the isolated mesas in Aeolis Mensae. NGL has a capping unit like the isolated mesas in Nepenthes Mensae (capping unit present in Aeolis Mensae isolated mesas). The relief of NGL (3.2 km) is larger than any isolated

mesas in Aeolis Mensae (<2.7 km) or Nepenthes Mensae (<700 m). The diameter of NGL (44 km) is larger than the isolated mesas in Aeolis Mensae (<30 km) and Nepenthes Mensae (<15 km). NGL and Isolated mesas may have formed by the same erosive processes that formed the platform mesas by more extreme erosion (Irwin III, et al., 2004).

Colles, which include hills, buttes and knobs (Figure 2-12, Figure 2-19) are significantly smaller than NGL in both diameter (<12 km vs 44 km) and relief (<1 km vs 3.2 km). Colles are observed to have curved shapes but they do not curve as much as NGL which has an arcuate shape. NGL has more angular boundaries and a wider, more angular capping unit than the rounded caps of the colles which appear relatively rounded. Colles also do not appear to have talus slopes or other slump deposits such as at NGL, but dunes often occur around their base.

Notably, NGL has the highest relief of any landform north of the dichotomy by over 600 m (Figure 2-1) with a maximum elevation of 581 m and a relief of over 3 km above the surrounding terrain. The entire western side of NGL's cap has an elevation over -400 m, this is higher than all but the highest points on the nearby mesas. The western side of NGL appears to be more degraded, there is also more evidence of landslides on the outside than the eastern side. The nearest mesas, colles and highland terrains are over 40 km away and most are grouped with other features of similar size and relief. Therefore, NGL is not a common dichotomy boundary feature.

2.4.1.2 Impact Crater Origin

Due to the large number of impact craters on Mars, it is reasonable to ask if NGL originated from an impact event, such as a degraded impact into a mesa. In this section, we first compare NGL with unmodified impact craters of similar size, then with raised rim impact craters, including pedestal craters, perched craters and excess ejecta craters, and finally with degraded impact structure.

An unmodified impact crater with a diameter of 25 km may be expected to have a circular shape, central peak, and an ejecta blanket. The rim may be raised above the surrounding terrain and the floor of the crater would be depressed below the surrounding terrain. An unmodified impact crater of a similar size to NGL is located to the east of NGL (Figure 2-1) is an example of this type of crater. Compared to craters of a similar size near Gale Crater (20 – 30 km diameter), NGL has a very distinct appearance (Figure 2-20). NGL has an extremely elevated "rim" (up to 3.1 km above surrounding terrain), the interior is elevated up to 1500 m above the surrounding terrain, tilts south ~5°, and no identified central peak. There are no impact craters observed to have the same combination of features as NGL. An elevated rim on a crater typically appears on one side of the crater and the elevated rim is not as high above the surrounding terrain as NGL. The floor of every crater measured sits below the surrounding terrain and many of those craters have a central peak. Very few of the crater floors in Figure 2-20 were tilted (1-2°), and none as extreme as NGL (5°). There is also no evidence of an ejecta blanket surrounding NGL. The plains to the north and west of NGL are not covered by an ejecta blanket originating from NGL. The plains to the south of NGL are covered by

irregular hills (hummocky terrain) and the plains to the west are covered by an ejecta blanket from a nearby crater. The presence of the impact crater's ejecta blanket to the east shows that the blanket of NGL would survive erosion in the area if it were an impact crater (at least since that crater was created). The differences in morphology (rim, interior, lack of ejecta blanket) indicate that the origin of NGL is not as an unmodified impact crater.

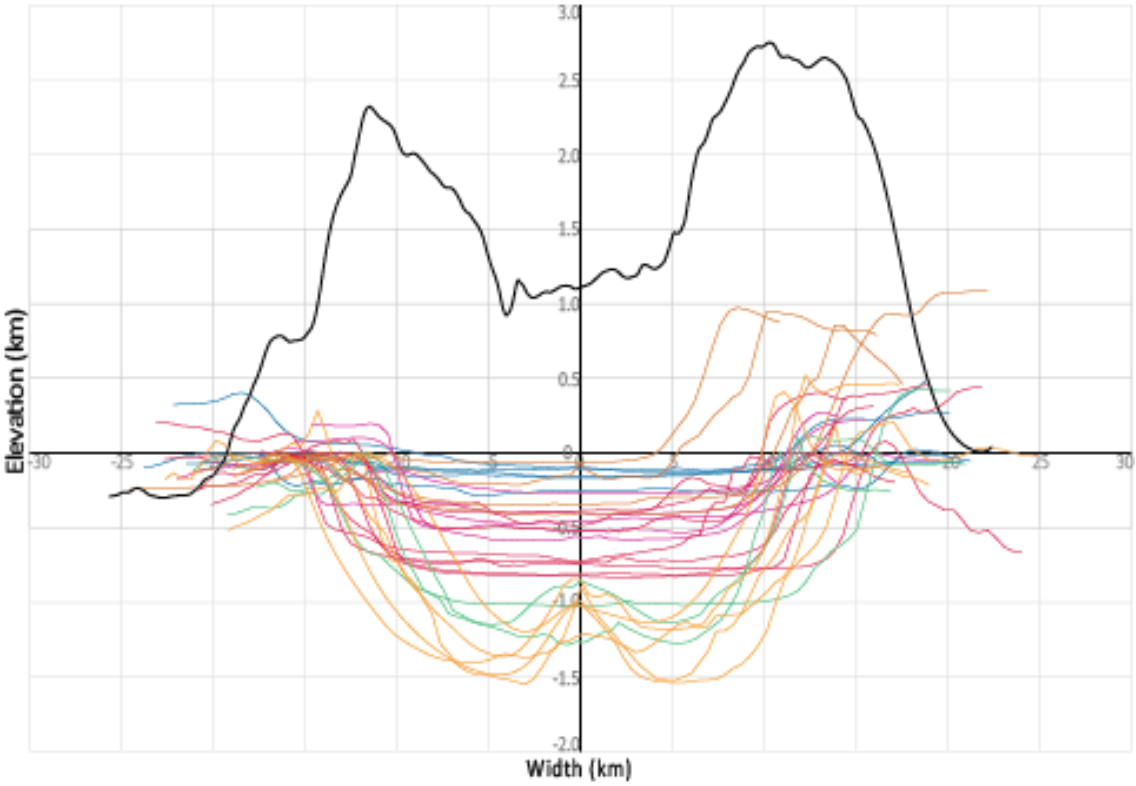

Figure 2-20: Comparison of the profile of North Gale Landform (black, W-E, CTX DEM (Hare, et al., 2016)) with the profiles of nearby craters (N-S, MOLA (Smith, et al., 1999)) of a similar diameter (20 - 30 km). Craters were selected both above and below the dichotomy boundary. Craters are grouped (colours) by similar degree of degradation. The entire structure of North Gale Landform appears above the surrounding terrain while every one of the craters has at least part of it below the surrounding terrain. The central region is over 1 km above the surrounding terrain in this part of North Gale Landform. The edges of North Gale Landform are over 1 km above the central region and over 2.5 km above the surrounding terrain. Some of the craters of this size have a large central peak and some have a flat central region. Some of the craters have a raised rim and others are a similar elevation to the surrounding terrain. The surrounding terrain is at different elevations for some of these craters as well. North Gale Landform looks distinct from the other craters in the area. The structure being entirely above the surrounding terrain is different than all the other craters in the area. The rims of the other craters are the only part that lies above the surrounding terrain, many of the rims are at the level of the surrounding terrain.

Degradation and modification of impact craters usually results in changes to the rim structure, central peak, floor and ejecta blankets (Figure 2-21F, Figure 2-22). NGL has obvious signs of modification by mass wasting, fluvial and aeolian erosion, including talus slopes, slumps and a large, tilted depression with dissected surface. The remaining NGL structure is much taller than any other feature in the region, while the rim of an eroded crater is more likely to be closer to in elevation to the surrounding terrain. NGL is surrounded by talus slopes, slumps and flow deposits, which suggests the surface is partially unconsolidated and not an erosional remnant of an impact crater. Erosion of the surrounding topography along the dichotomy boundary would be expected to also erode the unconsolidated material of NGL if it was a degraded/buried impact crater therefore it must have a different origin. A pristine crater 30 km east suggest that erosional processes were not very active (at least since that crater formed) and would be unlikely to remove >3 km of overburden to expose NGL. NGL has existed long enough that it has channeling in the amphitheatre floor (most likely from flowing surface water) which would suggest it could be >3.3 Ga (Grotzinger, et al., 2015b).

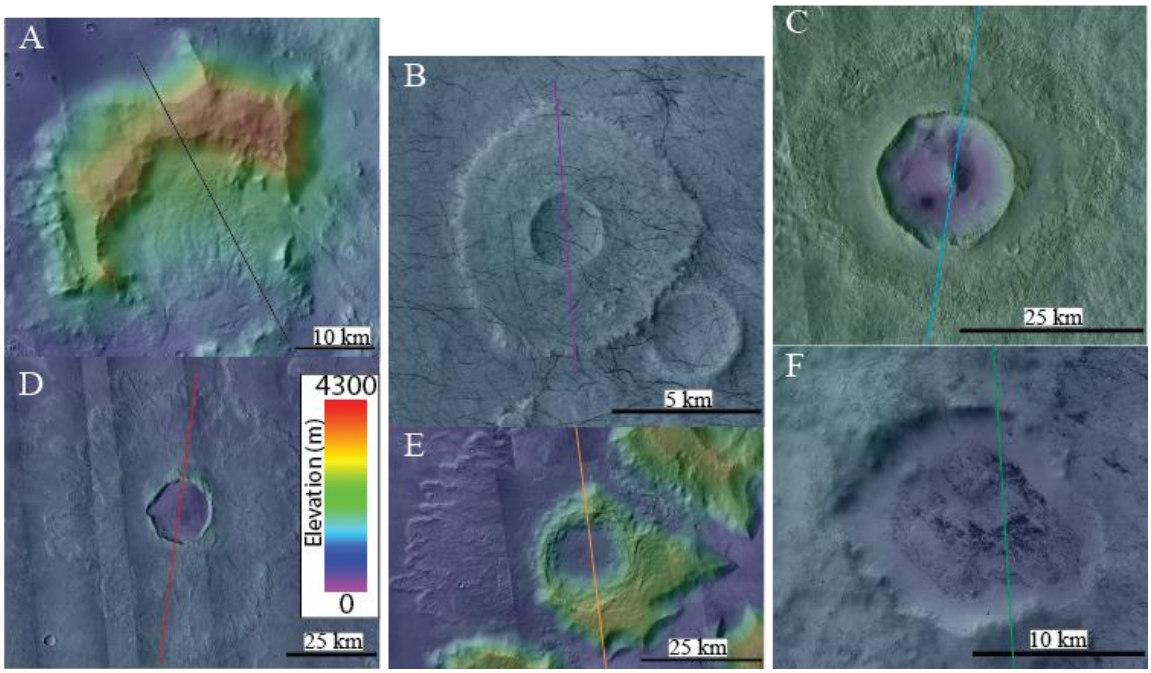

Figure 2-21: CTX (Malin, et al., 2007) images with overlain MOLA elevation data (Smith, et al., 1999) of different types of craters to compare to North Gale Landform. All images are at the same scale, but elevation is adjusted so the terrain surrounding the crater is set to 0 (purple). The types of craters were chosen as they may have an interior that is raised above the surrounding terrain or elevated from what it is to be expected during impacts. ***A****. North Gale Landform at 3.4S, 136.9E.* ***B****. 2.5 km wide pedestal crater at 56.9S, 43.7E.* ***C****. 18.5 km wide excess ejecta crater at 38.5N, 99.2E.* ***D****. 18 km wide perched crater at 37.4N, 159.1E.* ***E****. 17 km wide impact on a mesa at 0.9S, 136.6E.* ***F****. 13.4 km wide eroded crater at 51.5S, 173.9E.*

A variety of impact craters will result in an interior raised above the surrounding terrain and/or a rim raised significantly above the surrounding terrain: pedestal crater, perched crater and excess ejecta crater (Figure 2-21B-D, Figure 2-22). An evenly raised rim, flat raised interior, with a diameter <5 km sitting on a plateau created by the ejecta blanket are expected for a pedestal crater (Figure 2-21B). An unevenly raised rim, partially filled interior, with diameter 6 – 23 km and a visible ejecta blanket are expected for a perched crater (Figure 2-21D). An excess ejecta crater is expected to have a raised rim and ejecta blanket, depressed interior, central peak and 2.5 – 100 km diameter (Figure 2-21C). The exterior of NGL is raised above the surrounding terrain, but at a much higher relief than these craters. The southern portion of the rim is also missing,

whereas these crater types have complete, circular rims. NGL has a larger diameter than expected for pedestal and perched craters but is within the range of excess ejecta craters. The interior of NGL is raised above the surrounding terrain like perched and pedestal craters, but it is raised much higher above the surrounding terrain (~1 km) than expected for the other crater types (<500 m). The interior of NGL is sloped significantly more when compared to the relatively flat (besides central peak) interiors expected for other craters. There is no ejecta blanket identified surrounding NGL to protect the surrounding terrain from deflation as there is for the other crater types.

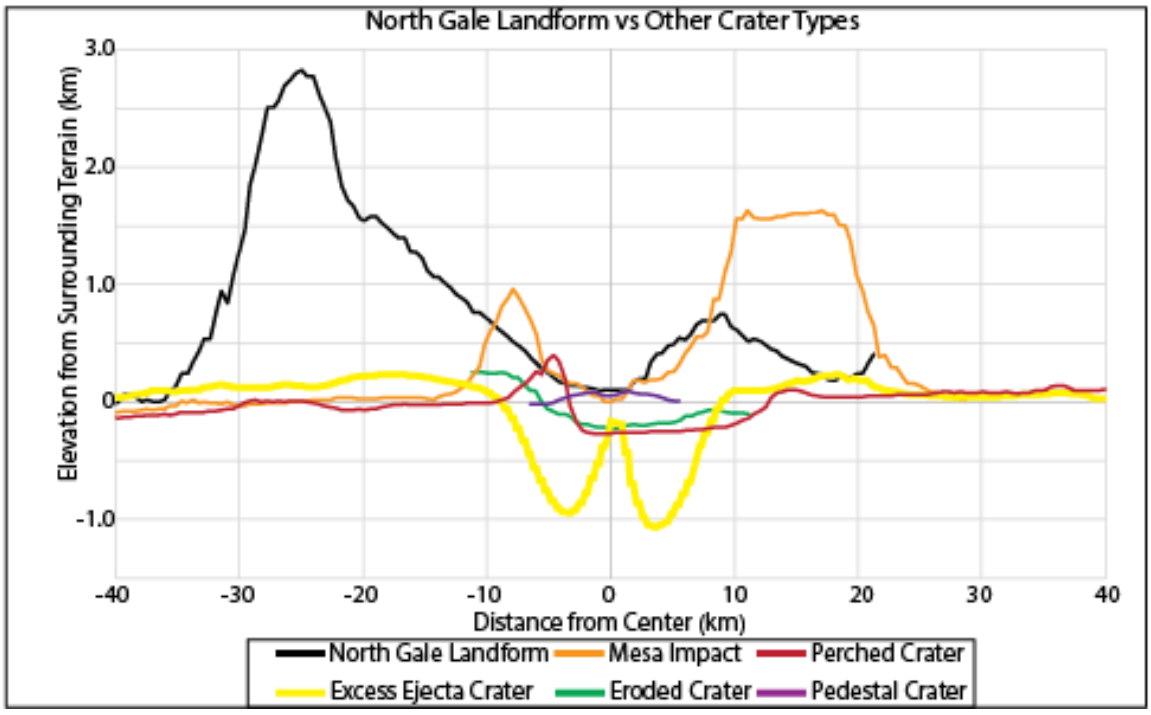

Figure 2-22: Profiles of examples for different crater types (MOLA (Smith, et al., 1999)) to compare against the profile of North Gale Landform (CTX (Hare, et al., 2016)). The types of craters were chosen as they may have an interior that is raised above the surrounding terrain or elevated from what is to be expected during impacts. The lower side of NGL in the profile is not actually part of the structure of North Gale Landform; it is an irregular hill emplaced close to NGL. It is likely blocks from North Gale Landform that were dislodged during the debris avalanche. The lowest point of the profile is still elevated with respect to the surrounding terrain.

Would an impact into a previously existing structure (e.g. mesa) explain the morphology of NGL? A previously existing structure could provide an elevated substrate

and the extreme relief seen on the exterior of NGL, while also providing a means for the interior of the crater to be raised above the surrounding terrain. A recognizable structure of a known landform, crater-like morphology of the rim and crater floor-like interior would be expected for an impact into an already existing structure. NGL does not appear to be like any dichotomy boundary landforms however, due to differences in size, dimensions and morphology (Section 2.4.1.1).

An example of an impact into a previously existing structure is found 120 km north of NGL where there is an impact crater in an isolated mesa (Figure 2-21E, Figure 2-22). This "impact mesa" features a large crater (16 km diameter) relative to the size of the previous structure (40 km wide mesa). This mesa has a high point at -367 m and a relief around 2.2 km (Figure 2-1). The mesa has a relatively flat cap with spurs on the edges and talus slopes surrounding the whole structure. The edge of the crater is composed of concentric rings in the mesa, the damage to the mesa has several tiers above the crater floor. The walls of the crater appear to be mass wasting into the interior of the crater. The floor of the crater is elevated above the surrounding terrain by ~170 m and the lowest point of the floor is in the center of the crater. There is a visible ejecta blanket extending up to 40 km away from the center of the crater on the north, west and south sides of the crater. The mesa may have prevented the ejecta blanket from spreading to the east.

The impact mesa is still recognizable as a typical mesa of the region with several similar mesas in its proximity. If a larger impact (relative to the size of the pre-existing landform) were to occur on a pre-existing landform then the original landform may not

be as well preserved (or destroyed completely). However, an impact would not significantly increase the relief of an existing landform, and NGL has a higher elevation (581 m) and relief (3.2 km) than any other landform north of the dichotomy near Gale Crater. The interior walls of NGL do not appear shattered/damaged like the impact mesa, nor are there concentric rings around the exterior of the depression and are covered with talus slopes. The interior depression of NGL has a more angular boundary than is seen in the circular impact crater in the mesa. The interior of NGL is filled in with a material that slopes southward, and the lowest point of the interior is in the southernmost section of NGL. The floor of the crater on impact mesa has a relatively smooth appearance with small hills and depressions (10s of meters) while NGL features a dissected surface morphology and a rougher surface texture. NGL does not appear to have an associated ejecta blanket while impact mesa and the crater to the east of NGL show that preservation of ejecta blankets is possible in this area, although this may be due to differences in age of the landforms. Therefore, due to the morphological and size differences between NGL and impact craters, it is not an impact related feature.

2.4.1.3 Volcanic Origin

This section will explore the possibility that NGL is volcanic. Volcanoes may experience constructive (edifice building), or destructive (edifice removing) phases (which may occur concurrently, see Anak Krakatau (Giachetti, et al., 2012)) and are typically built relatively quickly; it takes 1-5% of active lifetime for terrestrial stratovolcanoes to build a cone at 1-5 km^3/ky, and ~600 ky for terrestrial shield volcanoes to complete their shield building phase (Thouret, 1999). The structural

instability of volcanoes from their rapid construction often results in failures of the edifice (Thouret, 1999). NGL is a stand-alone ~44 km wide edifice with a relief of 3.2 km above surrounding terrain, suggesting that it underwent a constructive phase. NGL has also undergone a destructive phase as indicated by the lack of a conical shape, its 25 km-wide S-facing amphitheatre, extensive talus slopes covering sidewalls, and knobby deposits at the base of the slopes. The exact timeframe for the formation of NGL is unknown. There is minor cratering on NGL but not enough to be consistent with an early Noachian origin where more extensive degradation by craters would be expected. NGL does not appear to be covered in ejecta debris which would indicate that it formed after the Gale forming impact (~3.5-3.8 Ga). However, the collapse of NGL may have removed the portion of the structure with extensive crater degradation or Gale ejecta cover so it may not be possible to determine when it formed. The end of the major destructive phase which created the amphitheatre can be constrained to >3.2 Ga due to the presence of channeling on the amphitheatre floor and the end of significant fluvial activity (Grant, et al., 2014).

Volcanoes are composed of intermixed, indurated (e.g., lavas) and friable (e.g., tephras) materials. Typically, eroded volcanoes are mantled by talus and surrounded by debris aprons. These characteristics agree with what is observed on NGL: the exterior and interior slopes of NGL are covered by talus slopes (Figure 2-5, Figure 2-6, Figure 2-7) and other “slumping” deposits (knobby unit, Figure 2-5, Figure 2-7). Talus slopes are also seen on other features in the area (mesas, irregular landform to the northeast of NGL) and may be common to features in this region. The NGL depression floor is covered in

materials that appear to be unconsolidated due to the dissection of the surface. The material in the depression was likely deposited during mass wasting of the cap, spurs and sidewalls (Figure 2-5, Figure 2-6, Figure 2-7).

Martian volcanoes are typically thought to be large shield volcanoes and pateras or smaller features such as cinder cones and tuff rings (Table 2-2). Cinder cones can have slopes up to 20° but have much less relief, smaller diameters and height to width ratio (H/W) than NGL (Broz & Hauber, 2013). Shield volcanoes can have a vast range of dimensions from the giant shields of Tharsis to the small shields of Syria Planum (Baptista, et al., 2008; Plescia, 2004). Jovis Tholus, a shield volcano has a similar diameter to NGL but has lower relief, shallower slopes and smaller H/W (Plescia, 2004). Uranius Patera, also a shield volcano has a similar relief to NGL but has a wider diameter, shallower slopes and lesser H/W (Plescia, 2004). The dimensions of NGL suggest that it is not similar those types of Martian volcanoes and may be a type of volcano that is very uncommon on Mars: a stratovolcano.

A few stratovolcanoes, such as Zephyria Tholus (Figure 2-23) and Figure B, has been identified on Mars (Table 2-2) (Stewart & Head, 2001). Zephyria Tholus is smaller than NGL with shallower slopes although it has a similar H/W. Its flanks are dissected which is common on volcanic edifices built of pyroclastic materials. Zephyria Tholus has a summit crater and evidence of lobate flows. The summit region of Zephyria Tholus is dark under THEMIS Night IR similar to NGL (Figure 2-3). Spur-like regions appear around the rim of the summit and on the flanks, which are also bright under infrared like NGL.

Aside from the summit and spurs, the rest of the feature is mid toned like NGL, suggesting a similar mix of consolidated and unconsolidated material at the surface.

Table 2-2
Volcanic Attributes from Mars and Earth

Name (Location)	Type	Width[a]	Height[a]	Flank Slope	H/W[b]
North Gale Landform (Mars)	unknown	43.5 km	3.2 km	25°	0.07[h]
Cinder Cone/Tuff Ring (Mars)[c]	Cinder Cone/Tuff Ring	~7.8 km (3 – 15 km)	~120 m (30 – 370 m)	Up to 20°	0.02[h]
Shield Volcanoes (Mars)[d,e]	Shield Volcano	7 - 1400 km	0.1 – 21.9 km	Up to 10°	0.001 – 0.05[h]
Jovis Tholus (Mars)[d]	Shield Volcano	58 km	1.0 km	3°	0.02[h]
Uranius Patera (Mars)[d]	Shield Volcano	280 km	3.0 km	3°	0.01[h]
Zephyria Tholus (Mars)[f]	Stratovolcano	~30 km	2.5 km	14°	0.08[h]
Feature B (Mars)[f]	Stratovolcano	~30 km	~2 km	14°	0.07[h]
Stratovolcano (Earth)[g]	Stratovolcano	2.0 – 65.9 km	0.17 – 5.07 km	Up to 32.5°	0.023 – 0.30

[a] Range in parenthesis, [b] Height/Width ratio, [c] (Broz & Hauber, 2013), [d] (Plescia, 2004), [e] (Baptista, et al., 2008), [f] (Stewart & Head, 2001), [g] (Grosse, et al., 2014), [h]Calculated

Stewart & Head (2001) developed a set of criteria for identifying stratovolcano edifices for Mars: 1) size, 2) slope characteristics, 3) dissection processes common to pyroclastically built volcanoes 4) inability to explain the origin by other hypothesises. The size of NGL is within range of terrestrial stratovolcanoes (Table 2-2) and Zephyria Tholus (Grosse, et al., 2014; Stewart & Head, 2001). The slope and H/W of NGL are also within range of terrestrial stratovolcanoes and similar to Zephyria Tholus (Grosse, et al.,

2014). The amphitheatre of NGL has large scale dissections and the edifice has small scale dissections (visible in spurs and knobby unit). Talus slopes cover the edifice as well which hides the slopes of NGL. The previous subsections demonstrated that the other hypotheses (impact, dichotomy feature) fail to explain the origin of NGL. In addition, the amphitheatre in the southern flank of NGL appears to be a flank collapse which is common in terrestrial stratovolcanoes (Figure 2-24, Figure 2-25) (Siebert, 1984; Thouret, 1999). NGL appears to satisfy the conditions laid out by Stewart & Head (2001) and therefore may be a stratovolcano built from pyroclastic activity.

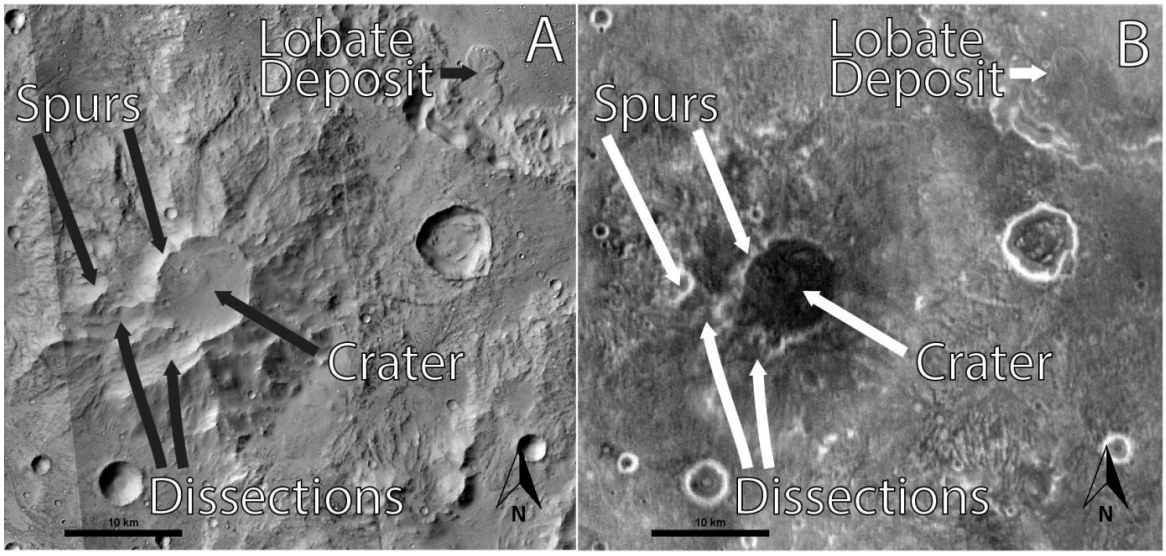

Figure 2-23: Zephyria Tholus in visible (A, CTX) and infrared (B, THEMIS). One of the few stratovolcanoes identified on Mars, Zephyria Tholus is identified as a stratovolcano in (Stewart & Head, 2001) through the criteria developed there. it has size and slope characteristics similar to terrestrial examples. There is evidence of dissections on the edifice common to terrestrial volcanoes. No other explanations for formation fit better.

Other potentially volcanic features in the region may provide supporting evidence for a volcanic origin for NGL, including chaotic terrain and a pit crater chain. A ~20-km wide, roughly square area of chaotic terrain (Figure 2-11) is located within 10 km of NGL (Figure 2-4) and composed of many sub kilometer scale blocks separated by

linear to arcuate troughs. There is also a smaller (~7 km x ~3.5 km), irregularly shaped collapse feature (potential outflow channel) just north of the main body of chaotic terrain that are likely related. The difference in relief between the blocks and troughs is <100 m suggesting it could not form through the Zegers, et al. (2010) model and must have a different heat source than the heat flux from Mars. The presence of pedestal craters in the transition area along the dichotomy boundary suggests that there was subsurface ice in the area (Irwin III, et al., 2004). However, the relief difference between blocks and troughs suggests there was not the required 1-2 km of ice and overburden for the chaotic terrain to form from this model (Zegers, et al., 2010). An underground magma body, possibly related to the nearby NGL (~10 km), might represent a heat source to melt the subsurface ice and form the small-scale chaotic terrain (Meresse, et al., 2008). A pit crater chain (Figure 2-10) is present 10 km further west of the chaotic terrain near NGL. A lava tube or magma chamber creating the original void space for the pit crater chain may have originated from NGL or be related to the magma body feeding it. The pit crater chain is oriented NE/SW toward NGL which may also indicate a link between this feature and NGL. However, there does not appear to be more than one pit crater chain near NGL, or any other evidence of lava flows in the area. A volcanic origin for this pit crater chain could also have been linked to the formation of the chaotic terrain providing the magma for its formation (pit crater chain <10 km west of chaotic terrain).

2.4.2 Origin of Hummocky Terrain

The hummocky terrain that lies between NGL and Gale crater is also relevant for understanding the history of these landforms. Hypothesises for the origin of the hummocky terrain include: (1) the hummocks are typical dichotomy boundary landforms (hills, knobs and buttes); (2) the hummocky terrain is part of another identified unit, such as Gale Crater ejecta (Figure 2-13) or highland rugged, knobby unit (Figure 2-14); and (3) the hummocky terrain is a debris avalanche deposit formed during the collapse of the southern flank of NGL. This subsection will explore each of these possibilities to determine the most likely scenario for the origin of the hummocky terrain.

Hummocks are morphologically distinct from other small hills, buttes and knobs (colles (Figure 2-12)), that are found near the dichotomy boundary in several locations on Mars (specifically those near Gale Crater). Colles appear consolidated and stand out among their immediate surroundings compared to hummocks which look to be a mixture of consolidated and unconsolidated material (competent blocks in large piles of debris) with unconsolidated material "connecting" the blocks together. While colles are often grouped, they do not appear to be as closely associated as hummocks (talus slopes converge, hummocks touching). Colles have angular sides more often than hummocks but often have a rounded appearance as well. Hummocks always have some talus slopes around their margins, while some colles may have some talus associated with them, but many do not. Individual hummocks are observed to have a diameter as small as 10s of meters. In contrast, small colles have diameters as small as 500 m. Both

hummocks and colles can have a relief up to ~1 km, but many of the hills are smaller than that.

The highlands to the west of the hummocky terrain include a knobby, hilly unit (Figure 2-14) that is similar to the hummocky terrain. It is more like the Gale Crater rim unit however, due to its more rugged appearance. The knobs and hills might be ejecta from Gale Crater or material slumping off the highland units as it appears near the transition between highland and lowland plains.

Here we propose that the hummocky terrain is a massive debris avalanche deposit. For this to be the case, several features are required (Siebert, 1984), including the morphology of the hummocks (described below), a source for the avalanche, and a contained location for the terrain.

The hummocks are morphologically distinct from dichotomy boundary landforms, crater rim and nearby knobby highland units. The combination of competent blocks partially buried in piles of rubble is distinct to this area. A massive debris avalanche would have large blocks of the original structure intermixed with smaller debris that broke up during the collapse and transport (Siebert, 1984). The blocks and rubble piles forming the hummocks fit this description. The competent blocks are likely large pieces of the original structure and the piles of rubble are likely material that was pulverised during the original collapse.

A debris avalanche from NGL would explain the amphitheatre in addition to the hummocky terrain. The partial collapse of a mountainous landform like NGL is expected

to leave a large scar in the original structure, depending on the volume of material moved relative to the landform (small landslide may not leave noticeable scar, large landslide may significantly impact the structure of the landform) (Siebert, 1984). The south-facing amphitheatre of NGL may represent a source for a debris avalanche that formed through the collapse of its southern flank. The original structure may have been quasi-circular, and there is potentially a large volume of the original structure that would have been transported away that now make up the hummocky terrain. There are sections of the amphitheatre sidewalls approximately 7-10 km long that are fairly straight, and the sidewalls may be tectonically controlled. The floor of the amphitheatre is sloped away from the elevated cap of NGL (5° south) and its dissected surface might be evidence of an unconsolidated surface that was modified by flowing water. THEMIS Night IR shows the interiors of the channels to be filled with fine sediments while the channel banks have little sediment cover and may be indurated.

The hummocky terrain is contained within an area that widens toward Gale crater and that would be expected if it were produced during the collapse of NGL. The largest hummocks occur concentrated along the center axis of the debris avalanche. Hummocks are also larger closer to their source. The largest hummock in the deposit has a relief of ~1 km and it is in the cluster of hummocks closest to NGL. Smaller hummocks are located nearer to the edges of the unit and are more common in the direction of Gale crater.

Tectonic features surrounding NGL including fault scarps, wrinkle ridges and linear outwash channels have a distinct trend of orientation of 66˚ (Figure 2-16, Figure

2-17, Figure 2-18) (Cole & Andrews-Hanna, 2017). It is also possible that there are unidentified dyke intrusions associated with these tectonic features. The dominant tectonic orientation is approximately perpendicular to the axis of the NGL amphitheatre and is consistent with tectonic stresses having a control in its formation, such as by a preferred orientation to a radial dyke swarm. The apparent tectonic control of the NGL amphitheatre is consistent with terrestrial debris avalanches, where tectonic features are usually perpendicular to the direction of the amphitheatre openings (Siebert, 1984).

2.4.3 Volcanic Debris Avalanche

Terrestrial stratovolcanoes and shield volcanoes are known to experience sector collapses, where a portion of the volcanic edifice is removed by debris avalanche and deposited near the volcano as hummocky terrain (Siebert, 1984). The sector collapse leaves a large horseshoe shaped crater with a steep sided scarp (referred to as an amphitheatre) in the edifice of the volcano which opens towards the debris avalanche deposit (referred to as hummocky terrain) (Siebert, 1984; Thouret, 1999). The amphitheatres have a width of 1 to 3 km and widen in the direction of the avalanche (Siebert, 1984). The amphitheatre can be 100s of meters deep and may extend through the "core" (central vent) of the volcano (Siebert, 1984). The headwall and sidewalls (scarp) surrounding the amphitheatre are over steepened by the collapse and are prone to further collapse. There is an extreme difference between the elevation and steepness of the amphitheatre walls and floor of the depression. The floor has a gentle slope out of the breach, which is interrupted by the headwall which is raised above the floor (Siebert, 1984). A sector collapse is unlike a non-volcanic landslide where only material

close to the surface is displaced (Siebert, 1984). Some sector collapse events are associated with explosive activity that can further disrupt the cone and may lead to over-steepened walls and further collapse (Siebert, 1984). Terrestrial stratovolcanoes that have experienced sector collapse and produced hummocky terrain include Mt. St. Helens in Oregon, USA (Figure 2-24) and Bezymianny in Kamchatka, Russia (Siebert, 1984). Shield volcanoes that have experienced a sector collapse include Mauna Loa Volcano in Hawaii, USA (Lipman, et al., 1988), Waianae Volcano in Hawaii, USA (Presley, et al., 1997) and the Canary Islands, Spain (Carracedo, 1999). A similar morphology to the terrestrial sector collapse volcano is seen in NGL.

Figure 2-24: Mt St Helens experienced a volcanic debris avalanche during its May 1980 eruption. The eruption caused the northern flank of the volcano to separate from the mountain, slide down the northern face and into the valley below. Left: Mt St Helens shortly before the 1980 eruption. Right: Mt St Helens after the 1980 eruption. Source: USGS.

The amphitheatre on NGL is a horseshoe shaped depression in the southern flank which opens towards hummocky terrain to the south (Figure 2-2). The

amphitheatre includes the central area of NGL and is surrounded by steep walls on the remaining sides (headwall and sidewalls). Talus slopes completely cover the head/sidewalls and a section of knobby material is on the wall in the northeast corner. The amphitheatre floor/wall contact is covered by talus and gently slopes from the headwall towards the hummocky terrain to the south. The dimensions of the amphitheatre on NGL are much larger than those on the terrestrial volcanoes (25 km vs <10 km). The depression of NGL is also much deeper than terrestrial volcanoes (>1 km vs 100s m). The depression may have been filled in with the eroded structure (talus slopes, knobby unit mobilization) which affected the slope compared to terrestrial examples. The head/sidewalls (~23°) of NGL are steeper than the floor (~5°) as seen in terrestrial examples (Figure 2-25). The NGL depression has a shallower backwall slope relative to terrestrial volcanic amphitheatres, but this may not reflect the underlying structure as there are talus slopes covering the backwall. The collapse of NGL is not like a non-volcanic landslide scarp as the amphitheatre suggests a significant amount of the structure was removed. A non-volcanic landslide scarp often only results in the mobilization of the surface material. There is no evidence of an explosive eruption during collapse of NGL such as occurred at Mt St Helens such as associated pyroclastic deposits (but that does not mean an explosive eruption did not occur).

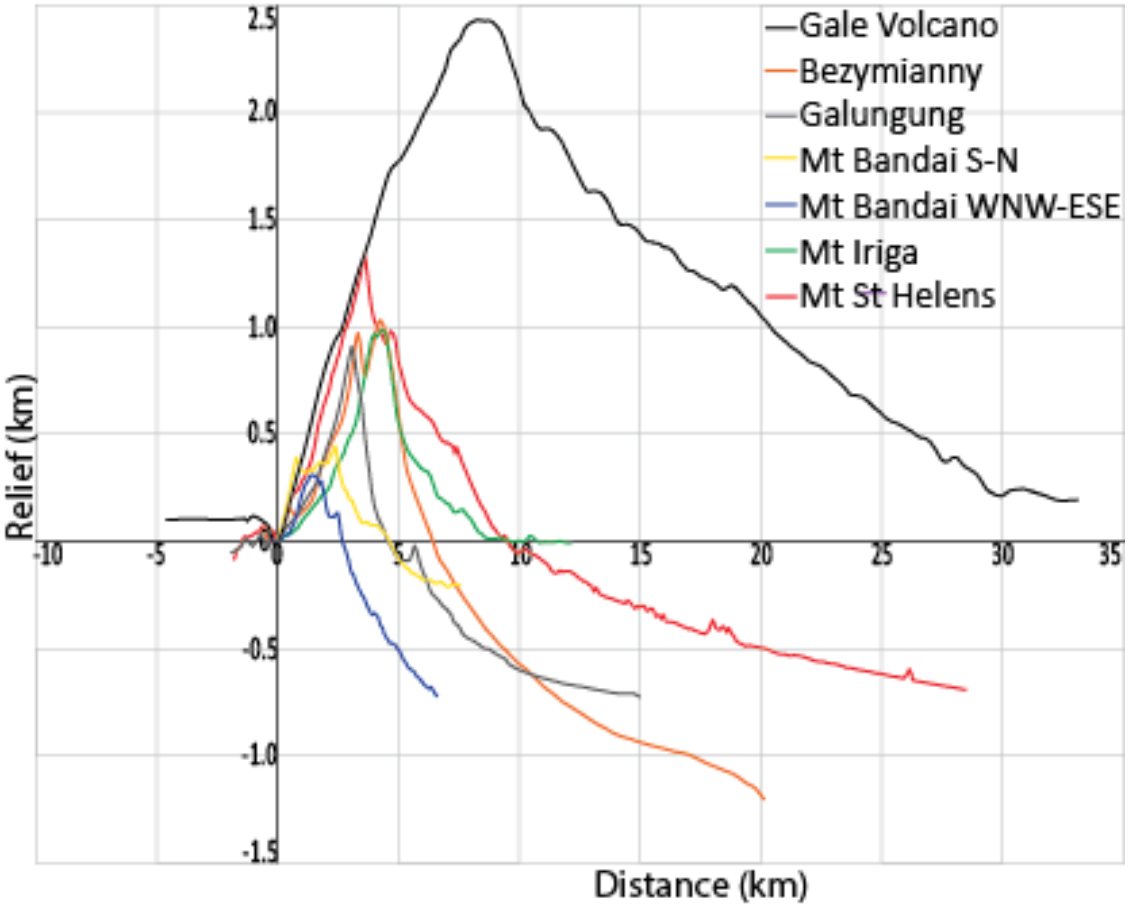

Figure 2-25: Profiles of North Gale landform (HRSC (Neukum & Jaumann, 2004)) and six terrestrial volcanoes (Google Earth) that have experienced major debris avalanches. Profiles were taken along the direction of the debris avalanche.

Mobilized volumes of up to almost 300 km^3 have been observed on terrestrial stratovolcanoes, with even larger debris avalanches removing half of several Hawaiian shield volcanoes (Coombs, et al., 2004). The avalanches appear to move longer distances than expected for non-volcanic landslides (possibly due to presence of pyroclastic and altered materials or hydrothermal fluids) reaching up to 50-60 km from the source (Siebert, 1984). The largest runout efficiency (runout efficiency = runout length / descent height) observed for terrestrial volcanoes was 21 (Siebert, 1984). An estimated volume between 670 – 4700 km^3 was mobilized from NGL depending on its

original height (4.3 – 13.7 km estimated original height for a cone-shaped landform). Gale Crater is 58.2 km away and a runout efficiency of the NGL debris avalanche of 4 to 11 (assuming 13.7 km and 4.3 km original height) would allow the debris flow to reach it in the vicinity of Peace Vallis. Such run out efficiencies are within accepted values for other landslides observed on Mars (2 – 23) (Coleman, 2003).

Terrestrial debris avalanche deposits are composed of lithic and minor juvenile material (Siebert, 1984). They consist of a poorly sorted mixture of brecciated debris extending from the base of the volcano outwards with a surface morphology that contains hills, depressions, longitudinal and transverse ridges, and megablocks of the former edifice (Siebert, 1984). There can be hundreds to thousands of hills that can be over 200 m in height and 100s of m in diameter (Siebert, 1984). These hills can have a range of morphologies from conical to elliptical with the long axis of the hill often pointing away from its source (Siebert, 1984). The largest hills tend to be along the central axis of the debris avalanche, but the density of hills increase towards the margins (Siebert, 1984). The fragmentation of blocks and fine materials increase as distance from the source increases (Siebert, 1984). The hills are also often in clusters resulting in areas with many hills and some areas with no hills (Siebert, 1984).

In the hummocky terrain near NGL, the hummocky unit (hills) may be intact blocks of the failed volcanic edifice and smaller debris. There are several transverse ridges composed of groups of hummocks and a few longitudinal ridges near the center axis of the deposit. There are several clusters of hummocks and flat depressions present in the deposit area. The large hummocks near NGL may be partially composed of

megablocks. The largest hummocks occur closest to the center axis and source of debris avalanche, are generally smaller away from the axis and source. This hummocky terrain is likely not Gale Crater impact ejecta because it is only found between the landform and Gale Crater and not in other locations around the crater rim.

2.4.3.1 Regional Considerations

Region and local stresses can have some influence over the location and direction of the amphitheatre. Radial dike swarms and parasitic cones will form parallel to the stresses experienced by the volcano. The intrusion of magma from those features causes some extensional stress perpendicular to the original stresses which can result in failure of the volcanic edifice and a debris avalanche. Amphitheatre openings at terrestrial volcanoes are often found to be approximately perpendicular to the preferred orientation of the dikes although some have no relationship between them. The direction can also be controlled by topography of the underlying surface, any internal faulting, or the shape of other structures inside the volcano (Siebert, 1984). An examination of lineations which may represent tectonic stresses was conducted (Figure 2-16, Figure 2-17, Figure 2-18) and indicates a dominant NE-SW direction (strike ~65°) that is perpendicular to the amphitheatre opening. The NE-SW orientation is also present in a nearby pit crater chain (Figure 2-10). Fissuring and dike swarms would likely also have a similar orientation to them due to that preferred direction of tectonic stress. The east side of NGL shows a radial spur (possible dike) with the same orientation. Therefore, we can conclude that NGL produced a volcanic debris avalanche which was deposited as the hummocky terrain between NGL and Gale Crater.

2.4.4 Implications for Gale Crater Geology

There are distinct igneous endmember sediment compositions which have been examined by the Curiosity rover after it landed in Gale Crater. The current hypothesis for the origin of the igneous sediments is that they are sourced from the wall and rim of Gale Crater through erosion and transport (Grotzinger, et al., 2015b). However, the endmember compositions of Jake M and Bathurst Inlet classes cannot be linked by igneous processes (Schmidt, et al., 2014; Schmidt M. E., et al., 2017). The crater wall and rim would not be able to produce both igneous endmember compositions so a new source for the compositions might be required. There have not been any volcanic centers previously identified within 2000 km of Gale Crater, making it unlikely that the igneous endmember compositions could have come from a distant volcanic source. However, a volcanic origin for NGL could satisfy this need for another discreet source of igneous endmember sediments. The volcaniclastic sediments may have been transported into Gale Crater by the debris avalanche or remobilized and carried through Peace Vallis. The Peace Vallis catchment area (Figure 2-4) is presently within the hummocky terrain deposit from NGL (Palucis, et al., 2014). Erosion and transport from the catchment area could also allow remobilization of sediments from NGL into the crater.

NGL might also provide both a magmatic and hydrothermal heat source for the widespread enrichment of Zn and Ge found sediments in Gale Crater (Berger, et al., 2017). A magmatic system underneath NGL could have provided the initial enrichment of Zn and Ge and the energy from that system may have provided heat for hydrothermal

systems nearby and possibly in Gale Crater. The catchment of Peace Vallis provides an area where there may be enrichment of Zn and Ge in sediments before transportation into Gale Crater if this process did not occur on NGL itself. There are two populations of Zn enrichment in Gale Crater which could indicate hydrothermal activity in situ in addition to the source region hydrothermal activity (Yen, et al., 2017). Acid sulfate alteration of fracture associated haloes in the Stimson unit of Mount Sharp might also require a hydrothermal source (Yen, et al., 2017). Since NGL is ~40 km away from Gale Crater, it might be close enough to provide a heat source for hydrothermal interactions in Gale Crater sediments.

Tridymite identified in the Buckskin drill sample suggests a low pressure, high temperature silicic volcanic environment for its (Morris, et al., 2016). The single layer suggests that this could be a solitary event such as an ash fall into Lake Gale rather than erosion of existing lithology although erosion and transport is still a viable transportation mechanism as well. Morris, et al. (2016) says that the source region for this tridymite would likely be from the crater rim or central peak (pre-existing lithology), however, a separate volcanic source close to Gale Crater could also be the source. The type of volcanism at NGL is not known so it cannot be identified as the definitive source for this tridymite, but if NGL and the tridymite are linked it may imply silicic volcanic activity at NGL. NGL could have produced an ash fall during an eruptive episode or rocks/sediments from NGL could have been eroded and transported into Gale Crater as well.

2.5 Conclusions

Volcaniclastic sediments found by the Curiosity rover in Gale Crater suggested there needs to be more igneous sediment sources than the rim and wall of Gale Crater. Orbital imagery and elevation data from HiRISE, CTX, THEMIS, HRSC and MOLA datasets showed there is a unique landform ~40 km north of Gale Crater which might represent such a source.

NGL appears to be distinct from those other dichotomy boundary features. Due to the large size difference (>1 km relief) it is unlikely that NGL is a knob, hill or butte despite morphological similarities such as spur-like features and talus slopes. NGL and mesas both have large diameters, high relief, talus slopes and spurs so it is possible that NGL is a heavily deformed mesa, however the extreme relief compared to all other dichotomy features in the region suggests it is a separate type of landform.

NGL has a unique morphology that is not typical of impact craters. Craters with elevated interiors have an associated ejecta blanket which allows for the elevation of the interiors while NGL has no apparent ejecta blanket. NGL has a different morphology than the examples of impacts in mesas observed and has been shown to be a distinct type of landform. NGL does not resemble any eroded craters due to the extreme relief of the landform and the unconsolidated material composing NGL (talus slopes, knobby unit) suggests that extreme erosion events would not selectively erode everything but NGL.

Given the physical characteristics of NGL and its close association with other potential volcanic features and the criteria laid out in (Stewart & Head, 2001), it strongly suggests it is a volcanic feature. However, NGL does not appear to be created by lava flows over time like most of the other volcanic edifices seen today on Mars (Werner, 2009). In fact, the lack of lava flows around NGL seems like it would cast doubt on the explanation for its origin. Volcanic edifices can be created through other means however, terrestrial stratovolcanoes are created through alternating eruptions of magma and pyroclastic deposits, so the lack of lava flows does not rule it out (Siebert, 1984; Stewart & Head, 2001). The edifice of NGL is a standalone feature with an extreme relief compared to regional landforms though it has experienced extreme modification indicated by the amphitheatre in the southern flank. Talus slopes are present on every side of NGL originating from spurs surrounding a consolidated capping unit consistent with the mixture of indurated and friable materials that typically comprise volcanic edifices. It is within range of terrestrial stratovolcanoes in terms of size and slope characteristics and has evidence of dissection processes. Stratovolcanoes are not unheard of on Mars, Zephyria Tholus has been determined to have a stratovolcano origin and it is ~2200 km away from Gale Crater (Stewart & Head, 2001). NGL is similar to Zephyria Tholus on Mars in terms of dimensions, common features and appearance under THEMIS Night IR.

The amphitheatre appears to have been created by a massive debris avalanche as it meets all the requirements for identification of a terrestrial volcanic debris avalanche outlined by Siebert (1984). A volcanic debris avalanche explains NGL and the

surrounding topography. The morphology of NGL (Figure 2-4), including the amphitheatre (Figure 2-7) and hummocky terrain (Figure 2-8), show that there was a catastrophic failure and collapse of a portion of the original structure. The remaining landform resembles terrestrial volcanic debris avalanches (Figure 2-25). While there have been massive debris avalanches on shield volcanoes, most terrestrial volcanoes that have experienced massive debris avalanches are stratovolcanoes. Stratovolcanoes are composed of intermixed lava and tephra layers and are often steeper than shield volcanoes which are composed of layers of lava flows like shield volcanoes. The evidence indicates that NGL may be a stratovolcano, although no compositional data is available to support the hypothesis at this time.

If NGL is a stratovolcano, it would be one of a few discovered on Mars. Evidence of basaltic volcanism on Mars is widespread, including large shield volcanoes, cinder cones/tuff rings and basaltic composition soils (Broz & Hauber, 2012; Schmidt & McCoy, 2010). Evidence for silicic volcanism on Mars is more limited, but orbital data shows evidence of silicic rocks on the surface (Christensen, et al., 2005; Sautter, et al., 2015; Wray, et al., 2013). Those papers indicate the silicic rocks are evidence for early continental crust on Mars that cooled from a magma ocean rather than erupted from volcanic landforms. Recent evidence of a tridymite layer in the Murray mudstone at Maria's Pass in Gale crater by MSL Curiosity suggests a need for a silicic volcanic source, however. NGL is ideally placed to be the source for the tridymite layer and this would constrain the volcanic activity at NGL to 3.7 – 3.2 Ga to coincide with lakes in Gale Crater (Grant, et al., 2014). The volcanic origin of NGL has more implications for the discoveries

of the Curiosity rover in Gale Crater as well. Igneous endmember compositions of the sediments in Gale Crater indicate that another source of volcanic materials besides the crater rim/wall is needed to produce the compositions observed. The enrichment of zinc and germanium in APXS targets could require a volcanic and hydrothermal source for both the original and secondary enrichment to reach the levels observed. Acid sulfate alteration haloes in the Stimson formation may also need an energy source for hydrothermal activity to explain their origin. A volcano near Gale Crater can help to solve some of the problems posed by what has been observed in Gale Crater and NGL is the likely candidate.

Chapter 3: Volcanic Sources of Sediment in Gale Crater, Mars

3.1 Introduction

The Mars Science Laboratory rover *Curiosity* landed in Gale Crater, Mars on August 6, 2012 and began its mission to evaluate the crater for ancient habitability and characterize the modern environment (Figure 3-1) (Grotzinger J. P., et al., 2015). It has been active on Mars for over 2300 sols (Martian days): driven more than 20 km, climbed over 300 m and conducted experiments at more than 70 sites. Curiosity is armed with a variety of sensors and instruments used to examine and conduct experiments on the geology of the crater. This study will focus on elemental compositions provided by the Alpha Particle X-ray Spectrometer (APXS) which examines small targets (1.7 cm) on the surface of a rock or soil (Campbell, et al., 2012).

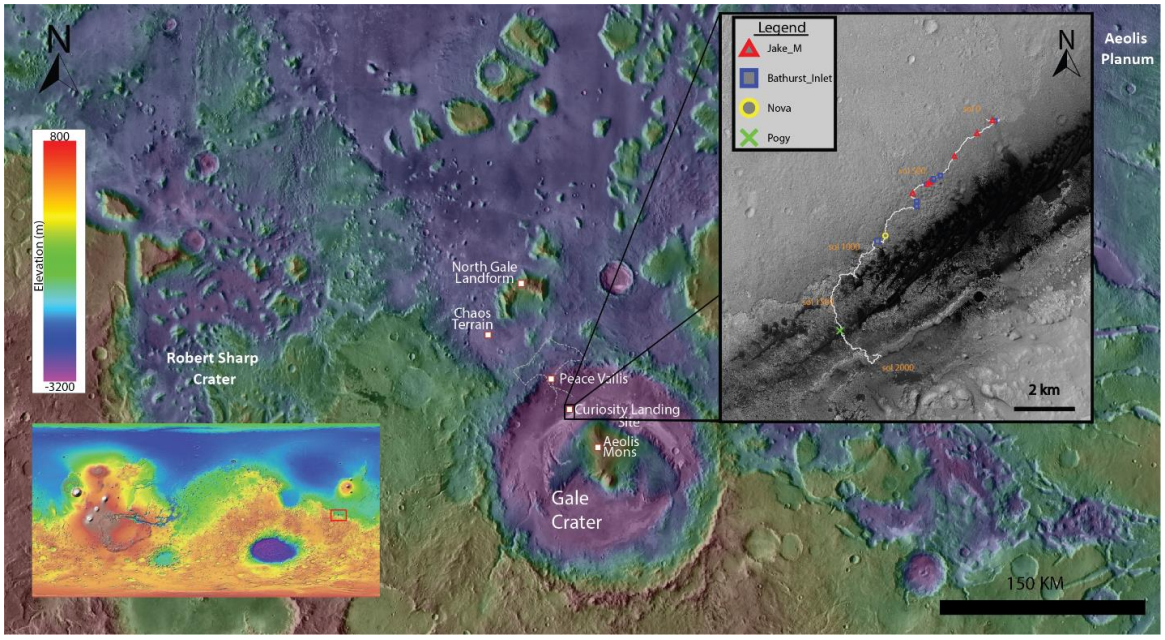

Figure 3-1: Overview map of the Mars Science Laboratory Mission to Gale Crater, Mars. Traverse of Curiosity during its ascent of Aeolis Mons during the first 2066 sols of its mission. All igneous composition targets examined by the APXS instrument are marked along their traverse according to their igneous classification. Gale Crater regional view (background) is THEMIS Day IR imagery (Edwards, et al., 2011). Overall Mars view (bottom left) is MGS MOLA Colorized Hillshade Map.

Gale Crater is a Noachian aged (3.6 – 3.8 Ga), large (155 km diameter) impact crater near the equator of Mars along the dichotomy boundary; it is located between the southern highlands and Elysium Planitia (Grotzinger, et al., 2015b). The surrounding terrain has a knobby, mottled, dissected and mantled appearance with mesas and plains (Anderson & Bell III, 2010). A large, arcuate, quasi circular landform (~40 km diameter, ~3.2 km relief) of likely volcanic origin, North Gale Landform, is located 60 km to the north of the crater (Chapter 2). The rim of Gale Crater is degraded and dissected by channels, which may have drained water and sediments into the crater in the past (Palucis, et al., 2014).

Gale Crater is a basin that filled with sediments deposited between ~3.6 and 3.2 Ga in aqueous environments (Anderson & Bell III, 2010; Grotzinger, et al., 2015b; Milliken, et al., 2010). Ancient river deltas indicate the edge of a lake once contained in the crater where the sediments taken from the crater wall/rim infilled the crater over time (Grotzinger, et al., 2015b). An age of 4.21 ± 0.35 Ga for a local mudstone sample by K-Ar dating is consistent with the possible age range for pre-existing bedrock at the Gale impact site, and the sediment source is interpreted to be the crater wall (Farley, et al., 2014). There is a large interior mountain, Aeolis Mons (also called Mount Sharp), which is composed of flat, stratified beds reaching approximately 6 km above the crater floor (Anderson & Bell III, 2010; Grotzinger, et al., 2015b). Wind-driven erosion over billions of years carved Aeolis Mons out of the sedimentary rock, removing possibly 100s of meters of material down to the current crater floor (Grotzinger, et al., 2015b; Milliken, et al., 2010). On the basis of cosmogenic dating, the rocks comprising the crater floor have

been exposed at the surface for 78 ± 30 Ma after having been buried since their deposition (Farley, et al., 2014).

This study examines the possibility that an external volcanic source has contributed sediments into Gale Crater. We attempt to answer whether more than one source is required to generate the different classes of volcaniclastic sediments examined by the APXS instrument. Petrologic models for partial melting, fractional crystallization and mineral accumulation will be used to help determine the minimum number of crystalline igneous sources that are needed for the different classes of igneous compositions. This work relies on mixing models while another study relies on a model of size sorting to explain the differences in volcaniclastic sediment compositions (Siebach, et al., 2017).

The rocks in Gale Crater examined by MSL *Curiosity* are sedimentary rocks that composed of the sediments that originally filled Gale Crater and lithified (Anderson & Bell III, 2010; Grotzinger, et al., 2015b; Milliken, et al., 2010). Some float rocks, conglomerate clasts and bedrock have a composition and texture that suggests that they have an igneous origin even though they are sedimentary rocks. (McLennan, et al., 2014; Sautter, et al., 2014; Schmidt, et al., 2014; Hurowitz, et al., 2017; Mangold, et al., 2017; Grotzinger J. P., et al., 2015; Siebach, et al., 2017). The volcaniclastic sediments that compose these rocks are thought to be detrital grains which were transported to their current location after weathering out of their source rocks (Siebach, et al., 2017). One source of the volcaniclastic sediments is thought to be through the erosion of the wall and rim of Gale Crater or possibly Mount Sharp (Grotzinger, et al., 2015b; Morris, et

al., 2016). However, the alluvial fan near Curiosity's landing site shows that sediments were transported into the crater from outside the walls through Peace Vallis, so it is possible that an external volcanic source was also contributing to the sediments found in Gale Crater (Palucis, et al., 2014). A potential source near Gale Crater, North Gale Landform, has been described in Chapter 2. Since the catchment area of Peace Vallis contains part of the deposit from a debris avalanche from North Gale Landform (hummocky terrain), it may represent a source of the volcaniclastic sediments.

As Mars is largely an igneous planet, it is reasonable to suggest the least altered endmember igneous compositions reflect the composition of the source rocks. Therefore, it is possible to use petrological modelling to determine the number of crystalline sources required to generate the compositions found in Gale Crater. The determination that two (or more) distinct igneous compositions are required would corroborate geomorphologic evidence that volcanic material from the North Gale Landform reached Gale crater.

3.1.1 Igneous Lithologies

The volcaniclastic sediments examined by MSL *Curiosity* are all part of the Bradbury Group that makes up the surface of Aeolis Palus (Gale Crater floor) and are not present in the Mount Sharp group (sedimentary mound in Gale Crater). Curiosity has examined two distinct classes of these targets with igneous lithologies: Jake_M class and Bathurst_Inlet class (Schmidt M. E., et al., 2017). Curiosity has also examined two targets that are similar to Jake_M and Bathurst_Inlet but have elemental variations which indicate they are distinct from those classes: Nova and Pogy (Schmidt M. E., et al., 2017).

Jake_M targets (n=13) (Figure 3-2) are largely igneous float blocks and cobbles which may have been sourced from a conglomerate bedrock (Schmidt M. , et al., 2017). They are very fine-medium grained, have dusty, pitted surfaces (possibly vesicular), light and dark toned (mostly dark toned with some light toned clasts) (Cousin, et al., 2017; Mangold, et al., 2017). They have compositions with elevated Na, K, P and Al as well as depleted Ni and Cr. Mineralogy may include plagioclase, Ca-rich pyroxene, olivine and Fe-Ti oxides (Stolper, et al., 2013). The targets have a fractionated, alkaline chemical composition and are classified as phonotephrites, tephriphonolites, mugearites and trachyandesites (Schmidt M. E., et al., 2017; Stolper, et al., 2013). Jake_M targets have two additional subclasses due to elemental variation and rock textures: Matthew and Clinton (Schmidt M. E., et al., 2017).

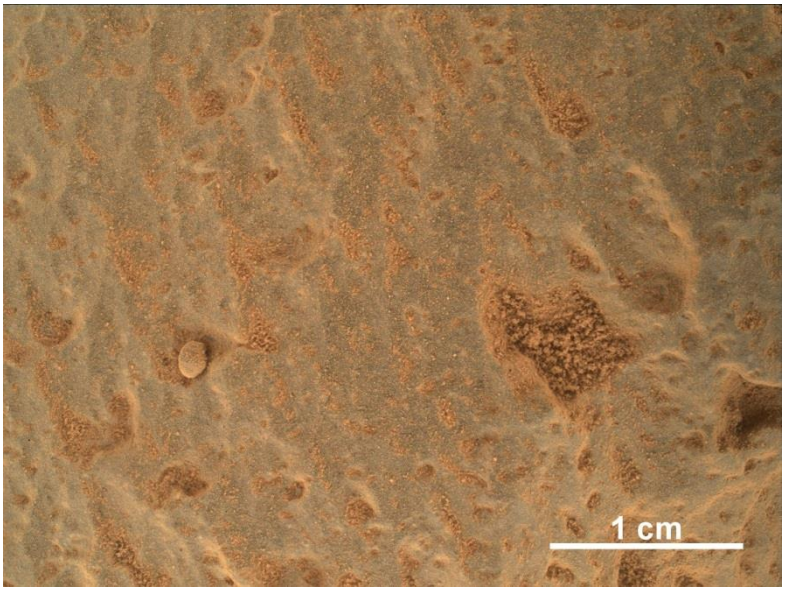

Figure 3-2: MAHLI Image an example of Jake_M class target: Matthew. It is a float rock with an igneous composition, it has a dusty, dark toned surface with pitted texture and fine grain size. It was the first target of the Jake_M subclass Matthew examined. MAHLI Image: 0360MH0003060020104191C00_DRCX

Bathurst_Inlet (n=19) (Figure 3-3) is composed of least altered potassic basaltic sediments in siltstone sandstone to matrix-supported conglomerates (Schmidt M. E., et al., 2017). They are fine to coarse grained, have dusty surfaces, smooth to mottled surfaces, dark to light toned and some are laminated (Cousin, et al., 2017; Mangold, et al., 2017). Their composition is thought to reflect the igneous protolith and has sanidine, plagioclase, pyroxene and magnetite phases (Schmidt M. E., et al., 2017; Treiman, et al., 2015). Bathurst_Inlet targets have a lower alkaline, more mafic composition than Jake_M targets and can be highly potassic. They are classified as tephrite basanite, basalt and trachybasalt. Bathurst_Inlet targets may be identified as Windjana subclass due to differences in SiO_2 in targets near the Windjana drill hole (Thompson, et al., 2016; Treiman, et al., 2015)

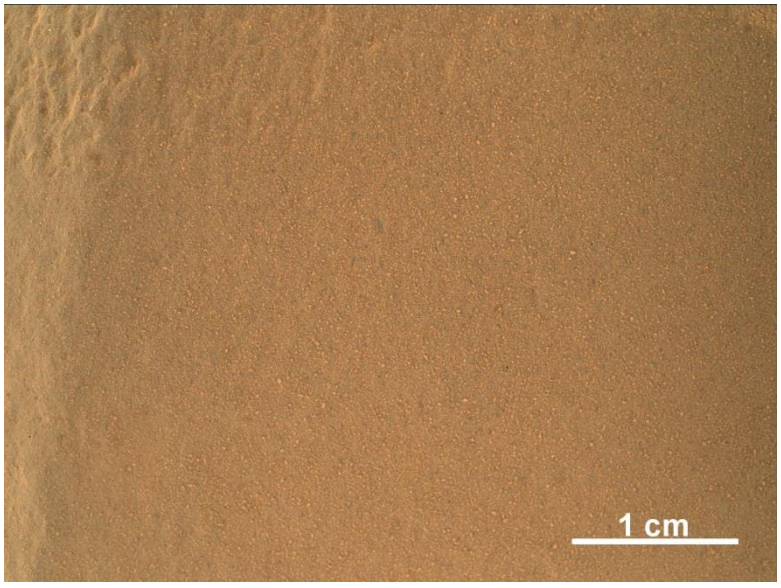

Figure 3-3: MAHLI Image of an example of Bathurst_Inlet class target: Bathurst_Inlet. Bathurst_Inlet is a sandstone bedrock target with very fine grain size. There were 2 APXS measurements taken at Bathurst_Inlet. MAHLI image: 0054MH0000180010100267E01_DRCX

Nova (n=1) and Pogy (n=1) are slight outliers when compared to the other classes. Nova is similar to Jake_M class (lithology and composition), it is a fine-grained, dark toned, angular, float rock with a basaltic composition and elevated P and Ca (Schmidt M. E., et al., 2017). Pogy is similar in composition to Bathurst_Inlet, it is a dark and light toned picrobasalt cap rock with a lightly pitted surface and elevated Ca (and other small elemental variations from Bathurst_Inlet in Al and K).

The distinct classes (Jake_M, Bathurst_Inlet, Nova, Pogy) could indicate that there may be more than one distinct crystalline sources for the volcaniclastic sediments that have been found in Gale Crater.

3.2 Methods

The elemental composition data for targets on Mars used in this study is provided by the APXS instrument on board the MSL Curiosity rover (Table 3-1, Table 3-2, Table 3-3, Table 3-4). The APXS is an X-ray spectrometer which is used to characterize the geochemical content of a variety of targets on the surface of Mars (Grotzinger J. P., et al., 2012; Schmidt, et al., 2014). The instrument uses a combination of PIXE (Particle-Induced X-Ray Emission) and XRF (X-Ray Fluorescence) to determine the elemental composition using a radioactive ^{244}Cm source. The APXS can detect major (Si, Fe, Al, etc.), minor (Na, K, Mg, etc.) and trace (Cr, Ni, Zn, etc.) elements near the surface (>20 µm penetration for large elements) of a target with high precision and has low detection limits. It is typically deployed as close to a surface as possible for a reading, in contact with hard targets and within 5 mm of the surface through proximity mode. Quick look

deployments last for 10 minutes and can identify elements at over 0.5% composition of the target while longer duration deployments (up to 8 hours) can detect trace elements as low as 20 ppm for Br (Campbell J. , 2012; Grotzinger J. P., et al., 2012; Schmidt, et al., 2014).

3.3 Results

APXS elemental compositions for the targets with igneous compositions are presented in Table 3-1, Table 3-2, Table 3-3 and Table 3-4. The results are normalized to be volatile-free by subtracting SO_3 and Cl concentrations. Igneous compositions targets have been classified in to two categories based on attributes such as geologic context and elemental composition: Jake_M class and Bathurst_Inlet class (Schmidt M. , et al., 2017).

CIPW norm calculations for selected targets in each class and subclass are presented in Table 3-5 (Johannsen, 1931). The norm calculation was modified to group albite and anorthite into plagioclase as well as enstatite, ferrosilite and wollastonite grouped into diopside. Fe_2O_3 is assumed to be 15% of FeO total as that is a standard assumption for terrestrial midocean ridge basalts. The differentiation index is a measure of how evolved or differentiated a composition is. It is the ratio of normative quartz, albite, orthoclase, nepheline, leucite, kalsilite, sodium carbonate and sodium sulfate to the total weight of the norm. It indicates the amount of differentiation undergone by the magma including fractional crystallization and the composition change towards

alkali-alumina silicate minerals which all magma systems progress towards (Thornton & Tuttle, 1960).

Elemental variation diagrams (Figure 3-4) demonstrate differences between the identified classes of igneous materials in Gale Crater. Terrestrial models typically use MgO as the x-axis for these types of diagrams, but for Mars SiO_2 was chosen to minimize the effects of Mg-rich Martian surface dust (Schmidt, et al., 2018).

Bathurst_Inlet class targets have elevated FeO, MgO, MnO, Cr_2O_3, Ni, and Zn compared to Jake_M. Jake_M class targets have elevated SiO_2, Al_2O_3, and Na_2O compared to Bathurst_Inlet (Figure 3-4). Nova has elevated CaO and P_2O_5 but is otherwise similar to Jake_M compositions. Pogy has elevated CaO, and depleted Zn relative to Bathurst_Inlet but all values are very close.

Table 3-1

APXS Analyses for Jake_M Class Targets of Gale Crater.

Target Name	Jake_ Matijevic	JM2_APXS_ RP2_OVERNIGHT	Matthew	Rucker RP	Nedrow RP	Morehouse RP	Oneida	Lowerre RP	Larrabee RP	Clinton RP	Kodak RP	Reedy twk	Monkey Yard
Class	Jake_M	Jake_M	Jake_M	Jake_M	Jake_M	Jake_M	Jake_M	Jake_M	Jake_M	Jake_M	Jake_M	Jake_M	Jake_M
Sub class			Matthew	Matthew	Matthew		Matthew	Matthew	Matthew	Clinton	Matthew	Clinton	Clinton
Sol	46	47	360	387	503	503	506	510	510	512	512	526	564
Duration	0:32:39	00:30:00	4:00:00	8:02:23	0:11:00	4:00:00	0:22:00	0:20:00	5:00:00	0:20:00	7:43:09	0:20:00	0:22:00
Temp	-3	-55	-53.4	-58.2	-27.7	-65.3	-36.6	-34.1	-73.1	-25.5	-50.4	-32.4	-27.1
FWHM	204.1	148.6	156.4	152.2	149.8	146.2	143.9	144.1	143.1	150.4	145.2	146.6	148.8
wt%													
SiO_2	52.56 (1.07)	50.80 (0.54)	51.80 (0.54)	56.11 (0.54)	53.20(0.75)	51.73 (0.54)	53.57 (0.64)	52.88 (0.64)	51.51 (0.54)	56.985(0.75)	54.27 (0.54)	54.33 (0.75)	55.17 (0.75)
TiO_2	0.51 (0.03)	0.76 (0.03)	0.80 (0.03)	1.42 (0.05)	0.62 (0.05)	0.74 (0.03)	0.59 (0.05)	0.56 (0.05)	1.24 (0.05)	0.37 (0.03)	0.74 (0.03)	0.89 (0.05)	0.38 (0.03)
Al_2O_3	16.68(0.87)	15.23 (0.38)	14.42 (0.29)	12.27 (0.29)	12.79(0.29)	15.92 (0.38)	15.77 (0.38)	16.75 (0.38)	15.85 (0.38)	17.72 (0.38)	15.96 (0.38)	16.80 (0.38)	17.58 (0.38)
FeO*	9.82 (0.20)	11.37 (0.13)	12.54 (0.13)	10.74(0.13)	11.46(0.13)	10.64 (0.13)	11.50 (0.13)	11.85 (0.13)	12.73 (0.13)	6.04 (0.13)	10.94 (0.13)	8.82 (0.13)	8.14 (0.13)
MnO	0.15 (0.02)	0.24 (0.02)	0.28 (0.02)	0.23 (0.02)	0.28 (0.04)	0.27 (0.02)	0.16 (0.02)	0.20 (0.02)	0.30 (0.02)	0.13 (0.02)	0.19 (0.02)	0.19 (0.04)	0.20 (0.04)
MgO	3.74 (0.33)	4.78 (0.17)	4.88 (0.17)	4.66 (0.17)	5.67 (0.25)	3.53 (0.08)	4.46 (0.17)	3.18 (0.17)	3.85 (0.08)	3.60 (0.17)	3.82 (0.08)	4.09 (0.17)	3.03 (0.17)
CaO	6.29 (0.31)	7.04 (0.08)	7.58 (0.08)	7.60 (0.08)	6.91 (0.13)	5.97 (0.07)	6.49 (0.08)	5.89 (0.08)	6.42 (0.07)	7.55 (0.11)	5.70 (0.06)	8.59 (0.11)	5.75 (0.10)
Na_2O	7.37 (0.41)	6.84 (0.20)	5.07 (0.20)	4.35 (0.14)	4.24 (0.20)	7.02 (0.27)	5.33 (0.20)	5.59 (0.20)	5.23 (0.20)	5.47 (0.20)	5.03 (0.20)	4.51 (0.20)	6.46 (0.20)
K_2O	2.31 (0.12)	1.96 (0.06)	1.75 (0.06)	0.98 (0.04)	3.67 (0.11)	3.05 (0.10)	1.27 (0.05)	2.31 (0.07)	1.97 (0.06)	1.44 (0.05)	2.59 (0.08)	0.70 (0.04)	2.24 (0.07)
P_2O_5	0.51 (0.07)	0.88 (0.05)	0.77 (0.05)	1.54 (0.09)	0.95 (0.07)	0.96 (0.07)	0.72 (0.05)	0.64 (0.05)	0.81 (0.05)	0.64 (0.05)	0.67 (0.05)	0.98 (0.07)	0.86 (0.07)
Cr_2O_3	0.04 (0.01)	0.05 (0.01)	0.07 (0.01)	0.09 (0.01)	0.10 (0.03)	0.05 (0.01)	0.07 (0.01)	0.07 (0.03)	0.04 (0.01)	0.06 (0.03)	0.04 (0.01)	0.07 (0.03)	0.05 (0.03)
ppm													
Ni	31 (20)	63 (20)	72 (10)	38 (5)	138 (35)	21 (10)	107 (25)	100 (25)	137 (10)	45 (10)	50 (5)	29 (25)	45 (25)
Zn	230 (15)	332 (15)	314 (10)	89 (5)	842 (40)	957 (30)	353 (20)	637 (25)	265 (10)	227 (20)	494 (15)	130 (15)	1463 (45)
Br	95 (10)	95 (5)	16 (5)	37 (5)	45 (10)	85 (5)	19 (10)	34 (10)	53 (5)	5 (10)	11 (5)	54 (10)	92 (20)

Duration is presented as H:MM:SS.

Temperature is in °C.

Compositions altered to be volatile free by subtraction of SO_3 and Cl and renormalized.

Total Fe is reported as FeO*.

Statistical errors are given in parenthesis.

Table 3-2

APXS Analyses for Bathurst_Inlet Class Targets of Gale Crater Up to Sol 537.

Target Name	Bathurst_Inlet RP For Real	Bathurst_Inlet Top RP	Pine Plains	Rensselaer	Oswego	Cumberland_dump substrate touch	Cumberland_dump _substrate_predicted peak	Fitzroy RP	Halls RP
Class	Bathurst Inlet	Bathurst Inlet	Bathurst Inlet	Bathurst Inlet	Bathurst Inlet	Bathurst Inlet	Bathurst Inlet	Bathurst Inlet	Bathurst Inlet
Sub class								Windjana	Windjana
Sol	54	54	441	442	472	485	485	537	537
Duration	0:22:14	0:22:15	0:20:00	2:30:00	0:20:00	0:10:00	0:20:00	0:17:00	4:00:00
Temp	-4	-2	-25.3	-59.5	-35.6	-30.5	-29.1	-19.1	-70.2
FWHM	196.7	212.7	149.1	149.9	144.0	145.2	147.7	160.8	143.7
wt%									
SiO_2	45.49 (0.64)	45.92 (0.96)	45.48 (0.43)	46.41 (0.54)	45.03 (0.64)	45.62 (0.75)	45.26 (0.54)	43.53 (0.54)	43.62 (0.43)
TiO_2	1.13 (0.09)	1.11 (0.07)	1.16 (0.05)	0.93 (0.03)	0.94 (0.05)	1.10 (0.07)	1.10 (0.07)	1.10 (0.07)	1.05 (0.03)
Al_2O_3	8.18 (0.38)	8.28 (0.48)	9.24 (0.19)	8.99 (0.19)	8.36 (0.19)	9.37 (0.029)	9.29 (0.19)	8.15 (0.19)	8.24 (0.19)
FeO	23.00 (0.26)	21.94 (0.46)	22.16 (0.26)	21.35 (0.26)	23.40 (0.26)	21.94 (0.26)	22.44 (0.26)	25.72 (0.26)	25.49 (0.26)
MnO	0.87 (0.06)	0.48 (0.06)	0.38 (0.04)	0.44 (0.02)	0.52 (0.04)	0.43 (0.06)	0.47 (0.04)	0.60 (0.06)	0.58 (0.02)
MgO	8.92 (0.33)	9.07 (0.50)	9.11 (0.25)	9.02 (0.25)	9.12 (0.25)	9.05 (0.25)	8.84 (0.17)	9.44 (0.25)	9.79 (0.25)
CaO	6.55 (0.08)	6.74 (0.34)	7.00 (0.08)	6.16 (0.07)	6.42 (0.08)	6.73 (0.11)	6.85 (0.08)	6.28 (0.08)	6.17 (0.06)
Na_2O	2.30 (0.27)	2.15 (0.14)	2.70 (0.14)	2.65 (0.14)	2.82 (0.14)	2.82 (0.20)	2.85 (0.14)	2.69 (0.14)	2.62 (0.14)
K_2O	2.27 (0.07)	3.01 (0.15)	1.13 (0.04)	2.71 (0.08)	2.05 (0.06)	1.49 (0.05)	1.34 (0.05)	1.11 (0.04)	0.98 (0.04)
P_2O_5	0.86 (0.07)	0.92 (0.09)	1.07 (0.07)	0.83 (0.05)	0.78 (0.05)	1.02 (0.07)	1.02 (0.07)	0.96 (0.07)	1.01 (0.05)
Cr_2O_3	0.43 (0.03)	0.37 (0.03)	0.56 (0.03)	0.52 (0.01)	0.57 (0.03)	0.44 (0.05)	0.56 (0.03)	0.42 (0.03)	0.44 (0.01)
ppm									
Ni	416 (40)	342 (30)	462 (35)	304 (15)	377 (35)	405 (50)	418 (35)	423 (45)	441 (20)
Zn	1416 (45)	1277 (65)	1198 (35)	1302 (40)	1271 (40)	1273 (50)	1194 (35)	1484 (45)	1192 (35)
Br	14 (10)	42 (10)	199 (10)	119 (5)	184 (15)	41 (15)	38 (10)	1116 (35)	819 (25)

Duration is presented as H:MM:SS.

Temperature is in °C.

Compositions altered to be volatile free by subtraction of SO_3 and Cl and renormalized.

Total Fe is reported as FeO*.

Statistical errors are given in parenthesis.

Table 3-3

APXS Analyses for Bathurst_Inlet Class Targets of Gale Crater After Sol 537.

Target Name	Square_Top_3 _raster1	Square_Top_3 _raster2	Square_Top_3 _raster3	Square_Top_3 _raster4	Square_Top_3 _overnight	Pandanus _Yard	Virgin_Hills	Wift_daytime	Wift_ overnight	Homewood _rp
Class	Bathurst_Inlet	Bathurst_Inlet	Bathurst_Inlet	Bathurst_Inlet	Bathurst_Inlet	Bathurst_Inlet	Bathurst_Inlet	Bathurst_Inlet	Bathurst_Inlet	Bathurst_Inlet
Sub class	Windjana	Windjana	Windjana	Windjana	Windjana		Windjana			
Sol	583	583	583	583	583	584	585	633	633	742
Duration	0:15:00	0:15:00	0:12:00	0:15:00	4:00:00	7:00:00	7:30:00	0:21:00	8:02:24	7:00:00
Temp °C	-34.4	-32.7	-31.5	-30.5	-60.4	-62.5	-66	-19	-62.1	-33.4
FWHM	146.6	148.8	147.9	148.4	152.7	150.6	148.0	164.5	153.3	148.6
wt%										
SiO_2	43.91 (0.64)	43.28 (0.64)	43.26 (0.64)	43.48 (0.64)	43.38 (0.43)	45.09 (0.43)	43.61 (0.43)	45.76 (0.54)	45.52 (0.54)	45.23 (0.43)
TiO_2	0.89 (0.05)	0.98 (0.05)	0.99 (0.05)	0.94 (0.05)	0.89 (0.03)	1.00 (0.03)	0.99 (0.03)	0.97 (0.03)	0.96 (0.03)	1.05 (0.03)
Al_2O_3	8.48 (0.19)	7.86 (0.19)	8.15 (0.19)	8.30 (0.19)	8.23 (0.19)	9.03 (0.19)	8.64 (0.19)	9.17 (0.19)	9.23 (0.19)	9.20 (0.19)
FeO	23.71 (0.26)	24.38 (0.26)	24.46 (0.26)	24.30 (0.26)	24.33 (0.26)	22.59 (0.26)	24.53 (0.26)	21.76 (0.26)	21.67 (0.26)	22.65 (0.26)
MnO	0.46 (0.06)	0.54 (0.06)	0.47 (0.06)	0.44 (0.06)	0.46 (0.02)	0.41 (0.02)	0.46 (0.02)	0.27 (0.04)	0.23 (0.02)	0.45 (0.02)
MgO	9.78 (0.25)	10.25 (0.25)	9.73 (0.25)	9.85 (0.25)	9.81 (0.25)	9.16 (0.17)	9.15 (0.25)	10.02 (0.25)	10.02 (0.25)	9.21 (0.25)
CaO	6.56 (0.11)	6.68 (0.10)	6.81 (0.11)	6.77 (0.11)	6.74 (0.07)	6.49 (0.07)	6.97 (0.07)	6.12 (0.08)	6.20 (0.07)	6.93 (0.07)
Na_2O	1.92 (0.20)	1.91 (0.14)	1.85 (0.20)	1.98 (0.14)	1.87 (0.07)	2.65 (0.14)	2.64 (0.14)	2.20 (0.14)	2.27 (0.07)	3.14 (0.13)
K_2O	2.90 (0.08)	2.69 (0.08)	2.74 (0.08)	2.56 (0.07)	2.85 (0.08)	2.15 (0.06)	1.34 (0.05)	2.56 (0.08)	2.58 (0.08)	0.81 (0.02)
P_2O_5	0.60 (0.05)	0.70 (0.05)	0.67 (0.05)	0.71 (0.05)	0.66 (0.05)	1.00 (0.05)	0.98 (0.05)	0.68 (0.05)	0.77 (0.05)	0.93 (0.05)
Cr_2O_3	0.77 (0.05)	0.72 (0.05)	0.86 (0.05)	0.67 (0.05)	0.76 (0.01)	0.42 (0.01)	0.68 (0.01)	0.50 (0.03)	0.54 (0.01)	0.41 (0.01)
ppm										
Ni	181 (40)	259 (40)	251 (40)	337 (45)	247 (15)	470 (25)	371 (20)	168 (30)	210 (10)	517 (25)
Zn	1906 (60)	1926 (55)	1833 (55)	1934 (60)	2004 (60)	1628 (45)	1469 (45)	802 (30)	833 (25)	805 (25)
Br	206 (15)	199 (15)	199 (15)	164 (15)	118 (5)	896 (25)	677 (20)	99 (10)	102 (5)	281 (10)

Duration is presented as H:MM:SS.

Temperature is in °C.

Compositions altered to be volatile free by subtraction of SO_3 and Cl and renormalized.

Total Fe is reported as FeO*.

Statistical errors are given in parenthesis.

Table 3-4

APXS Analyses for Nova and Pogy Targets of Gale Crater

Target Name	Nova_RP	Pogy
Class	Nova	Pogy
Sol	687	1606
Duration	1:30:00	7:00:00
Temp °C	-51.7	-44.3
FWHM	173.7	146.0
wt%		
SiO_2	50.70 (0.54)	44.71(0.43)
TiO_2	0.46 (0.03)	0.80(0.03)
Al_2O_3	14.43 (0.29)	10.60(0.29)
FeO	9.86 (0.13)	20.85(0.26)
MnO	0.22 (0.02)	0.47(0.01)
MgO	5.46 (0.17)	8.27(0.17)
CaO	10.63 (0.11)	10.46(0.11)
Na_2O	4.00 (0.14)	2.44(0.14)
K_2O	0.66 (0.02)	0.17(0.01)
P_2O_5	3.45 (0.16)	0.78(0.05)
Cr_2O_3	0.09 (0.01)	0.41(0.01)
ppm		
Ni	75 (15)	138 (10)
Zn	419 (15)	103 (5)
Br	56 (5)	53 (10)

Duration is presented as H:MM:SS.

Temperature is in °C.

Compositions altered to be volatile free by subtraction of SO_3 and Cl and renormalized.

Total Fe is reported as FeO*.

Statistical errors are given in parenthesis.

Table 3-5

CIPW Normative Mineralogy and Differentiation Index of APXS Igneous Targets in Gale Crater

	Class	Subclass	Quartz wt%	Plagioclase wt%	Orthoclase wt%	Nepheline wt%	Diopside wt%	Hypersthene wt%	Olivine wt%	Ilmenite wt%	Magnetite wt%	Apatite wt%	Chromite wt%	Total	Differentiation Index[a]
Jake_M	Jake_M		0	36.14	13.59	17.17	18.57	0	9.89	0.97	2.36	1.18	0.09	99.96	66.87
Monkey_Yard	Jake_M	Clinton	1.25	61.6	4.14	0	10.5	16.3	0	1.69	2.13	2.27	0.15	100.03	75.36
Matthew	Jake_M	Matthew	0	46.17	10.34	4.35	17.65	0	15.03	1.5	3.03	1.78	0.15	100	60.82
Bathurst_Inlet _RP_For_Real	Bathurst_Inlet		0	24.66	13.36	0	18.02	0.85	32.78	2.15	5.54	1.97	0.93	100.26	38.02
Halls_RP	Bathurst_Inlet	Windjana	0	56.89	13.24	5.42	8.89	0	10.68	0.7	1.97	1.97	0.1	99.86	35.64
Nova_RP	Nova		0	53.26	3.9	0	8.84	22.08	0.5	0.85	2.38	7.99	0.19	99.99	57.16
Pogy	Pogy		0	38.01	1	0	24.51	0.22	27.23	1.52	5.02	1.81	0.87	100.19	39.01

CIPW norm calculations were determined using volatile free APXS compositions

Fe^{3+} is calculated as 0.15 of FeO

[a] Differentiation Index is measure of how evolved or differentiated a composition is. Ratio of normative quartz, albite, orthoclase, nepheline, leucite, kalsilite, sodium carbonate and sodium sulfate to the total weight.

Bathurst_Inlet class compositions have higher concentrations of compatible elements (Fe, Mg, Cr, Ni), mafic minerals (olivine, pyroxenes) and lower differentiation index (~35-48) reflecting its mafic composition (Table 3-5). Jake_M compositions have lower concentrations in those same compatible elements, higher differentiation index (~60-75) demonstrating a more evolved composition. Pogy concentrations of compatible elements are on the low end of Bathurst_Inlet ranges, has high concentration of mafic minerals and a low differentiation index (~39) which suggests that it is also has a more mafic composition. Nova concentrations of compatible elements are all within range of Jake_M and it has a high differentiation index (~57) indicating it also has an evolved composition.

Mafic compositions have higher Mg and Fe as well as Mg and Fe bearing minerals such as olivine, pyroxene, amphibole, and biotite (amphibole and biotite do not appear in Table 3-5 as CIPW norm models do not include hydrous minerals). Mafic compositions represent a more primitive melt than an evolved composition in which the parental magma may have undergone fractional crystallization, assimilation, replenishment or magma mixing. How evolved a magma is can be classified through the differentiation index which measures the enrichment in alkali-alumina silicates through fractional crystallization (Thornton & Tuttle, 1960) (Table 3-5).

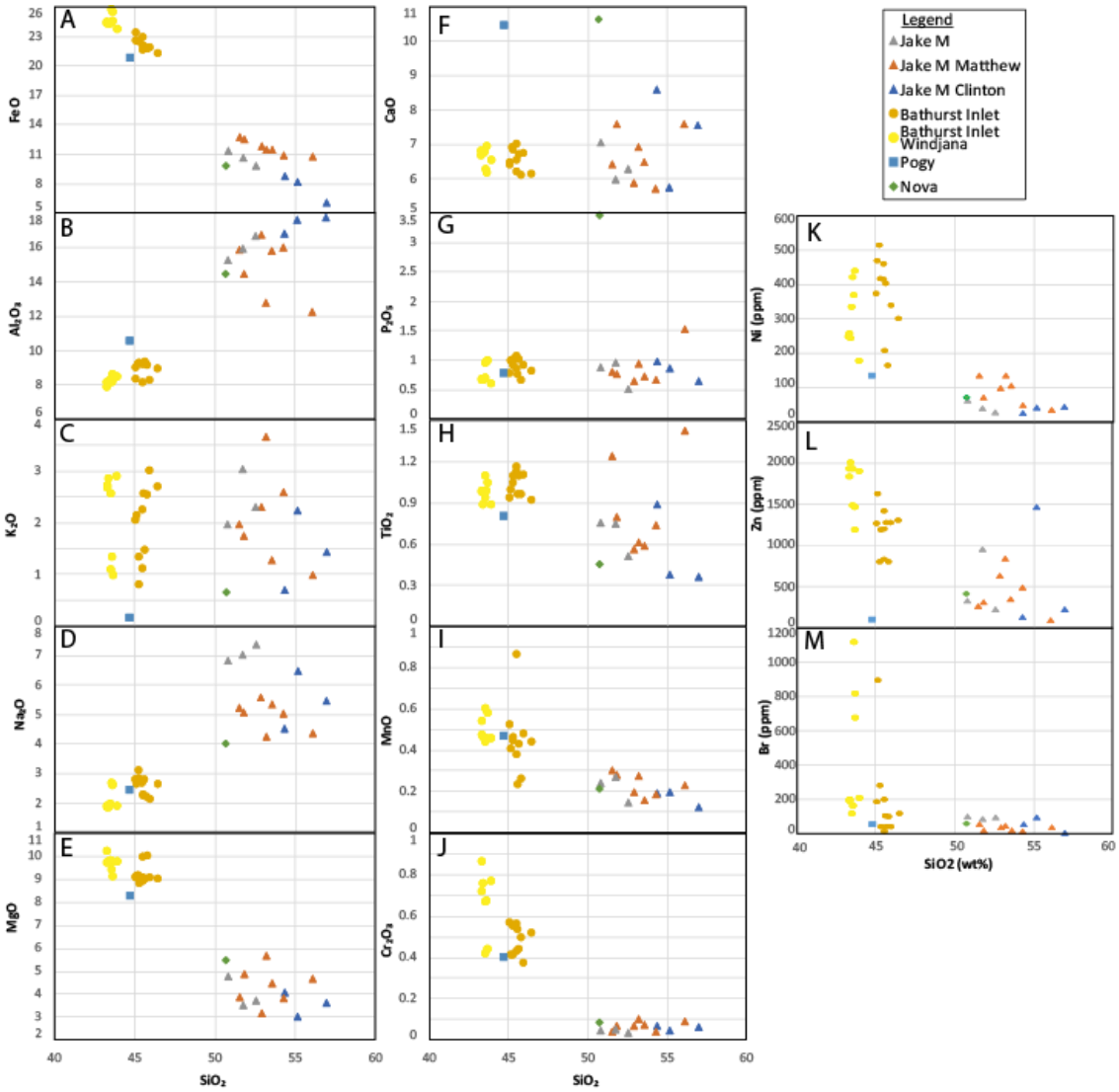

Figure 3-4: SiO_2 elemental variation diagrams for igneous composition targets identified by the APXS instrument of the Curiosity rover at Gale Crater, Mars. Major and minor elements detectable by the APXS instrument are plotted. They have been altered to be volatile free (removed SO_3 and Cl). Targets are divided into Bathurst_Inlet, Jake_M, Jake_M Matthew, Jake_M Clinton, Nova and Pogy classes. A) FeO vs SiO_2; B) Al_2O_3 vs SiO_2; C) K_2O vs SiO_2; D) Na_2O vs SiO_2; E) MgO vs SiO_2; F) CaO vs SiO_2; G) P_2O_5 vs SiO_2; H) TiO_2 vs SiO_2; I) MnO vs SiO_2; J) Cr_2O_3 vs SiO_2; K) Ni vs SiO_2; L) Zn vs SiO_2; M) Br vs SiO_2.

The total Alkali-Silica (TAS) diagram (Le Bas, et al., 1986) is used to classify the igneous rock classes discovered in Gale Crater (Figure 3-5). If the sample has Na_2O wt% – 2 > K_2O wt% the sample is considered sodic, if a sample has K_2O wt% > Na_2O wt% than it is considered potassic.

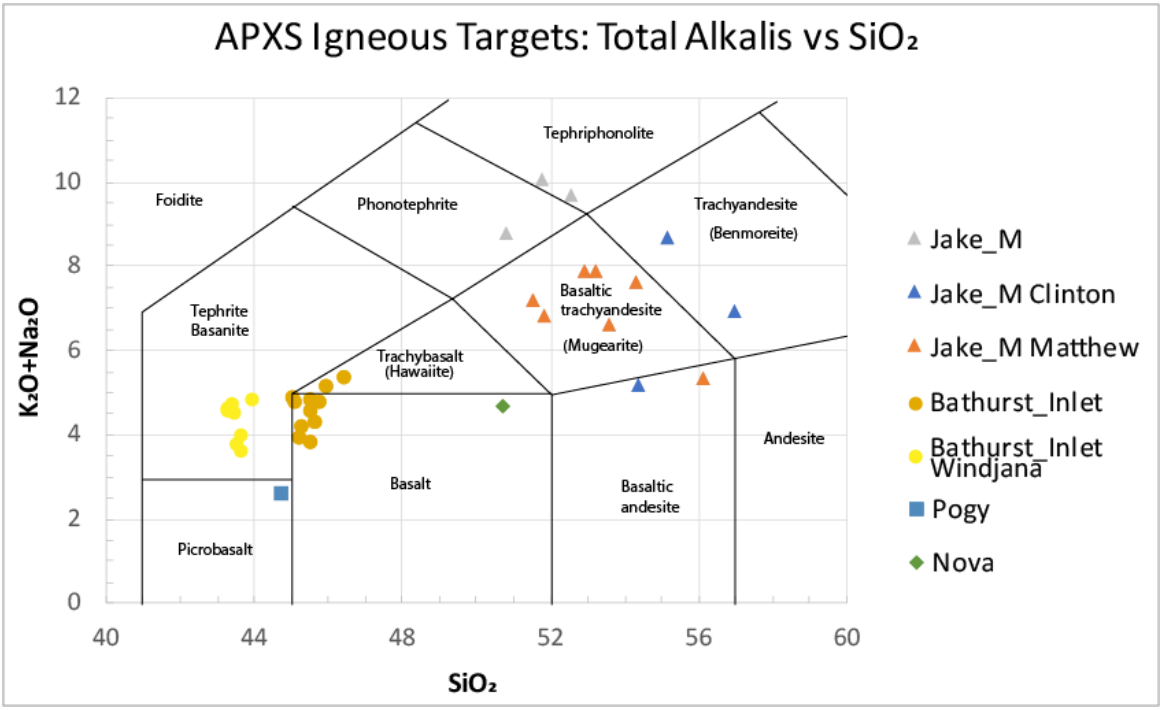

Figure 3-5: Total Alkali vs SiO_2 diagram of APXS igneous targets with an igneous classification scheme (Le Bas, et al., 1986). Sodic rock compositions for rock classes are shown in brackets, targets with $(Na_2O - 2) > K_2O$ will use these designations instead of the default name. Targets with $K_2O > Na_2O$ can be referred to as potassic and targets with $(Na_2O - 4) > K_2O$ can be referred to as sodic. The compositions of targets in Gale Crater, Mars were determined by the APXS instrument on MSL Curiosity and altered to be free of volatiles (SO_3 and Cl). Targets are divided into Bathurst_Inlet, Jake_M, Jake_M Matthew, Jake_M Clinton, Nova and Pogy classes. Bathurst_Inlet targets are in the tephrite basanite, (potassic) trachybasalt and basalt classes; Jake_M targets are in the phonotephrite and tephriphonolite classes; Jake_M Matthew targets are in the basaltic andesite and mugearite classes; Jake_M Clinton are in the basaltic andesite and benmoreite classes; Nova is a basalt class; Pogy is a picrobasalt class.

The TAS diagram classifies Jake_M targets as phonotephrite and tephriphonolite. Clinton targets are classified as benmoreite and basaltic andesite. Matthew targets are mostly classified as mugearite and one is a basaltic andesite. Bathurst_Inlet targets are classified as basalt and (potassic) trachybasalt. Windjana targets are classified as tephrite basanite. Nova is classified as basalt and Pogy is classified as picrobasalt.

3.4 Discussion

This section explores the igneous composition lithologies found in Gale Crater and attempts to constrain the minimum number of crystalline sediment sources that are

required to generate them. Since the igneous composition targets analyzed by the APXS instrument are found in the same general area along Curiosity's early traverse ("Bradbury Rise") of Gale Crater at the foot of Aeolis Mons (Figure 3-1), it is not unreasonable to hypothesize that they all came from the same source. Grotzinger and others (2015) suggested their source is the (now eroded) upper 2 km wall of the Gale crater rim. Erosion of the crater wall would readily contribute sediments to the interior and the composition of some igneous targets likely reflects the composition of the Pre-Noachian to Noachian-age crystalline basement prior to the Gale impact. However, Jake_M and Bathurst_Inlet classes differ in several regards (geologic context, grain size, texture and composition) that complicate the hypothesis of a single sediment source.

The compositions of Jake_M and Bathurst_Inlet are distinct in several key ways and represent the least altered igneous compositions in Gale Crater (Figure 3-4). Overall, Jake_M has elevated SiO_2, Al_2O_3 and Na_2O while Bathurst_Inlet has elevated FeO, MgO, TiO_2, MnO and Cr_2O_3. The two other igneous compositions, Pogy and Nova, seem to be similar to one of the classes in many aspects but with significant differences. Pogy is basaltic like Bathurst_Inlet, but has elevated Al_2O_3 and CaO and lower FeO, K_2O, MgO and TiO_2 contents. Nova is more similar to lower SiO_2 Jake_M rocks but is highly elevated in CaO and P_2O_5 (CaO 10.63 wt%, P_2O_5 3.45 wt%) (Figure 3-4F,G).

The TAS diagram (Figure 3-5) demonstrates that Jake_M and Bathurst_Inlet targets can be classified as igneous compositions. The high Na content of Jake_M targets also classifies them as the sodic, while some Bathurst_Inlet targets are potassic.

However, as outlined below, different rock types can be generated by the same volcano over time and even during the same eruptive event.

There can be changes in magma composition generated from a single source, so the elemental compositions do not necessarily indicate that more than one crystalline source for the volcaniclastic sediments of Gale Crater are needed. The magma composition can change over time at terrestrial volcanoes and the same is true for Martian volcanoes (Baratoux, et al., 2011). The Hawaiian Islands generated tholeiitic magmas before producing alkaline magmas near the end of the shield building stage in each volcano through a combination of fractional crystallization and a decrease in the degree of partial melting over time (Moore & Clague, 1992). Heimaey volcano in Iceland generated rocks that ranged from mugearitic to hawaiitic through eruption of old and new magmas as well as magma mixing over week long timescales during a single eruptive event in 1973 (Jakobsson, et al., 1973). Hypothesises for these changes include small magma batches of mugearitic lavas were produced through fractional crystallization of a parental hawaiitic composition (Furman, et al., 1991) and varying degrees of plagioclase nucleation/growth, coarsening and clinopyroxene fractionation (Higgins & Roberge, 2007). Magma from Mt Erebus in Antarctica had stages producing tephrite basanite to phonotephrites to tephriphonolites magmas over its ~1.3 million-year eruptive history caused by crustal assimilation and fractional crystallization (Esser, et al., 2004). Nyiragongo volcano in Democratic Republic of the Congo has generated magmas with compositions of melilitites to melilite nephelinites to nephelinites and back to melilite nephelinites during various eruptive stages from differentiation in a

shallow reservoir and periodic mixing of reservoirs at different depths (Demant, et al., 1994). The Usal-Selendi-Emet (USE) area of Western Turkey produced potassic volcanism in the Miocene which evolved into sodic during the Quaternary through continued extension and decompression melting of the asthenosphere and magma mixing (Seyitoglu, et al., 1997). Volcanism in Southern Italy produced ultrapotassic and sodic alkaline magmatism (and others) from the same mantle source through mixing of basaltic ocean crust, subducted sediments and mantle wedge material (Ellam, et al., 1989).

The composition of a magma is affected by igneous processes, from its generation in the mantle until it is erupted or emplaced as a pluton. The compositions seen in Jake_M, Bathurst_Inlet, Pogy and Nova class targets may reflect their mantle sources or have been altered by some process. The lower differentiation index (~35-39, Table 3-5) of Bathurst_Inlet and Pogy targets indicate it is more primitive and more likely to be a primary partial melt of the mantle. The evolved compositions of Jake_M and Nova targets were likely generated by magma differentiation processes such as fractional crystallization, assimilation, replenishment or mixing. A Bathurst_Inlet-like composition may or may not be parental to Jake_M compositions. In subsequent sections, petrological modelling of Martian mantle melting, and later magma differentiation processes will be used to test whether any of the APXS igneous targets can be linked through those simple igneous processes. If it is possible then both Jake_M and Bathurst_Inlet could come from the same source, however if there is no link between them then another source of volcaniclastic sediments is required.

Siebach et al. (2017) have proposed that the compositional differences of Jake_M and Bathurst_Inlet can be reconciled through grain size sorting during fluvial transport. Jake_M targets are high in Al_2O_3, SiO_2 and Na_2O and are generally coarser grained than the fine grained Bathurst_Inlet targets which have more mafic components. It is expected that the hydrodynamic sorting used in this model would have separated the deposition locations for the coarser Jake_M and finer Bathurst_Inlet sediments. As the mean velocity of the flowing water drops, the larger sized sediments (Jake_M) would have dropped out of suspension and stopped transportation earlier than the smaller sediments (Bathurst_Inlet) (Ritter, et al., 2011). However, as Jake_M and Bathurst_Inlet compositions are not found in exclusive locations and are often very near to each other this indicates that there is a problem with the sedimentary sorting model; this is not a problem with mixing models. Figure 3-1 inset shows how Jake_M and Bathurst_Inlet targets alternate along the traverse of the rover and are found in similar locations.

3.4.1 Models

Petrological models provide constraints on the origin of the igneous compositions as well as their possible evolution. In particular, we test whether Jake_M and Bathurst_Inlet classes can be linked by igneous processes. Models were constructed to evaluate both major and trace elements and include simple models of partial melting, fractional crystallization, and mineral accumulation.

1) Partial melting models were constructed to investigate if the trace element compositions (K, P, Ti, Cr and Ni) of Bathurst_Inlet class can be generated

through partial melting of the WD Martian mantle (Wänke & Dreibus, 1988). Compatible and incompatible trace elements behave in predictable ways in igneous systems which allows for the prediction of compositions of melts generated from the Martian mantle (Schmidt & McCoy, 2010). Two models of partial melting (batch melting and two-stage batch melting) were applied. The melt generated in batch melting models remains in equilibrium at its melting site (here, the Martian mantle) until it is removed as a single batch. Two-stage batch melting generates a first batch melt that is removed and is followed by another batch melt of the residuum.

2) Fractional Crystallization (FC) models tested how crystallization and removal of either olivine or plagioclase feldspar from a selected composition would change compositions of major elements (FeO, Al_2O_3, K_2O, Na_2O, SiO_2) in APXS targets. Fractional crystallization is a differentiation process in which a magma chamber will change its composition from processes such as minerals crystallizing out of the melt. It is one of the processes through which a volcanic source can change the composition of the lava generated during eruptions (Esser, et al., 2004; Jakobsson, et al., 1973; Moore & Clague, 1992). Olivine and plagioclase feldspar were chosen for the model as they are the first minerals to crystallize as a magma cools in each reaction series and reasonable Martian compositions are known from Martian meteorites (Bowen, 1922; Papike, 1998). The model simulated removing 1% of olivine and plagioclase feldspar (Shergottite EETA79001 (Papike, 1998)) from the

composition of a Jake_M (Monkey_yard), Bathurst_Inlet (Halls_RP) and Adirondack (from MER *Spirit* mission (McSween, et al., 2004)) target.

3) Mineral Accumulation (MA) models were constructed to investigate how the addition of olivine or plagioclase feldspar crystals will change the compositions of major elements (FeO, Al_2O_3, K_2O, Na_2O, SiO_2) in the APXS targets. Mineral accumulation is a differentiation process that occurs along with fractional crystallization, the minerals crystalized might accumulate at the bottom of a magma chamber after settling or along the sides of a vent. Accumulation of minerals in the lower magma chamber is a side effect from fractional crystallization which is known to change the composition of a magma (Esser, et al., 2004; Jakobsson, et al., 1973; Moore & Clague, 1992). Olivine and plagioclase feldspar were chosen for this model as they are the first minerals to crystallize as a magma cools in each reaction series and have reasonable known compositions from Martian meteorites (Bowen, 1922; Papike, 1998). The model simulated adding 1% of olivine and plagioclase feldspar (Shergottite EETA79001 (Papike, 1998)) from the composition of a Jake_M (Monkey_yard), Bathurst_Inlet (Halls_RP) and Adirondack (from MER *Spirit* mission (McSween, et al., 2004)) target.

3.4.2 Partial Melting

Partial Melting models were used to determine if Bathurst_Inlet compositions could be generated from the WD Martian mantle elemental composition (Table 3-6). The trace elements focused on for this study are K, P, Ti, Cr, and Ni because they have

known partitioning behaviour during melting processes and are detectable by APXS. Partition coefficients and proportions of minerals in the mantle follow the conditions established in Schmidt & McCoy (2010) and Bertka & Fei (1997)(Table 3-6). Partition coefficients were calculated using

$$D_{Bulk} = \sum (Kd^{i}_{min} \times X_{min}) \quad (1)$$

where D_{Bulk} is the bulk partition coefficient, Kd^{i}_{min} is the partition coefficient of element, *i*, in each mineral, *min*, and X_{min} is the molar proportion of each mineral. Molar proportions of the minerals of the mantle are listed in Table 3-6 as X_1 and X_2. Two partial melting models were used for this study: batch melting (Table 3-7) and two-stage batch melting (Table 3-8).

The batch melting model melts the same original mantle source at 2% intervals up to 35% (highest degree of partial melting on Mars is ~25% for Gusev basalt (Baratoux, et al., 2011)). Melts are calculated using the equation

$$\frac{C^{i}_{liq}}{C_0} = \frac{1}{F + D - FD} \quad (2)$$

where C^{i}_{liq} is the composition of the melt, C_0 is the composition of the mantle source, F is the degree of partial melting (melt fraction or weight % of the sample melted) and D is the bulk distribution coefficient. The two-stage batch melting model melts the mantle

source at 5% degree of partial melting and then at 5% again. Melts are calculated using the equation

$$\frac{C_{1,2}^{i}}{C_{0}^{i}} = \frac{D_{1}^{i}}{(F_1 + D_{1}^{i} - F_1 D_{1}^{i})(F_2 + D_{2}^{i} - F_2 D_{2}^{i})} \quad (3)$$

where $C^{i}_{1,2}$ is the concentration in the incremental batch generated, C_0 is the concentration of mantle source, D_1 is the first stage bulk distribution coefficient, D_2 is the second stage bulk distribution coefficient, F_1 is the first stage melt fraction and F_2 is the second stage melt fraction. The composition of the melt and the residuum is calculated for both of the models. All results are normalized to C1 Chondrite (Sun & McDonough, 1989) for the figures and the tables show actual values.

Table 3-6

D_{bulk} Values for Trace Elements[a] and Mineral Composition of the Mantle[b].

	Plagioclase	Olivine	Garnet	Clinopyroxene	Orthopyroxene	Spinel	Chromite	D_{bulk1}	D_{bulk2}
D_K	0.117	0.00018	0.0007	0.007	0.0003	0.00	0.00	0.0027	0.0024
D_P	0.071	0.050	0.150	0.030	0.030	0.00	0.00	0.04	0.04
D_{Ti}	0.04	0.006	0.688	0.384	0.074	0.97	0.97	0.17	0.15
D_{Cr}	0.02	0.9	2.01	3.5	4	3.4	174	3.05	2.95
D_{Ni}	0.06	12.2	5.1	2.6	1.1	30	30	4.40	4.78
X_1	0%	25%	0%	35%	40%	0%	0%		
X_2	0%	29%	0%	31%	40%	0%	0%		

D is the partition coefficient.
X_1 composition of the Martian mantle.
X_2 composition of mantle after a melt.
[a] (Schmidt & McCoy, 2010)
[b] (Bertka & Fei, 1997)

The batch partial melting model (Table 3-7, Figure 3-6) demonstrates that melts of the Martian mantle can generate K and P compositions that are within range of Bathurst_Inlet class compositions. Melts can achieve a Bathurst_Inlet-like concentration

in K and P at 2.72 – 3.86% melt fraction. The partial melt has a Pogy concentration in K, P and Ti but never simultaneously.

Table 3-7

Model for Batch Melting of Martian Mantle

Element	**K**	**P**	**Ti**	**Cr**	**Ni (ppm)**
Mantle Composition	0.06	0.54	1.91	1.88	314
$\mathbf{D_{bulk}}$	0.002	0.04	0.17	3.05	4.4
Melt fraction					
0.19%	7.22	1.78	0.50	0.16	75
0.50%	4.33	1.64	0.49	0.16	75
1%	2.62	1.47	0.48	0.16	76
3%	1.02	1.02	0.44	0.17	77
5%	0.63	0.79	0.40	0.17	78
7%	0.46	0.64	0.37	0.17	79
9%	0.36	0.54	0.35	0.17	81
11%	0.30	0.46	0.33	0.18	82
13%	0.25	0.41	0.31	0.18	83
15%	0.22	0.36	0.29	0.18	85
17%	0.19	0.33	0.27	0.18	86
19%	0.17	0.30	0.26	0.19	88
21%	0.16	0.28	0.25	0.19	90
23%	0.14	0.25	0.23	0.19	91
25%	0.13	0.24	0.22	0.20	93
27%	0.12	0.22	0.21	0.20	95
29%	0.11	0.21	0.21	0.20	97
31%	0.11	0.20	0.20	0.21	99
33%	0.10	0.19	0.19	0.21	101
35%	0.09	0.18	0.18	0.21	103

WD Mantle Composition (Wänke & Dreibus, 1988).
Yellow shading indicates the melt has a Bathurst_Inlet composition.

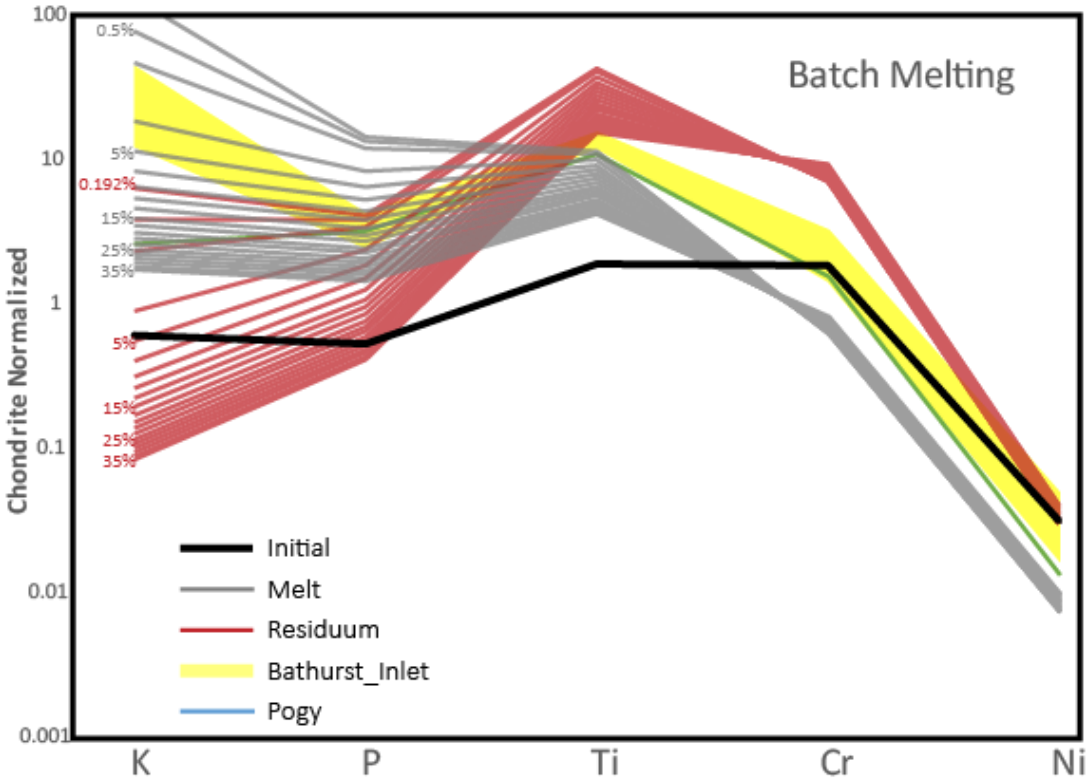

Figure 3-6: Chondrite normalized trace element abundance diagram from modelling partial melting of WD mantle in 2% steps. The range of Bathurst_Inlet compositions indicates if and when melt or residuum has a similar composition.

Within these model conditions, the required melt fractions for WD mantle to generate a complete trace element package within the range of each class is not possible for batch melting. Bathurst_Inlet composition of Ti cannot be generated. Ti and Cr compositions of Pogy are not possible. Bathurst_Inlet compositions could require a WD mantle source with higher Cr and Ni to generate a fitting melt at ~3% melt fraction.

Mantle melts would have a mafic composition (Fe, Mg, Cr, Ni, olivine, pyroxene, plagioclase feldspar) as seen in Bathurst_Inlet and Pogy targets however, Bathurst_Inlet compositions could not be generated by batch melting Martian mantle; the big misfits are Ti, Cr and Ni. This may be do to the composition of the source mantle as Shergottites may be higher in Ti and meteorite olivine has high Cr and Ni which may not be relevant

to Gale Crater rocks (Wänke & Dreibus, 1988). The mantle source required for generating a trace element composition within range of Bathurst_Inlet at 5% melt fraction would be enriched in K (0.04 wt% vs 0.03 wt%), Ti (0.18 wt% vs 0.08 wt%), Cr (1.10 wt% vs 0.50 wt%) and Ni (709 ppm vs 330 ppm). A non-WD mantle source could be possible as Windjana (Treiman, et al., 2015) and the parental magma for Jake_M (Stolper, et al., 2013) have been hypothesized to have a non-WD mantle source.

As the mineral modes of the Martian mantle are not exactly known, we can experiment by changing the mineral composition to examine the effects on the melt composition. Increasing the amount of olivine will cause an increase in K, P, Ti and Cr but causes Ni to decrease. Increasing clinopyroxene increases P, Cr and Ni while decreasing K and Ti. Orthopyroxene increases P, Ti, Cr and Ni as the mode increases. The amount of Ni and Ti decreases, and Cr and P increase with added spinel. Addition of chromite causes Ti, Cr and Ni to decrease with P increasing. No combination of mineral modes of the mantle is able to match Bathurst_Inlet completely.

The two-stage batch melting model (Table 3-8, Figure 3-7) demonstrates that first stage melting (5% melt fraction) can generate Bathurst_Inlet-like compositions of P. No matching Pogy compositions could be made. The second stage melt (5%) cannot generate a composition similar to Bathurst_Inlet or Pogy.

Table 3-8

Model for Two-Stage Melt of Martian Mantle

Element	K	P	Ti	Cr	Ni
Mantle Composition	0.06	0.54	1.91	1.88	314
D_{bulk1}	0.0027	0.04	0.17	3.05	4.4
D_{bulk2}	0.0024	0.04	0.15	2.95	4.78
First Melt (5%)	0.63	0.79	0.40	0.17	78
Second Melt (5%)	0.03	0.33	0.35	0.18	75

WD Mantle Composition (Wänke & Dreibus, 1988).

Yellow shading indicates the melt has a Bathurst_Inlet composition.

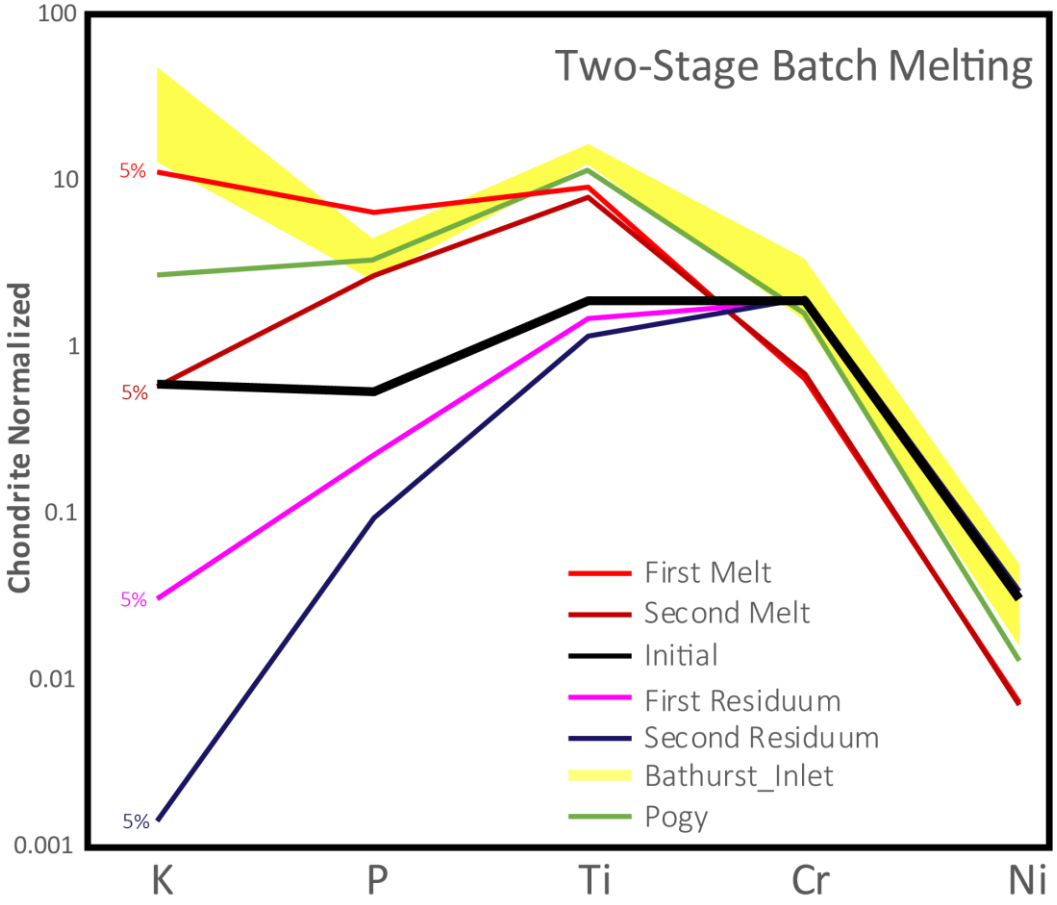

Figure 3-7: Chondrite normalized trace element abundance diagram from modelling partial melting of WD mantle by two-stage batch melting. The mantle is melted in two 5% stages each producing residuum. The range of Bathurst_Inlet compositions indicates if and when melt or residuum has a similar composition.

The required melt fractions for WD mantle to generate a complete trace element package within the range of each class is not possible for the second stage melt in a two-stage batch melting model after a 5% first stage (Table 3-10). Bathurst_Inlet

compositions are not possible in anything but Ni at a high melt fraction. Pogy compositions can only be achieved in Ni both at high melt fractions.

Bathurst_Inlet is expected to be able to be generated from partial melting because of its mafic composition however there is a misfit with all elements. A mantle source with elevated K (0.83 wt% vs 0.03 wt%), P (0.13 wt% vs 0.07 wt%), Ti (0.22 wt% vs 0.08 wt%), Cr (1.03 wt% vs 0.50 wt%) and Ni (740 ppm vs 330 ppm) might generate an average Bathurst_Inlet composition after two-stage batch melting (both 5%).

3.4.3 Fractional Crystallization

Fractional crystallization models were constructed to test if compositions of the Jake_M and Bathurst_Inlet classes of rocks could be linked through removal of olivine or plagioclase feldspar crystals with Martian meteorite compositions (Shergottite EETA79001 (Papike, 1998)) from the "end member" compositions (with respect to total alkali vs silica) of Jake_M (Monkey_yard) and Bathurst_Inlet (Halls_RP) class compositions as well as Adirondack (from MER *Spirit* mission (McSween, et al., 2004)). Monkey_yard and Halls_RP were chosen as starting compositions because they were the furthest outliers of their class (TAS diagram, Figure 3-5). Adirondack was chosen as it considered a primary Mars mantle melt with high MgO and olivine phenocrysts present (Monders, et al., 2007). FC was applied in 1% increments until each of the targets ran out of an element (MgO for olivine, Al_2O_3 or CaO for plagioclase feldspar).

Olivine and plagioclase fractionation trend Monkey_yard away from Bathurst_Inlet compositions (Figure 3-8). Olivine fractionation trends Halls_RP towards

Jake_M compositions in all examined elements but FeO, plagioclase fractionation trends Halls_RP away from Jake_M compositions. Adirondack trends towards Jake_M compositions during olivine fractionation and towards Halls_RP during plagioclase fractionation.

The best fitting model is for Bathurst_Inlet to form from plagioclase fractionation of Adirondack, however it is not a perfect fit as the K_2O composition of Adirondack is too low. The next best fitting model is for olivine fractionation of Adirondack to form Jake_M, however this model only matches in Al_2O_3. None of the Jake_M or Bathurst_Inlet models have a good fit with each other.

Therefore, it is unlikely that Jake_M and Bathurst_Inlet classes are linked through fractional crystallization processes. Adirondack is not linked to Jake_M through fractional crystallization and while it does match Bathurst_Inlet in all but K_2O composition it is not a complete match and likely not linked. Fractional crystallization of olivine removes the mafic components of the targets and trends them away from Bathurst_Inlet (mafic composition). Removing plagioclase feldspar from the targets has the opposite effect and concentrates the mafic minerals in the target and pushes them towards Bathurst_Inlet.

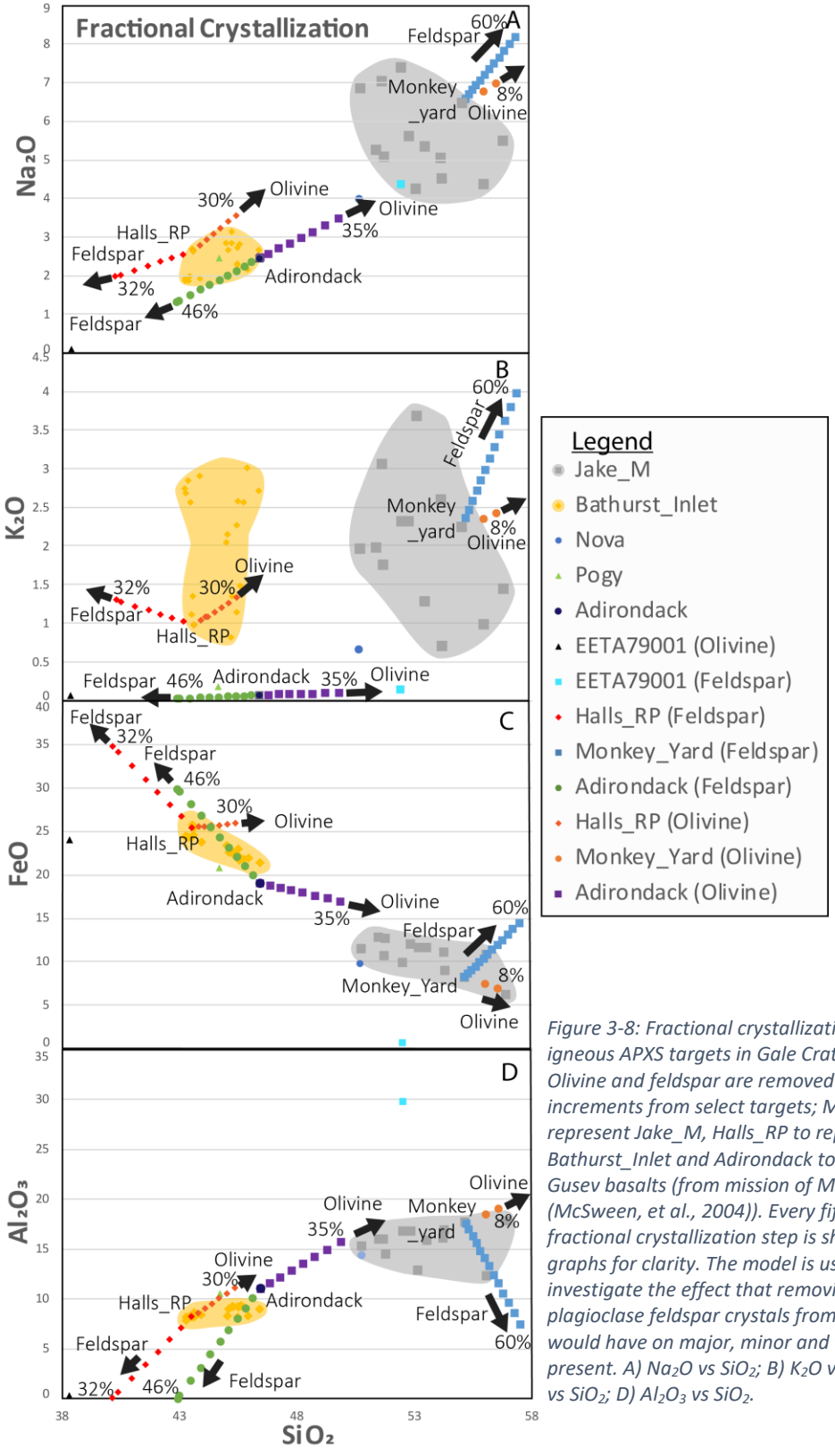

Figure 3-8: Fractional crystallization models for igneous APXS targets in Gale Crater, Mars. Olivine and feldspar are removed in 1% increments from select targets; Monkey_yard to represent Jake_M, Halls_RP to represent Bathurst_Inlet and Adirondack to represent Gusev basalts (from mission of MER rover Spirit (McSween, et al., 2004)). Every fifth (and final) fractional crystallization step is shown on the graphs for clarity. The model is used to investigate the effect that removing olivine and plagioclase feldspar crystals from each class would have on major, minor and trace elements present. A) Na_2O vs SiO_2; B) K_2O vs SiO_2; C) FeO vs SiO_2; D) Al_2O_3 vs SiO_2.

3.4.4 Mineral Accumulation

Mineral accumulation modeling was used to determine if accumulation of plagioclase feldspar or olivine crystals would link the composition of Jake_M, Bathurst_Inlet or Adirondack (Gusev plains basalt from MER *Spirit* mission (McSween, et al., 2004)) to another class of igneous targets. This model simulates the addition of olivine and plagioclase feldspar crystals with Martian meteorite compositions (Shergottite EETA79001 (Papike, 1998)) to the composition of Monkey_yard (Jake_M), Halls_RP (Bathurst_Inlet) and Adirondack (Gusev plains basalt). Monkey_yard and Halls_RP were chosen as representatives from their respective classes as they were the furthest outliers (TAS diagram, Figure 3-5). Adirondack was chosen as it considered a primary Mars mantle melt with high MgO and olivine phenocrysts present (Monders, et al., 2007). Mineral accumulation in 1% increments was applied for the same number of increments as fractional crystallization (there is no limiting factor to how long this process can occur unlike fractional crystallization).

Olivine accumulation demonstrates a trend of Monkey_yard towards the Bathurst_Inlet class compositions, plagioclase accumulation only caused Na_2O to approach Bathurst_Inlet composition (Figure 3-9). Olivine accumulation trends Halls_RP away from Jake_M compositions, plagioclase fractionation trends Halls_RP towards Jake_M compositions of Na_2O, FeO and Al_2O_3. Adirondack trends towards Jake_M compositions during plagioclase feldspar accumulation and towards Halls_RP during olivine accumulation.

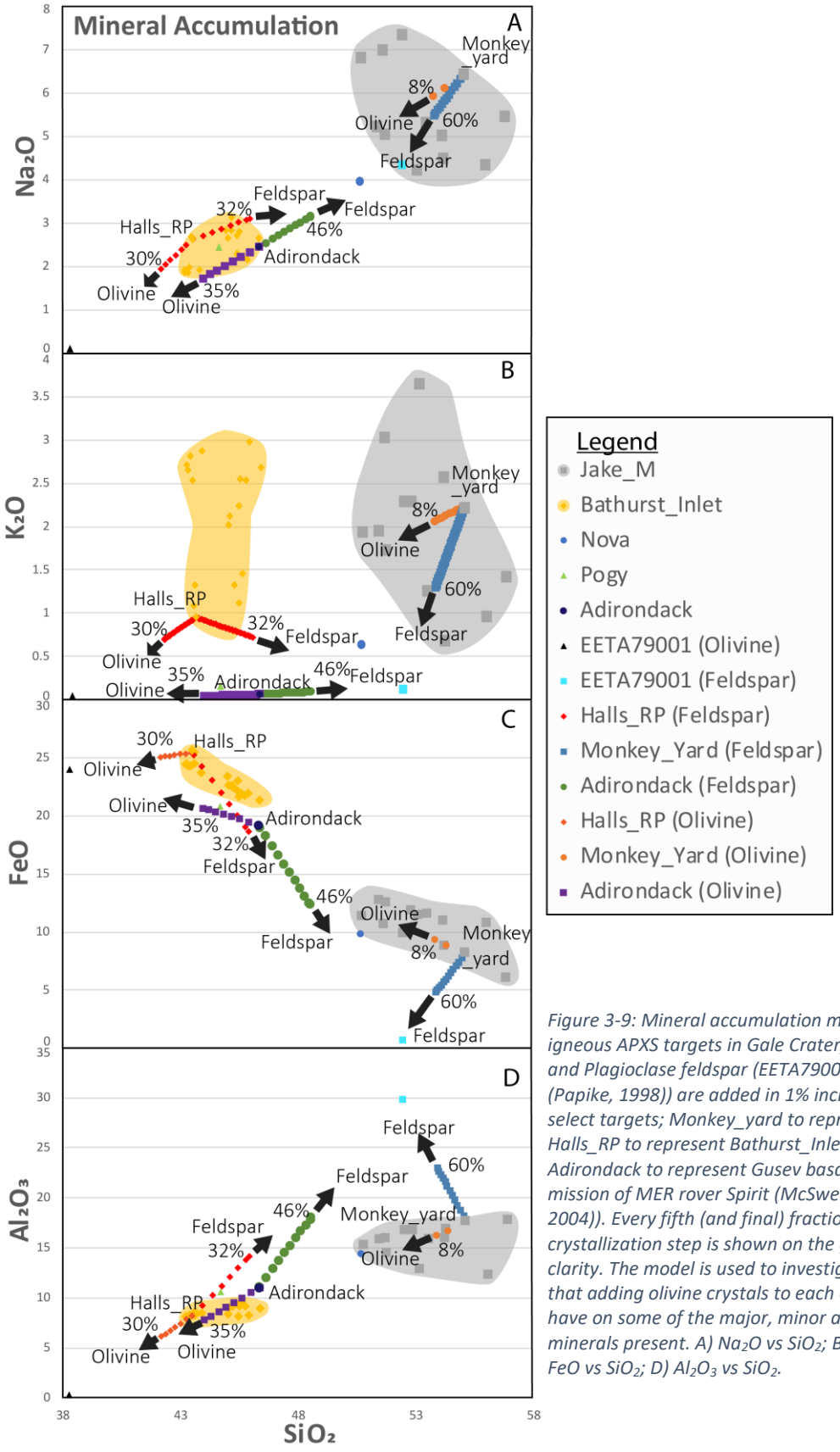

Figure 3-9: Mineral accumulation models for igneous APXS targets in Gale Crater, Mars. Olivine and Plagioclase feldspar (EETA79001 Shergottite (Papike, 1998)) are added in 1% increments to select targets; Monkey_yard to represent Jake_M, Halls_RP to represent Bathurst_Inlet and Adirondack to represent Gusev basalts (from mission of MER rover Spirit (McSween, et al., 2004)). Every fifth (and final) fractional crystallization step is shown on the graphs for clarity. The model is used to investigate the effect that adding olivine crystals to each class would have on some of the major, minor and trace minerals present. A) Na_2O vs SiO_2; B) K_2O vs SiO_2; C) FeO vs SiO_2; D) Al_2O_3 vs SiO_2.

The best fitting model is for Bathurst_Inlet to form from olivine accumulation in Adirondack, however it is not a perfect fit as the K_2O and FeO compositions of Bathurst_Inlet are too high. The next best fitting model is for olivine fractionation of Adirondack to form Jake_M, however this model only matches in FeO and Al_2O_3. None of the Jake_M or Bathurst_Inlet models have a good fit with each other.

Therefore, it is unlikely that Jake_M and Bathurst_Inlet classes are linked by mineral accumulation processes. Adirondack is not a full match in major elements to Jake_M or Bathurst_Inlet through mineral accumulation despite matching some elemental compositions. Mineral accumulation of olivine trends each target towards Bathurst_Inlet since it is a mafic composition. Adding plagioclase feldspar trends each target towards the more evolved Jake_M compositions.

3.4.5 Summary of Models

The batch partial melting model demonstrates that there is not any complete match between the melts (up to 35%) and the APXS igneous classes. Bathurst_Inlet does not match with more than two trace element at a time (K and P at 2.72 – 3.86% melt fraction) and neither do Nova and Pogy. A section of heterogeneous mantle enriched in K, Ti, Cr and Ni would be needed to generate a Bathurst_Inlet-like composition for batch melting at 5% melt fraction. Changing the mineral mode of the mantle used in the model is not able to generate a Bathurst_Inlet-like melt either.

The two-stage batch partial melting model also indicates that there is not a good match between the melts (5% and 5%) and the APXS igneous classes. The first stage

melts do not match with Bathurst_Inlet in more than P in the first melt. The second stage melt does not match with Bathurst_Inlet or Pogy in any element. A mantle source with higher concentrations of all of the trace elements would be needed to generate a Bathurst_Inlet-like composition for the second stage of a two-stage batch melt. Again, changing the mantle mineral mode is not able to generate a match with Bathurst_Inlet.

Fractional crystallization modelling demonstrates that while some of the major elements may match after FC of olivine and plagioclase feldspar, there is not a complete match with the APXS igneous classes. Monkey_yard trends away from Bathurst_Inlet during FC of both olivine and plagioclase feldspar. Halls_RP and Adirondack both trend towards Jake_M during olivine FC but away during plagioclase feldspar FC. Olivine FC causes the targets to get less mafic (less like Bathurst_Inlet) while FC of plagioclase feldspar causes targets to get less like Jake_M (evolved). The best fitting models do not match with every element: olivine fractionation of Adirondack to Bathurst_Inlet and plagioclase fractionation of Adirondack to Jake_M.

Mineral accumulation modelling suggests that there is not a complete match between the APXS igneous classes though some of the major elements match during MA of olivine and plagioclase feldspar. Monkey_yard trends towards Bathurst_Inlet during olivine MA, but the change is not sufficient to reach its basaltic composition. Halls_RP and Adirondack both trend toward Jake_M with plagioclase feldspar MA and towards Bathurst_Inlet with olivine MA. MA of olivine causes the targets to get more like Bathurst_Inlet (mafic) while plagioclase feldspar MA causes targets to get more a more Jake_M-like composition (evolved). The best fitting models again do not match

with every element: plagioclase accumulation in Adirondack towards Bathurst_Inlet and olivine accumulation in Adirondack towards Jake_M.

3.5 Conclusion

These volcaniclastic APXS targets are sedimentary rocks with igneous compositions found in a large sedimentary basin. Only one source for volcaniclastic sediments in Gale Crater has been identified previously: the rim/wall of Gale Crater. The distinct compositions, textures, grain sizes and type (bedrock vs float rock) of the igneous classes demonstrate that they are not the same now. This study shows that more than one source for the volcaniclastic sediment is required as there is no simple igneous petrological link between Jake_M and Bathurst_Inlet classes.

While Jake_M compositions are not expected to be generated through partial mantle melting due to the evolved composition, generation of mafic Bathurst_Inlet compositions would be expected to be possible. However, the partial melting models suggest Bathurst_Inlet is likely not the result of a partial melt of the WD mantle. Bathurst_Inlet could be from a mantle source with elevated K, Ti, Cr and Ni after a 5% batch melt or a mantle source with elevated K, P, Ti, Cr and Ni after two-stage batch melting. No combination of mantle mineral modes is able to generate Bathurst_Inlet from WD mantle composition. Windjana and Jake_M parent compositions are also shown to be from a different mantle source than WD mantle which indicates that there could be a heterogeneity in the mantle near Gale Crater. Heterogeneities in the Martian mantle are thought to be possible (Agee & Draper, 2004; Schmidt & McCoy, 2010).

As Jake_M and Nova are more differentiated than Bathurst_Inlet and Pogy, they could be evolved compositions of Bathurst_Inlet or Adirondack. However, fractional crystallization models demonstrate that Jake_M and Bathurst_Inlet cannot be linked through fractional crystallization of olivine or plagioclase feldspar. The best fractional crystallization models demonstrate that fractionation of Adirondack trends towards Jake_M (olivine) and towards Bathurst_Inlet (plagioclase feldspar) but fail to match compositions. Mineral accumulation models also demonstrate that Jake_M and Bathurst_Inlet are not linked through olivine or plagioclase feldspar. The best mineral accumulation models show that Adirondack will trend towards Bathurst_Inlet (olivine) and Jake_M (plagioclase feldspar) but fail to match either composition. The models demonstrate that one crystalline source could not be modified by fractional crystallization or mineral accumulation of olivine or plagioclase feldspar to produce both Jake_M and Bathurst_Inlet compositions. The models also suggest that a basaltic primary melt of Martian mantle like Adirondack could not be altered by these processes to generate Jake_M or Bathurst_Inlet compositions.

Therefore, Jake_M and Bathurst_Inlet are not linked and likely derive from different crystalline sources. There is a requirement for at least two crystalline sources for the volcaniclastic sediments in Gale Crater. While the wall of Gale Crater rim is likely one of the sources, the other is not known at this time. However, the volcanic landform North Gale Landform, located ~60 km north of Gale Crater is a likely candidate to be another source. The composition of the wall of Gale Crater rim is not known so there is

not enough information to determine which igneous composition is sourced from there nor is there any compositional data on North Gale Landform.

Chapter 4: Summary, Final Discussion and Overall Conclusions

4.1 Summary of Previous Chapters

In Chapter 2, the investigation into the nature of North Gale Landform, a previously unidentified landform north of Gale Crater, Mars has led to the following conclusions: 1) There was a collapse of the landform at an unknown time in the past of Mars. 2) A large portion of materials produced during the collapse moved to the south-southeast towards the rim of Gale Crater and created the hummocky terrain that can be seen there currently. 3) The collapse of NGL created a large horseshoe shaped depression in the southern flank called an amphitheatre. 4) The tectonic environment of the area surrounding NGL shows a trend in lineations perpendicular to the direction of the avalanche. 5) The morphology of NGL was not the result of an impact, it does not have the characteristics of elevated craters or an impact in a pre-existing structure nor is NGL the result of heavy degradation of an impact crater. 6) NGL is likely not a typical dichotomy boundary feature like a mesa, knob or plateau. 7) There is evidence to suggest that NGL is a volcanic feature, including its morphology and associated landforms.

In Chapter 3, the investigation into the igneous end member sediments in Gale Crater, Mars by the MSL Curiosity rover has led to the following conclusions. 1) There are significant differences in the composition of Jake_M and Bathurst_Inlet classes in SiO_2, FeO, Al_2O_3, Na_2O, MgO, MnO, TiO_2, Cr_2O_3 and Ni. 2) Jake_M rocks are classified as mugearites, basaltic andesite, benmoreite, tephriphonolite and phonotephrite while

Bathurst_Inlet rocks are classified as tephrite basanite, trachybasalt and basalt. Nova is a basalt and Pogy is a picrobasalt. 3) Partial melting models of the Martian mantle are unable to generate Bathurst_Inlet compositions for all of the trace elements examined simultaneously. The mantle source would need to be enriched in K, Ti, Cr and Ni compared to the WD mantle for a 5% melt fraction batch melt. It would need to be enriched in K,P, Ti, Cr, and Ni for a second stage 5% melt fraction in two-stage batch melting. 4) Mineral accumulation of olivine or plagioclase feldspar is not sufficient to generate Jake_M from Bathurst_Inlet class rocks, or vice versa. Adirondack is also not able to generate or be generated from Jake_M or Bathurst_Inlet. 5) Fractional crystallization of olivine and plagioclase feldspar is also not able to generate Jake_M from Bathurst_Inlet class rocks nor Bathurst_Inlet from Jake_M. Adirondack is also not able to generate or be generated from Jake_M or Bathurst_Inlet. 6) The number of crystalline sources for igneous composition material in Gale Crater is therefore more than one. Jake_M and Bathurst_Inlet are different enough to require discrete sources, and neither can be linked by simple igneous processes.

4.2 Final Discussion and Conclusions

Grotzinger, et al. (2015b) suggests that the source for igneous sediments is the rim of the Gale crater, which consists of pre-existing crystalline bedrock. The crystalline bedrock in the rim would be expected to have a basaltic (mafic) composition similar to the average Martian crust (McSween Jr, et al., 2009). This would make it the likely source for the Bathurst_Inlet class compositions found in Gale Crater. Treiman, et al. (2015), suggests that the Windjana sample (Bathurst_Inlet class) is sourced from the rim

of Gale Crater by fluvial transport before aeolian remobilization and deposition. As Bathurst_Inlet and Jake_M have been shown to be unrelated through simple igneous processes, Jake_M would need a different crystalline source. Adirondack was also demonstrated to not be related to Jake_M through simple differentiation processes (Schmidt & McCoy, 2010). Jake_M likely did not evolve from the same mantle reservoir as Adirondack implying that Jake_M was not differentiated from an Adirondack-like composition. A secondary crystalline source for the evolved Jake_M compositions is still needed and there is no evidence of another source within Gale Crater.

NGL might represent an external igneous source which could have contributed volcaniclastic sediments. Gale Crater is very far away (>2000 km) from previously identified volcanic edifices (Apollonaris Mons, Elysium Mons province volcanoes, Tyrrhenus Mons), so it is unlikely that associated igneous materials would have been carried into Gale Crater by sedimentary processes. NGL is closer to Gale Crater (~60 km) than any other identified volcanic source so it more plausible that it might be an outside source of volcanic material (Figure 2-4).

NGL was demonstrated to likely have a volcanic origin because it fits the criteria of Stewart & Head (2001), including morphology (capping unit, spur unit, talus slopes, etc. (Figure 2-15)), evidence of constructive/destructive phases (high relief, stand alone structure (Figure 2-1), amphitheatre, talus slopes, knobby deposits (Figure 2-6)), and associated volcanic features (pit crater chain (Figure 2-10), chaotic terrain (Figure 2-11)). NGL was determined to have experienced massive flank failure (amphitheatre (Figure 2-4)) that produced a massive debris avalanche (hummocky terrain (Figure 2-8)) in the

direction of Gale Crater. The hummocky terrain covers the area between NGL and the northern rim of Gale Crater (possibly inside Gale Crater) that includes the current catchment for Peace Vallis. These all provides avenues for sediments from NGL to be transported into Gale Crater.

It is not known what kind of volcanic eruptions NGL would have produced. Possible eruptive styles that could act as a delivery mechanism for sediments into or near Gale Crater could be lava flows, plinian column collapse, or pyroclastic flows. Wilson and Head (1994) also claim that plinian (explosive) eruptions would be common on Mars due to the lower atmospheric pressure, increased volatiles in magma and groundwater intrusion. Tharsis volcanoes are mantled in a material that was determined to be explosive debris from the volcanoes themselves (El Maarry, et al., 2009). The ease of explosiveness of Martian volcanic eruptions and the extended travel distance would likely leave Gale Crater within range of the deposits they create (Wilson & Head III, 1994; Stewart & Head, 2001). Volcanic eruptions which involved pyroclastic activity could be linked to the high tridymite content (14 wt%) of the Buckskin drill site as the proposed scenario involves silicic volcanism and ash fall into an ancient lake (Morris, et al., 2016).

However, the most obvious method of sediment delivery into Gale Crater for NGL has to be the massive debris avalanche that removed the southern flank. A large portion of NGL is missing and the most likely scenario is it has been deposited to the south of NGL as the hummocky terrain. Massive debris avalanches are common on terrestrial stratovolcanoes and terrestrial shield volcanoes also experience flank failures

creating large avalanches (Coombs, et al., 2004; Siebert, 1984). It is reasonable to assume that Martian volcanoes may also experience sector collapse events. Terrestrial flank failures and Martian landslides provided constraints (runout efficiency) for the expected distance of material dispersal and the ~60 km between NGL and Gale Crater is within those constraints. The massive debris avalanche did not necessarily stop at the rim of Gale Crater. There are large blocks inside the crater, near Peace Vallis, that have a stronger resemblance to the large blocks in the hummocky terrain rather than the rim of Gale Crater (lighter tone spurs, lighter toned under THEMIS Night IR, smoother appearance) (Figure 2-13). The Jake_M and Nova class float rocks seem like ideal candidates to be from NGL in this scenario because of the energy required to transport the larger float rocks (Jake_M is ~50 cm tall (Stolper, et al., 2013)).

The hummocky terrain spanning the region between NGL and Gale Crater's northern rim partially drains into the crater (Figure 2-4) (Palucis, et al., 2014). The current drainage basin for Peace Vallis appears to have been created from the massive debris avalanche of NGL as its borders are linear collections of hummocks. Incised valleys in the hummocky terrain were likely formed by flowing water when that was still possible on Mars (Palucis, et al., 2014). If NGL material was being eroded from the hummocks (talus slopes (Figure 2-8)) into river channels and transported away by flowing water, then the water would have drained into Gale Crater through Peace Vallis. The eroded material might have been transported into Gale Crater through the river systems as demonstrated by the Peace Vallis alluvial fan system that terminates near the Curiosity rover landing site (Figure 2-4). The Bathurst_Inlet bedrock sediments or

Jake_M igneous cobbles seem like ideal candidates to be from NGL in this scenario because of the spatial relationship between the hummocky terrain and Peace Vallis catchment. Weathering and transport of volcaniclastic material is already proposed as a delivery mechanism for crater rim and wall materials and it makes sense for NGL material outside the crater as well (Ehlman & Buz, 2015; Grotzinger, et al., 2015b; Le Deit, et al., 2013; Siebach, et al., 2017).

4.3 Limitations of Study

There were several limitations for this study that have likely impacted the results and/or interpretations. There is a lack of compositional data from NGL and the massive debris avalanche deposit which could clear up which class (if any) was sourced from the collapse of NGL. There is only one available HiRISE image for NGL and none for the massive debris avalanche deposit which limits the amount of detail observable for each of those targets. The blocks in the hummocky terrain could be examined in higher detail to determine if there is a jigsaw fit between them which would indicate that they used to be touching as part of the volcanic edifice. More high resolution images of NGL (including the interior) may also provide more details about its morphology and look for volcanic features such as dikes. There is a lack of CRISM coverage on NGL and hummocky terrain which may provide some compositional data which could help link them with the interior of Gale Crater. The WD mantle model composition may not represent the mantle source for Gale Crater as the source for that model (SNC meteorites) may have a different composition than the mantle.

4.4 Future Work

Future work on this topic would require compositional data and samples from both NGL and the hummocky terrain which can be used for more direct comparisons as well as concluding if this work has determined the correct origin for NGL and its link to Gale Crater. When better coverage of NGL with advanced orbital datasets such as HiRISE and CRISM is available, it would be possible to further investigate this problem as well.

References

Agee, C. B., & Draper, D. S. (2004). Experimental constraints on the origin of Martian meteorites and the composition of the Martian mantle. *Earth and Planetary Science Letters*, 415-429.

Anderson, H. R. (1965). Mariner IV Measurements near Mars: Initial Results. *Science*, 1226-1228.

Anderson, R. B., & Bell III, J. F. (2010). Geologic mapping and characterization of Gale Crater and implications for its potential as a Mars Science Laboratory landing site. *The International Journal of Mars Science and Exploration*, 76-128.

Andrews-Hanna, J. C., Zuber, M. T., & Banerdt, W. B. (2008). The Borealis basin and the origin of the martian crustal dichotomy. *Nature*, 1212-1215.

Bandfield, J. L., Edwards, C. S., Montgomery, D., & Brand, B. D. (2013). The dual nature of the martian crust: Young lavas and old clastic materials. *Icarus*, 188-199.

Baptista, A. R., Mangold, N., Ansan, V., Baratoux, D., Lognonne, P., Alves, E. I., . . . Neukem, G. (2008). A swarm of small shield volcanoes on Syria Planum, Mars. *Journal of Geophysical Research*, 19.

Baratoux, D., Toplis, M. J., Monnereay, M., & Gasnault, O. (2011). Thermal history of Mars inferred from orbital geochmistry of volcanic provinces. *Nature*, 1-5.

Bell III, J. F., McSween, H. Y., Crisp, J. A., Morris, R. V., Murchie, S. L., Bridges, N. T., . . . Soderblom, L. (2000). Mineralogic and compositional properties of Martian soil and dust: Results from Mars Pathfinder. *Journal of Geophysical Research, 105*(E1), 1721-1755.

Berger, J. A., Schmidt, M. E., Gellert, R., Boyd, N. L., Desouza, E. D., Flemming, R. L., . . . Yen, A. S. (2017). Zinc and germanium in the sedimentary rocks of Gale Crater on Mars indicate hydrothermal enrichment followed by diagenetic fractionation. *Journal of Geophysical Research: Planets, 122*(8), 1747-1772.

Berger, J. A., Schmidt, M. E., Gellert, R., Campbell, J. L., King, P. L., Flemming, R. L., . . . Desouza, E. (2016). A global Mars dust composition refined by the Alpha-Particle X-ray Spectrometer in Gale Crater. *Geophysical Research Letters, 43*, 67-75.

Bertka, C. M., & Fei, Y. (1997). Mineralogy of the Martian interior up to core-mantle boundary pressures. *JOURNAL OF GEOPHYSICAL RESEARCH*, 5251-5264.

Bish, D. L., Blake, D. F., Vaniman, D. T., Chipera, S. J., Morris, R. V., Ming, D. W., . . . Spanovich, N. (2013). X-ray Diffraction Results from Mars Science Laboratory: Mineralogy of Rocknest at Gale Crater. *Science, 341*, 6.

Bowen, N. L. (1922). The reaction principle in petrogenesis. *The Journal of Geology*, 177-198.

Broz, P., & Hauber, E. (2012). A unique volcanic field in Tharsis, Mars: Pyroclastic cones as evidence for explosive eruptions. *Icarus*, 88-99.

Broz, P., & Hauber, E. (2013). Hydrovolcanic tuff rings and cones as indicators for phreatomagmatic explosive eruptions on Mars. *Journal of Geophysical Research: Planets*, 1656-1675.

Campbell, J. (2012). The instrumental blank of the Mars Science Laboratory alpha particle X-ray spectrometer. *Nuclear Instruments and Methods in Physics Research*, 102-110.

Campbell, J. L., Perret, G. M., Gellert, R., Andrushenko, S. M., Boyd, N. I., Maxwell, J. A., . . . Schofield, C. D. (2012). Calibration of the Mars Science Laboratory Alpha Particle X-Ray Spectrometer. *Space Sci Rev*, 319-340.

Carr, M. H., & Head III, J. W. (2010). Geologic history of Mars. *Earth and Planetary Science Letters*, 185-203.

Carracedo, J. (1999). Growth, structure, instability and collapse of Canarian volcanoes and comparisons with Hawaiian volcanoes. *Journal of Volcanology and Geothermal Research, 94*(1-4), 1-19.

Chapman, M. G., & Tanaka, K. L. (2002). Related Magma–Ice Interactions: Possible Origins of Chasmata, Chaos, and Surface Materials in Xanthe, Margaritifer, and Meridiani Terrae, Mars. *Icarus*, 324-339.

Christensen, P. R., Engle, E., Anwar, S., Dickenshied, S., Noss, D., Gorelick, N., & Weiss-Malik, M. (2009). JMARS - A Planetary GIS. Retrieved from http://adsabs.harvard.edu/abs/2009AGUFMIN22A..06C

Christensen, P. R., McSween Jr, H. Y., Bandfield, J. L., Ruff, S. W., Rogers, A. D., Hamilton, V. E., . . . Moersch, J. E. (2005). Evidence for magmatic evolution and diversity on Mars from infrared observations. *Nature*, 504-509.

Citron, R. I., Manga, M., & Hemingway, D. J. (2018). Timing of oceans on Mars from shoreline deformation. *Nature*, 643-646.

Cole, H. M., & Andrews-Hanna, J. C. (2017). The anatomy of a wrinkle ridge revealed in the wall of Melas Chasma, Mars. *Journal of Geophysical Research: Planets, 171*(2), 889-900.

Coleman, N. M. (2003). Aqueous flows carved the outflow channels on Mars. *Journal of Geophysical Research , 108*(E5), 11.

Coombs, M. L., Clague, D. A., Moore, G. F., & Cousens, B. L. (2004). Growth and collapse of Waianae Volcano, Hawaii, as revealed by exploration of its submarine flanks. *Geochemistry Geophysics Geosystems, 5*(8), 1-30.

Cousin, A., Sautter, V., Payre, V., Forni, O., Mangold, N., Gasnault, O., . . . Rapin, W. (2017). Classification of igneous rocks analyzed by ChemCam at Gale crater, Mars. *Icarus*, 265-283.

Cousin, C. R., & Crawford, I. A. (2011). Volcano-Ice Interaction as a Microbial Habitat on Earth and Mars. *Astrobiology*, 695-710.

Crisp, J. A., Adler, M., Matijevic, J. R., Squyres, S. W., Arvidson, R. E., & Kass, D. M. (2003). Mars Exploration Rover mission. *Journal of Geophysical Research Planets*, 17.

Crosta, G. B., Frattini, P., Valbuzzi, E., & De Blassio, F. V. (2018). Introducing a New Inventory of Large Martian Landslides. *Earth and Space Science*, 89-119.

Demant, A., Lestrade, P., Lubala, R. T., Kampunzu, A. B., & Durieux, J. (1994). Volcanological and petrological evolution of Nyiragongo volcano, Virunga volcanic field, Zaire. *Bulletin of Volcanology*, 47-61.

Downs, R. T., & MSLScienceTeam. (2015). Determining Mineralogy on Mars with the CheMin X-Ray Diffractometer. *Elements, 11*, 45-50.

Edwards, C. S., Nowicki, K. J., Christensen, P. R., Hill, J., Gorelick, N., & Murray, K. (2011). Mosaicking of global planetary image datasets: 1. Techniques and data processing for Thermal Emission Imaging System (THEMIS) multi-spectral data. *Journal of Geophysical Research Planets*.

Ehlman, B. L., & Buz, J. (2015). Mineralogy and fluvial history of the watersheds of Gale, Knobel, and Sharp craters: A regional context for the Mars Science Laboratory Curiosity's exploration. *Geophysical Research Letters*, 264-273.

El Maarry, M. R., Gasnault, O., Toplis, M. J., Baratoux, D., Dohm, J. M., Newsom, H. E., . . . Karunatillake, S. (2009). Gamma-ray constraints on the chemical composition of the martian surface in the Tharsis region: A signature of partial melting of the mantle? *Journal of Volcanology and Geothermal Research*, 116-122.

Ellam, R. M., Hawkesworth, C. J., Menzies, M. A., & Rogers, N. W. (1989). The Volcanism of Southern Italy: Role of Subduction and the Relationship Between Potassic and Sodic Alkaline Magmatism. *Jounral of Geophysical Research*, 4589-4601.

Esser, R. P., Kyle, P. R., & McIntosh, W. C. (2004). 40Ar/39Ar dating of the eruptive history of Mount Erebus, Antarctica:. *Bulletin of Volcanology*, 671-686.

Farley, K. A., Malespin, C., Mahaffy, P., Grotzinger, J. P., Vasconcelos, P. M., Milliken, R. E., . . . MSL Science Team. (2014). In Situ Radiometric and Exposure Age Dating of the Martian Surface. *Science*.

Furman, T., Frey, F. A., & Park, K.-H. (1991). Chemical constratins on the petrogenesis of mildly alkine lavas from Vestmannaeyjar, Iceland: The Eldfell (1973) and Surtsey (1963-1967) eruptions. *Contributions to Mineralogy and Petrology*, 19-37.

Gellert, R., Rieder, R., Bruckner, J., Clark, B. C., Dreibus, G., Klingelhofer, G., . . . Squyres, S. W. (2006). Alpha Particle X-Ray Spectrometer (APXS): Results from Gusev crater and calibration report. *Journal of Geophysical Research: Planets*, 32.

Giachetti, T., Paris, R., Kelfoun, K., & Ontowirjo, B. (2012). Tsunami hazard related to a flank collapse of Anak Krakatau Volcano, Sunda Strait, Indonesia. *Geological Society, London, Special Publications*, 79-90.

Golabek, G. J., Keller, T., Gerya, T. V., Zhu, G., Tackley, P. J., & Connolly, J. A. (2011). Origin of the martian dichotomy and Tharsis from a giant impact causing massive magmatism. *Icarus*, 346-357.

Graf, J. E., Zurek, R. W., Eisen, H. J., Jai, B., Johnston, M., & DePaula, R. (2005). The Mars Reconnaissance Orbiter Mission. *Acta Astronautica*, 566-578.

Grant, J. A., Wilson, S. A., Mangold, N., Calef III, F., & Grotzinger, J. P. (2014). The timing of alluvial activity in Gale crater, Mars. *Geophysical Research Letters* , 1142-1148.

Grosse, P., Euillades, P. A., Euillades, L. D., & van Wyk de Vries, B. (2014). A global database of composite volcano morphometry. *Bull Volcanol*, 16.

Grotzinger, J. P., & Milliken, R. E. (2012). The Sedimentary Rock Record of Mars: Distribution, Origins and Global Stratigraphy. *Sedimentary Geology of Mars*, 1-48.

Grotzinger, J. P., Crisp, J. A., Vasavada, A. R., & MSLScienceTeam. (2015). Curiosity's Mission of Exploration at Gale Crater, Mars. *Elements*, 19-26.

Grotzinger, J. P., Crisp, J., Vasavada, A. R., Anderson, R. C., Baker, C. J., Barry, R., . . . Wiens, R. C. (2012). Mars Science Laboratory Mission and Science Investigation. *Space Sci Rev*, 5-56.

Grotzinger, J. P., Gupta, S., Malin, M. C., Rubin, D. M., Schieber, J., Siebach, K., . . . Wilson, S. A. (2015b). Deposition, exhumation, and paleoclimate of an ancient lake deposit, Gale crater, Mars. *Science, 350*(6257), 1-12.

Hare, T. M., Cushing, G., Shinamen, J., Day, B., & Law, E. (2016, July 1). *Context Camera (CTX) Image Mosaics for Mars Human Exploration Zones 5m* . Retrieved from USGS Astrogeology Science Center: http://bit.ly/CTX_EZs

Hargitai, H., & Kereszturi, A. (Eds.). (2015). *Encyclopedia of Planetary Landforms.* New York: Springer.

Higgins, M. D., & Roberge, J. (2007). Three magmatic components in the 1973 eruption of Eldfell volcano, Iceland: Evidence from plagioclase crystal size distribution (CSD) and geochemistry. *Journal of Volcanology and Geothermal Research*, 247-260.

Hurowitz, J. A., Grotzinger, J. P., Fischer, W. W., McLennan, S. M., Milliken, R. E., Stein, N., . . . Wiens, R. C. (2017). Redox stratification of an ancient lake in Gale Crater, Mars. *Science*, 1-10.

Irwin III, R. P., Watters, T. R., Howard, A. D., & Zimbelman, J. R. (2004). Sedimentary resurfacing and fretted terrain development along the crustal dichotomy boundary, Aeolis Mensae, Mars. *Journal of Geophysical Research, 109*(E09011), 20.

Jakobsson, S. P., Pedersen, A. K., Ronsbo, J. G., & Melchior Larsen, L. (1973). Petrology of mugearite-hawaiite: Early extrusives in the 1973 Heimaey eruption, Iceland. *Lithos*, 203-214.

Johannsen, A. (1931). *A Descriptive Petrolgraphy of Igneous Rocks.* Chicago: The University of Chicago Press.

Lanagan, P. D., McEwen, A. S., & Keszthelyi, L. P. (2001). Rootless cones on Mars indicating the presence of shallow equatorial ground ice in recent times. *Geophysical Research Letters*, 2365-2367.

Le Bas, M. J., Le Maitre, R. W., Streckeisen, A., & Zanettin, B. (1986). A Chemical Classification of Volcanic Rocks Based on the Total Alkali-Silica Diagram. *Journal of Petrology*, 745-750.

Le Deit, L., Hauber, E., Fueten, F., Pondrelli, M., Rossi, A. P., & Jaumann, R. (2013). Sequence of infilling events in Gale Crater, Mars: Results from morphology, stratigraphy, and mineralogy. *Journal of Geophysical Research: Planets*, 2439-2473.

Lipman, P. W., Normark, W. R., Moore, J. G., Wilson, J. B., & Gutmacher, C. E. (1988). The Giant Submarine Alika Debris Slide, Mauna Loa, Hawaii. *Journal of Geophysical Research, 93*(B5), 4279-4299.

Malin, M. C., Bell III, J. F., Cantor, B. A., Caplinger, M. A., Calvin, W. M., Clancy, R. T., . . . Wolff, M. J. (2007). Context Camera Investigation on board the Mars Reconnaissance Orbiter. *Journal of Geophysical Research Planets*.

Mangold, N., Schmidt, M. E., Fisk, M. R., Forni, O., McLennan, S. M., Ming, D. W., . . . Wiens, R. C. (2017). Classification scheme for sedimentary and igneous rocks in Gale crater, Mars. *Icarus, 284*, 1-17.

Marshak, S. (2008). *earth Portrait of a Planet.* New York: W.W. Norton & Company, Inc.

McEwen, A. S., Eliason, E. M., Bergstrom, J. W., Bridges, N. T., Hansen, C. J., Delamere, W. A., . . . Weitz, C. M. (2007). Mars Reconnaissance Orbiter's High Resolution Imaging Science Experiment. *Journal of Geophysical Research Planets*.

McLennan, S. M., Anderson, R. B., Bell III, J. F., Bridges, J. C., Calef III, F., Campbell, J. L., . . . MSLScienceTeam. (2014). Elemental Geochemistry of Sedimentary Rocks at Yellowknife Bay, Gale Crater, Mars. *Science*, 1-10.

McSween Jr, H. Y., Taylor, G. J., & Wyatt, M. B. (2009). Elemental Composition of the Martian Crust. *Science*, 736-739.

McSween, H. Y., Arvidson, R. E., Bell III, J. F., Blaney, D., Cabrol, N. A., Christensen, P. R., . . . Zipfel, J. (2004). Basaltic Rocks Analyzed by the Spirit Rover in Gusev Crater. *Science*, 842-845.

McSween, H. Y., Murchie, S. L., Crisp, J. A., Bridges, N. T., Anderson, R. C., Bell III, J. F., . . . Wanke, H. (1999). Chemical, multispectral and textureal constraints on the composition and origin of rocks at the Mars Pathfinder landing site . *Journal of Geophysical Research*, 8679-8715.

Meresse, S., Costard, F., Mangold, N., Masson, P., Neukem, G., & HRSCTeam. (2008). Formation and evolution of the chaotic terrains by subsidence and magmatism: Hydraotes Chaos, Mars. *Icarus*, 487-500.

Michalski, J. R., & Bleacher, J. E. (2013). Supervolcanoes within an ancient volcanic province in Arabia Terra, Mars. *Nature*, 47-52.

Milliken, R. E., Grotzinger, J. P., & Thomson, B. J. (2010). Paleoclimate of Mars as captured by the stratigraphic record in Gale Crater. *Geophysical Research Letters*.

Minin, M., Vargas, L., Fueten, F., Stesky, R., & Hauber, E. (2015). A new automated technique within ArcGIS to compute the attitudes of planar topographic features. *LPSC XLVI*, 1-2.

Monders, A. G., Medard, E., & Grove, T. L. (2007). Phase equilibrium investigtions of the Adirondack class basalts from the Gusev plains, Gusev crater, Mars. *Meteoritics & Planetary Science*, 131-148.

Moore, J. G., & Clague, D. A. (1992). Volcano growth and evolution of the island of Hawaii. *Geological Society of America Bulletin*, 1471-1484.

Morris, R. V., Vaniman, D. T., Blake, D. F., Gellert, R., Chipera, S. J., Rampe, E. B., . . . Schwenzer, S. P. (2016). Silicic volcanism on Mars evidenced by tridymite in high-SiO2 sedimentary rock at Gale crater. *Proceedings of the National Academy of Sciences of the United States of America, 113*(26), 7071-7076.

Neukum, G., & Jaumann, R. (2004). HRSC: the High Resolution Stereo Camera of Mars Express. In A. Wilson, *Mars Express The Scientific Payload* (pp. 17-35). Noordwijk: ESA Publications Division.

Newsom, H. E., Scuderi, L. A., Gallegos, Z. E., Tornabene, L. L., & Wiens, R. C. (2019). REVISED LARGER WATERSHED OF THE MULTI-STAGE PEACE VALLIS ALLUVIAL FAN SYSTEM, GALE CRATER, MARS. *50th Lunar and Planetary Sciences Conference* (p. 2). Houston: Lunar and Planetary Institute and NASA Johnson Space Center.

Ojha, L., Lewis, K., Karunatillake, S., & Schmidt, M. E. (2018). Global Dust from the Deflation of the Medusae Fossae Formation on Mars. Houston: Lunar and Planetary Science Conference 2018.

Palucis, M. C., Dietrich, W. E., Hayes, A. G., Williams, R. M., Gupta, S., Mangold, N., . . . Sumner, D. Y. (2014). The origin and evolution of the Peace Vallis fan system that drains to the Curiosity landing area, Gale Crater, Mars. *Jounral of Geophyscal Research: Planets*, 705-728.

Papike, J. J. (Ed.). (1998). *Planetary Materials.* Washington DC: The Mineralogical Society of America.

Parfitt, E. A., & Wilson, L. (2011). *Fundamentals of Physical Volcanology.* Malden: Blackwell Publsihing.

Platz, T., Byrne, P. K., Massironi, M., & Hiesinger, H. (2015). Volcanism and tectonism across the inner solar system: an overview. *Geological Society, London, Special Publications*, 1-56.

Plescia, J. B. (2004). Morphometric properties of Martian volcanoes. *Journal of Geophysical Research*, 26.

Presley, T. K., Sinton, J. M., & Pringle, M. (1997). Postshield volcanism and catastrophic mass wasting of the Waianae Volcano, Oahu, Hawaii. *Bulletin of Volcanology, 58*(8), 597-616.

Ritter, D. F., Kochel, R. C., & Miller, J. R. (2011). *Process Geomorphology* (5th ed.). Long Grove: Waveland Press, Inc.

Robbins, S. J., Di Achille, G., & Hynek , B. M. (2011). The volcanic history of Mars: High-resolution crater-based studies of the calderas of 20 volcanoes. *Icarus*, 1179-1203.

Rotto, S., & Tanaka, K. L. (1995). Geologic/geomorphic map of the Chryse Planitia Region of Mars, 1:5000,000. *U.S. Geol. Surv. Misc. Invest. Ser. Map I-2441-A*.

Sautter, V., Fabre, C., Forni, O., Toplis, M. J., Cousin, A., Ollila, A. M., . . . Pinet, P. (2014). Igneous mineralogy at Bradbury Rise: The first ChemCam campaign at Gale Crater. *Journal of Geophysical Research: Planets*, 30-46.

Sautter, V., Toplis, M. J., Wiens, R. C., Cousin, A., Fabre, C., Gasnault, O., . . . Wray, J. J. (2015). In situ evidence for continental crust on early Mars. *Nature Geoscience*, 605-609.

Schmidt, M. E., & McCoy, T. J. (2010). The evolution of a heterogeneous Martian mantle: Clues from K, P, Ti, Cr, and Ni variations in Gusev basalts and shergottite meteorites. *Earth and Planetary Science Letters*, 67-77.

Schmidt, M. E., Campbell, J. L., Gellert, R., Perrett, G. M., Treiman, A. H., Blaney, D. L., . . . Wiens, R. C. (2014). Geochemical Diversity in first rocks examined by the Curiosity Rover in Gale Crater: Evidence for and significance of an alkali and volatile-rich igneous source. *Journal of Geophysical Research: Planets*, 1-18.

Schmidt, M. E., Izawa, M. R., Thomas, A. P., Thompson, L., & Gellert, R. (2017). Diverse Igneous Protolith Contributions to Sediments in Gale Crater: Variable Metasomatism of the Mars Mantle. *48th Lunar and Planetary Science Conference.* Houston.

Schmidt, M. E., Perrett, G. M., Bray, S. L., Bradley, N. J., Lee, R. E., Berger, J. A., . . . Tesselaar, D. (2018). Dusty Rocks in Gale Crater: Assessing Areal Coverage and Separating Dust nad Rock Contributions in APXS Analyses. *Journal of Geophysical Research: Planets, 123*, 1649-1673.

Schmidt, M., Izawa, M., Thomas, A., Thompson, L., & Gellert, R. (2017). Diverse Igneous Protolith Contributions to Sediments in Gale Crater: Variable Metasomatism of the Mars Mantle. *Lunar and Planetary Science XLVIII* (p. 2). Houston: Lunar and Planetary Science.

Scott, E. D., & Wilson, L. (2002). Plinian eruptions and passive collapse events as mechanisms of formation for Martian pit chain craters. *Journal of Geophysical Research, 107*(E4), 11.

Seyitoglu, G., Anderson, D., Nowell, G., & Scott, B. (1997). The evolution of Miocene potassic to Quaternary sodic magmatism in western Turkey: implications for enrichment processes in the lithospheric mantle. *Journal of Volcanology and Geothermal Research* , 127-147.

Siebach, K. L., Baker, M. B., Grotzinger, J. P., McLennan, S. M., Gellert, R., Thompson, L. M., & Hurowitz, J. A. (2017). Sorting out compositional trends in sedimentary rocks of the Bradbury group (Aeolis Palus), Gale crater, Mars. *Journal of Geophysical Research: Planets, 122*, 295-328.

Siebert, L. (1984). Large Volcanic Debris Avalanches: Characteristics of Source Areas, Deposits, and Associated Eruptions. *Journal of Volcanology and Geothermal Research*, 163-197.

Sigurdsson, H., Houghton, B., McNutt, S. R., Rymer, H., & Stix, J. (. (2000). *Encyclopedia of Volcanoes.* San Diego: Academic Press.

Smith, D., Neumann, G., Ford, P., Guiness, E. A., & Slavney, S. (1999). Mars Global Surveyor Laser Altimeter Precision Experiment Data Record. *NASA Planetary Data System, MGS-M-MOLA-3-PEDR-L1A-V1.0, vols. MGSL_0001 - MGSL_0002*.

Šrámek, O., & Zhong, S. (2012). Martian crustal dichotomy and Tharsis formation by partial melting coupled to early plume migration. *Journal of Geophysical Research*, 1-14.

Stewart, E. M., & Head, J. W. (2001). Ancient Martian volcanoes in the Aeolis region: New evidence from MOLA data. *Journal of Geophysical Research Planets*, 17505-17513.

Stolper, E. M., Baker, M. B., Newcombe, M. E., Schmidt, M. E., Treiman, A. H., Cousin, A., . . . MSL_Science_Team. (2013). The Petrochemistry of Jake_M: A Martian Mugearite. *Science*, 1-7.

Sun, S. -s., & McDonough, W. F. (1989). Chemical and isotopic systematics of oceanic basalts: implications for mantle composition and processes. In A. D. Saunders, & M. J. Norry (Eds.), *Magmatism in the Ocean Basins* (pp. 313-345). Geological Society Special Publication.

Tanaka, K. L., Skinner Jr, J. A., Dohm, J. M., Irwin III, R. P., Kolb, E. J., Fortezzo, C. M., . . . Hare, T. M. (2014). Geologic Map of Mars. *U.S. Geological Survey*.

Thompson, L. M., Schmidt, M. E., Spray, J. G., Berger, J. A., Fairen, A. G., Campbell, J. L., . . . VanBommel, S. J. (2016). Potassium-rich sandstones within the Gale impact crater, Mars: The APXS perspective. *Journal of Geophysical Research: Planets*, 1981-2003.

Thomson, B. J., Bridges, N. T., Milliken, R., Baldridge, A., Hook, S. J., Crowley, J. K., . . . Weitz, C. M. (2011). Constraints on the origin and evolution of the layered mound in Gale Crater, Mars using Mars Reconnaissance Orbiter data. *Icarus*, 413-432.

Thornton, C. P., & Tuttle, O. F. (1960). Chemistry of Igneous Rocks I. Differentiation Index*. *American Journal of Science*, 664-684.

Thouret, J.-C. (1999). Volcanic geomorphology - and overview. *Earth Science Reviews*, 95-131.

Treiman, A. H., Bish, D. L., Vaniman, D. T., Chipera, S. J., Blake, D. F., Ming, D. W., . . . Yen, A. S. (2015). Mineralogy, provenance, and diagenesis of a potassic basaltic sandstone on Mars: CheMin X-ray diffraction of the Windjana sample (Kimberly area, Gale Crater). *Journal of Geophysical Research: Planets*, 75-106.

Vaniman, D. T., Bish, D. L., Ming, D. W., Bristow, T. F., Morris, R. V., Blake, D. F., . . . Spanovich, N. (2014). Mineralogy of a Mudstone at Yellowknife Bay, Gale Crater, Mars. *Science, 343*, 9.

Wänke, H., & Dreibus, G. (1988). Chemical Composition and Accretion History of Terrestrial Planets. *Philos. Trans. R. Soc. London*, 545-557.

Werner, S. C. (2009). The global martian volcanic evolutionary history. *Icarus*, 44-68.

Wilson, L., & Head III, J. W. (1994). Mars: Review and Analysis of Volcanic Eruption Theory and Relationships to Observed Landforms. *Review of Geophysics*, 221-263.

Wray, J. J., Hansen, S. T., Dufek, J., Swayze, G. A., Murchie, S. L., Seelos, F. P., . . . Ghiorso, M. S. (2013). Prolonged magmatic activity on Mars inferred from the detection of felsic rocks. *Nature Geoscience*, 1013-1017.

Wyrick, D., Ferrill, D. A., Morris, A. P., Colton, S. L., & Sims, D. W. (2004). Distribution, morphology, and origins of Martian pit crater chains. *Journal of Geophysical Research, 109*(E06005), 20.

Yen, A., Morris, D., Ming, D., Gellert, R., Thompson, L., Bristow, T., . . . Chipera, S. (2017). Hydrothermal Signatures in Gale Crater.

Zegers, T. E., Oosthoek, J. H., Rossi, A. P., Blom, J. K., & Schumacher, S. (2010). Melt and collapse of buried water ice: An alternative hypothesis for the formation of chaotic terrains on Mars. *Earth and Planetary Science Letters, 297*, 496-504.

Appendix

Morphological Map - A morphological map of the NGL and surrounding area consisting of 25 units classified using visible and thermal infrared orbital images. A set of CTX images was used as a basemap for production of the morphological map. The surface was divided into different morphologies using criteria such as tone, texture, crater content, landforms and THEMIS Night IR data. The morphological map was created to provide more detail of the northern Gale Crater region than shown in the current Geological Map of Mars (Tanaka, et al., 2014).

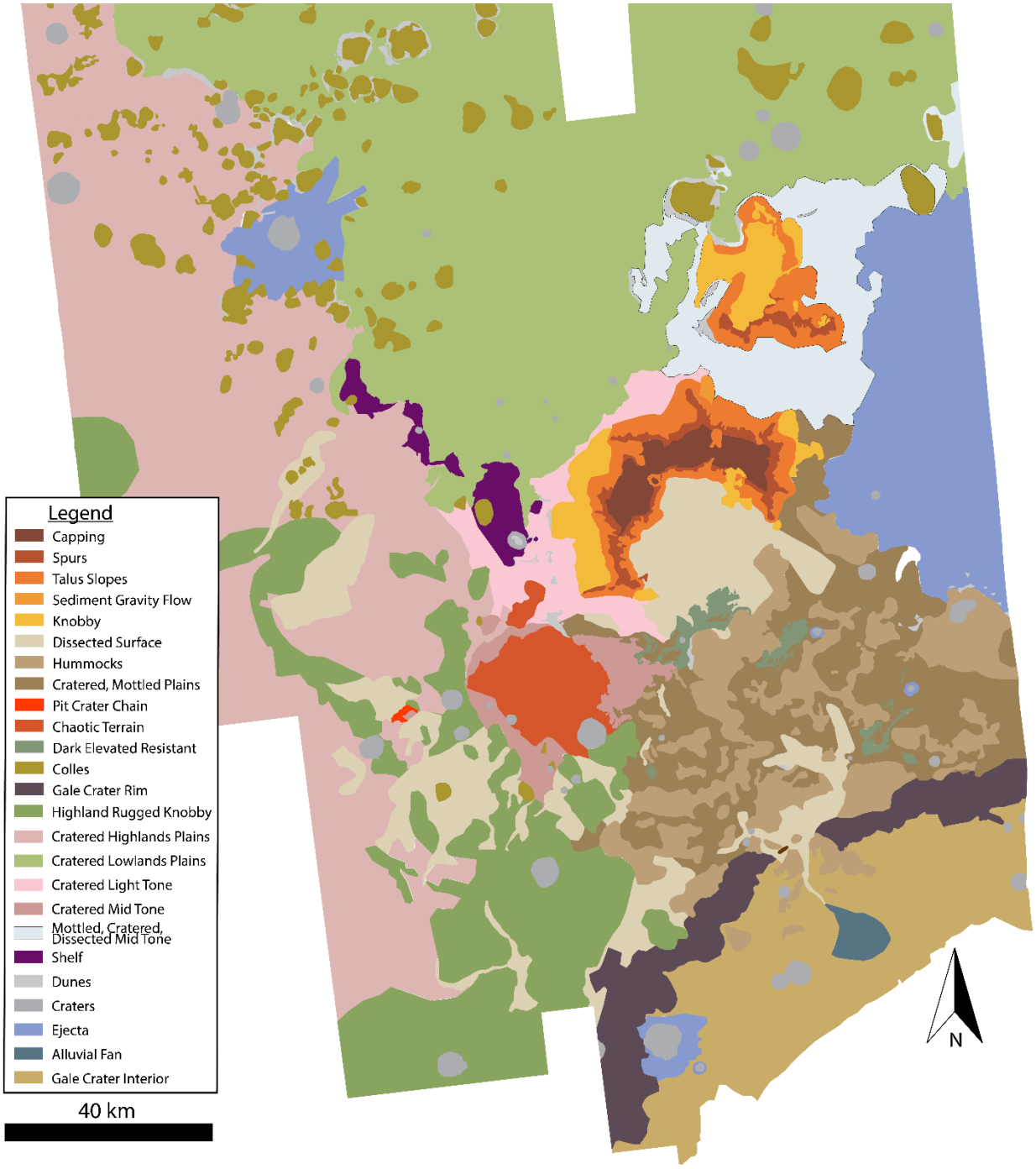

Unit Descriptions

Locations for images used to describe each unit.

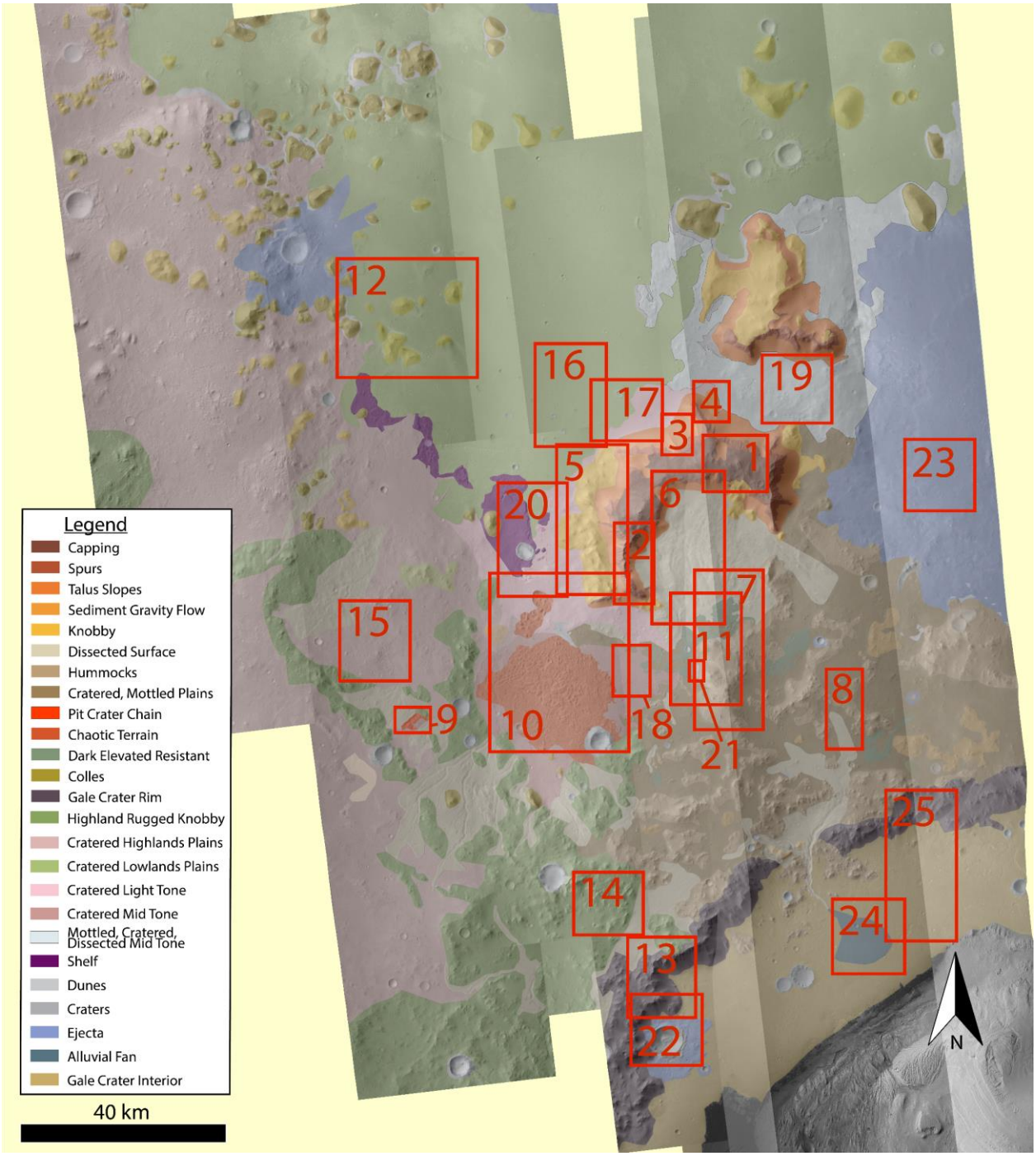

1. Capping Unit - Resistant capping unit on top of NGL with smooth and mottled textures. It is sparsely cratered and has depressions and rises (small hills, platforms, and ridges). The capping unit appears dark with bright areas on the edges of internal features in THEMIS Night IR images, indicating an unconsolidated surface (dust, sediments, etc.) covering an indurated material underneath. The center of the capping unit has a higher relief than near the edges and slopes towards the spur unit that lines the exterior of the capping unit. The eastern side of the capping unit is higher than the western side.

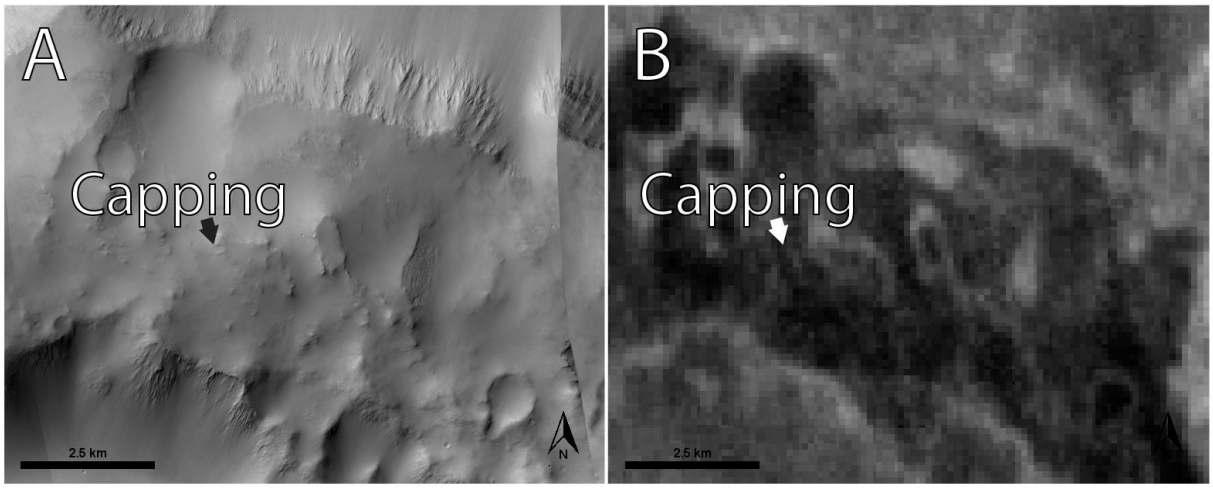

2. Spurs Unit - The rocky outcrops surrounding the capping unit extend radially outward as branching spurs (spur unit) around portions of the NGL. The spur unit appears bright under THEMIS Night IR, indicating indurated material not covered in dust/sediments. There are several radial spurs on NGL that extend up to 10 km from the capping unit and range in relief from level with the capping unit (~35m) to within a couple hundred meters of the surrounding terrain's elevation (~-2300m). The lower terminus of the spurs may be buried in talus or other sediment deposits.

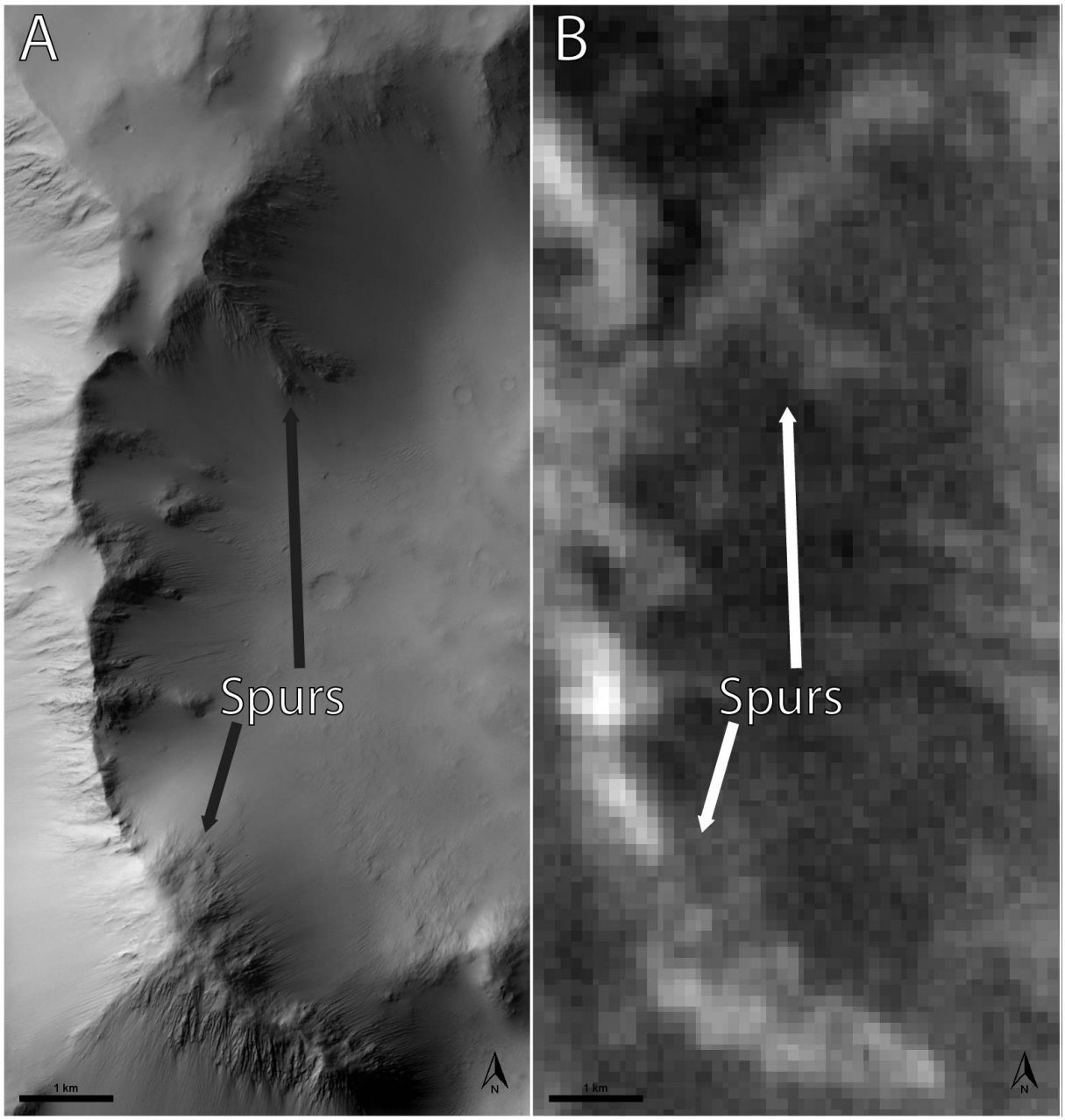

3. Talus Slopes Unit - The talus slopes surrounding NGL occur downslope from the spur unit and capping unit. Talus slopes often have linear streaks (bright/dark on mid tone in CTX images) that point downslope. In THEMIS Night IR, the talus slopes are slightly lighter than the capping unit but are darker than the spurs, indicating a friable, unconsolidated surface with a larger grain size than the dust/sediment covering the capping unit. There are no boulders observed in the talus slopes in HiRISE images (up to 30 cm/pixel). There are few elliptical craters in the talus slopes of the amphitheatre interior and none on the exterior slopes, indicating poor crater retention.

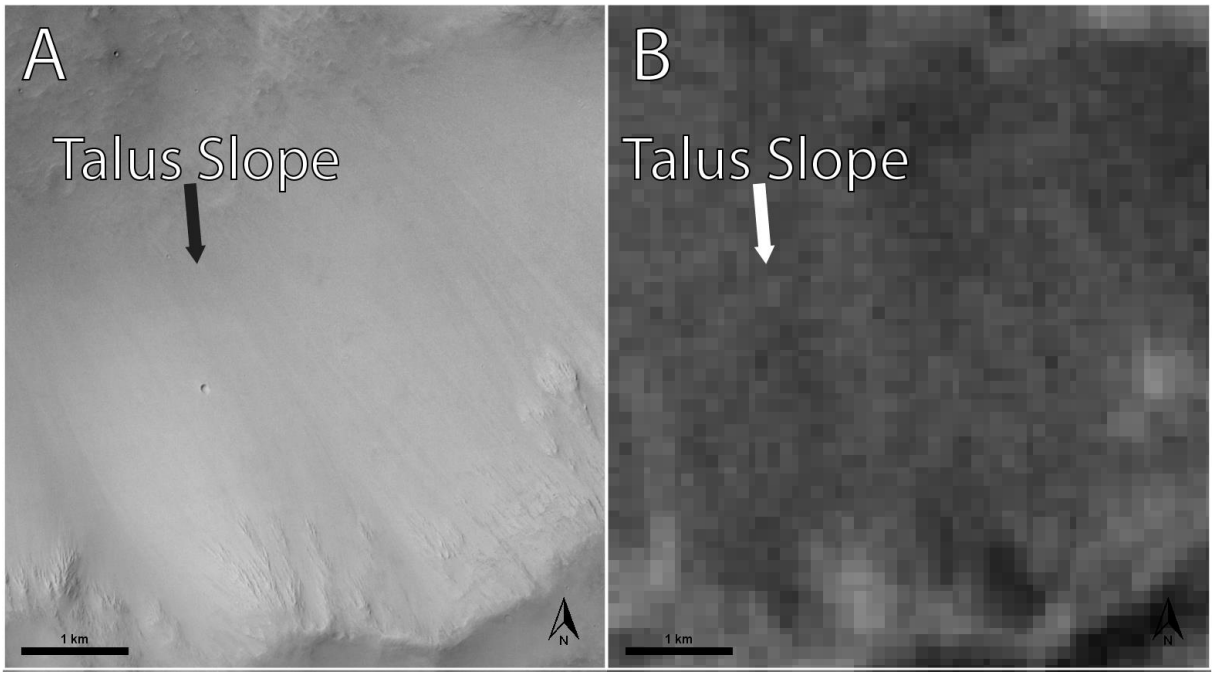

4. Sediment Gravity Flow Unit - A leveed sediment gravity flow (~2 x 5 km, possibly a slump or debris flow) occurs at the north side of NGL. The sediment gravity flow appears to have pushed up material as it moved and created a large lip (approximately 25 m higher relief than material in the flow) at the end of the flow. The edges of the flow are also elevated above the interior portion.

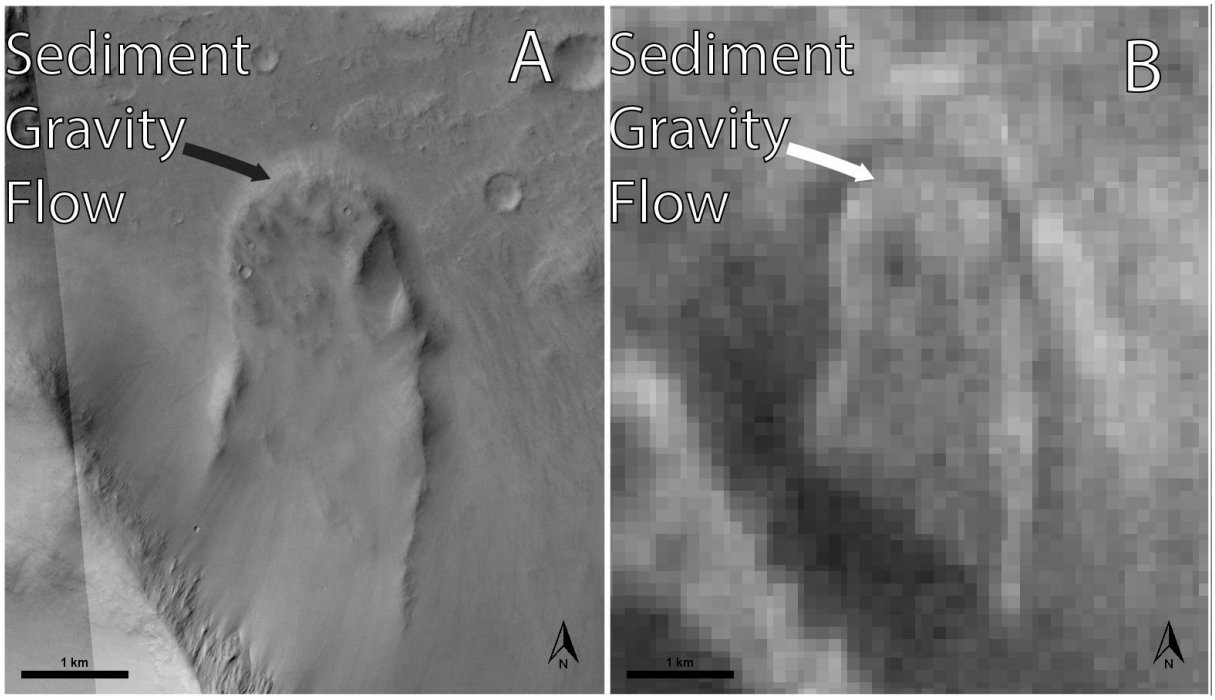

5. Knobby Unit - A knobby unit occurs below the talus slopes on the western exterior and northeastern interior of NGL. They have a knobby appearance with indurated spurs (bright THEMIS Night IR with a softer, darker, eroded appearance compared to spur unit) on top of friable debris aprons (dark THEMIS Night IR with sporadic craters and dunes compared to talus slope unit) and are either at the base of the talus slopes (exterior) or on the slope itself (interior). Knobs appears mottled and consolidated. They are also brighter than the talus slopes in THEMIS Night IR but darker than the spurs so we interpret the knobby unit to represent an accumulated debris apron with large slump blocks that originated from the capping unit suggesting the knobby unit may have been part of the capping/spur unit before being transported downslope. Where in association with the knobby unit, the talus slopes are interpreted to represent scarps of mass movement.

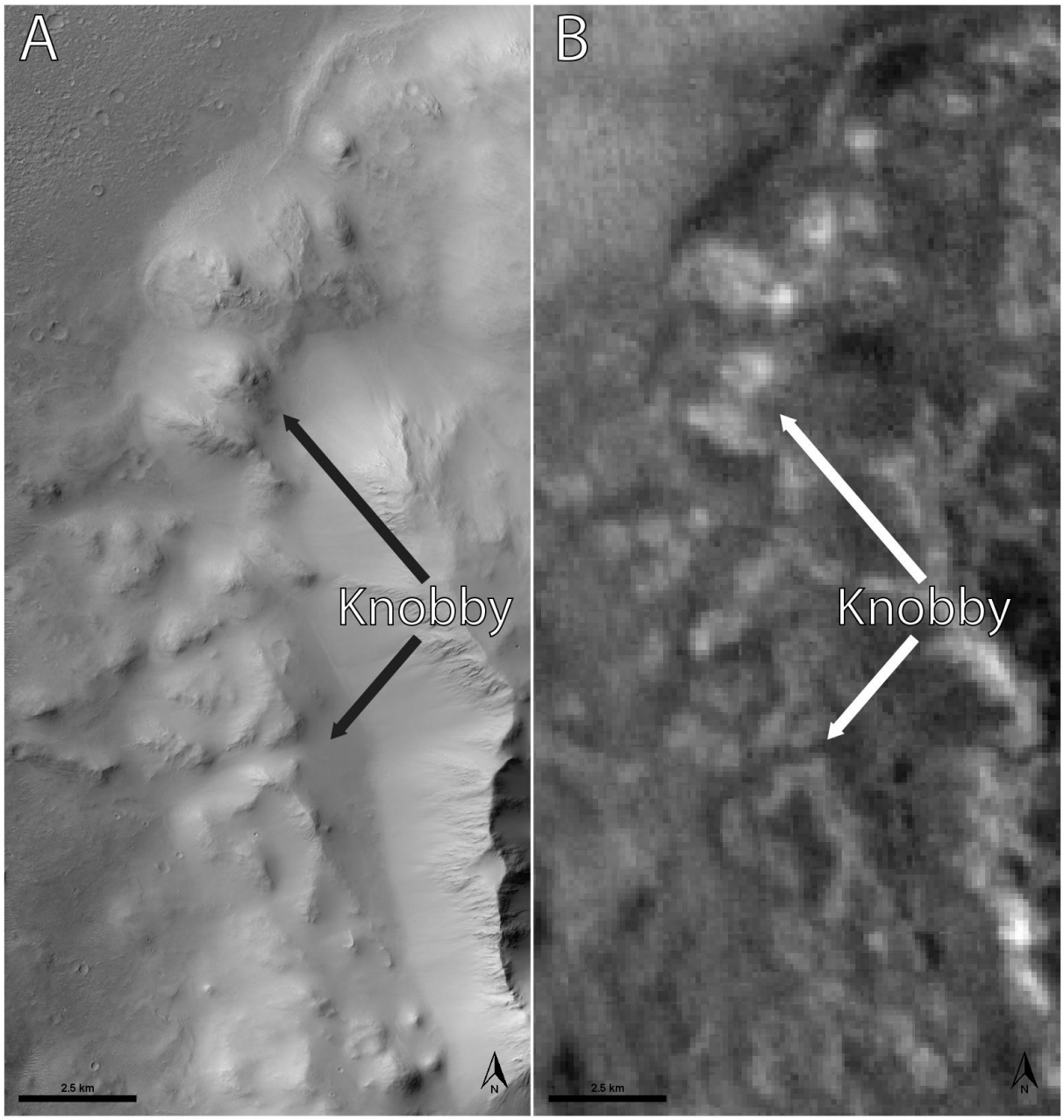

6. Dissected Surface Unit - Surfaces which have large channels on the surface which could have contained flowing water at one point in the past. The channels appear to be much wider than they are deep and have a branching pattern to them. The bottoms of the channels have a dark to light-medium appearance in THEMIS Night IR. The surface is brighter on channel banks, the center of the larger channels is dark, and the surface has medium brightness away from the channels/banks. This suggests there are fine sediments in the interior of the channels, less sediment coverage on the banks of the channel (possibly indurated material) and friable material covering the surface away from the channels. The amphitheatre in NGL has a heavily dissected surface with many channels oriented mostly north-south. Peace Vallis and its catchment have fewer large channels in them.

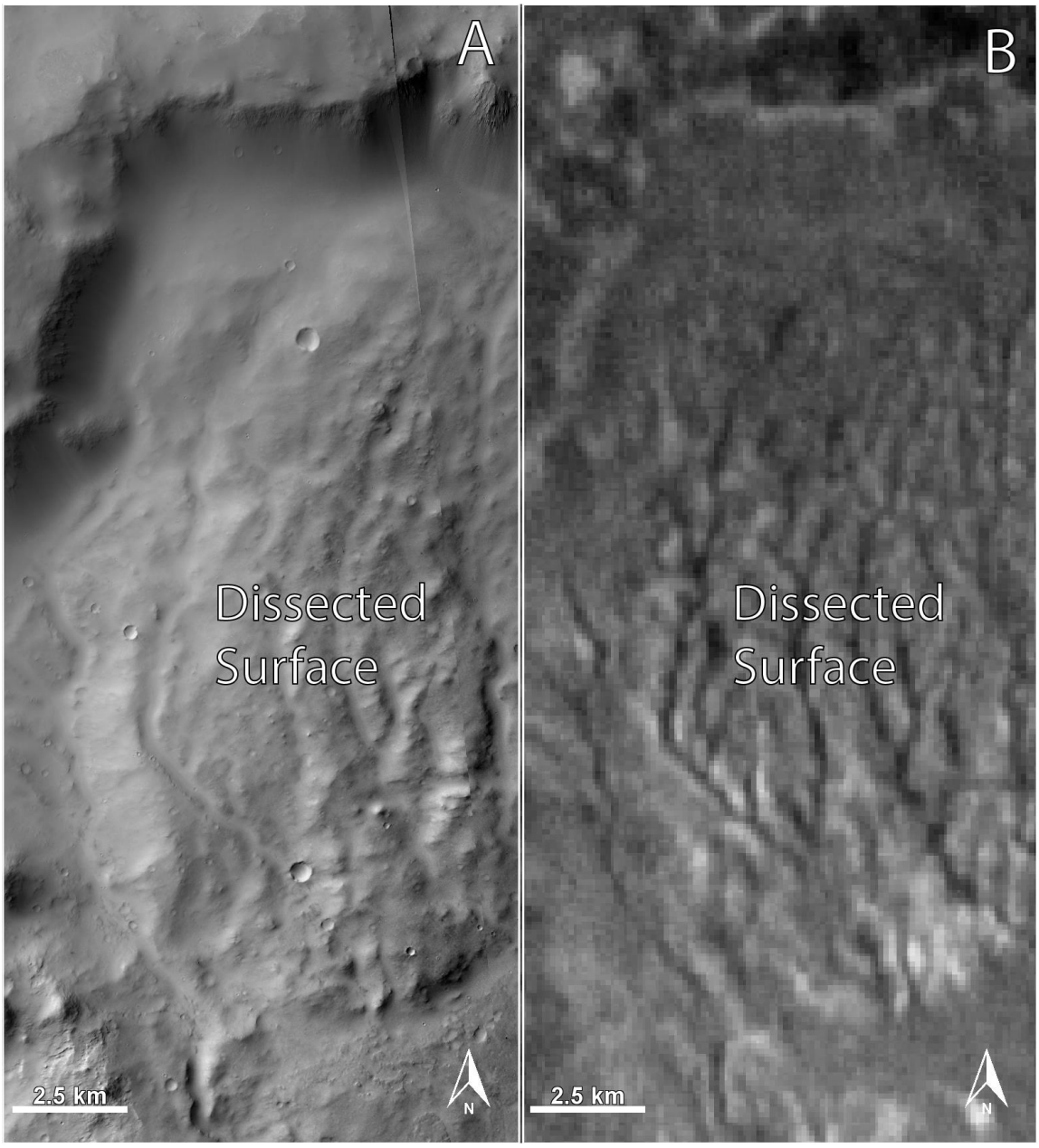

7. Hummocks Unit - Hummocks unit consists of large, irregularly shaped hills that only appears in the area between NGL and the northern rim of Gale Crater in a fan shape about 40 km long. The hummocks appear in clusters most often, sometimes the groups of hummocks form a linear, longitudinal ridge rising above the dissected, cratered plains surrounding it. Some of the hummocks have visible spurs however they are not as prominent as the spurs on the rim of Gale Crater or on NGL. Hummocks of all sizes have some talus on the steeper slopes and possibly unconsolidated debris piled up between the blocks.

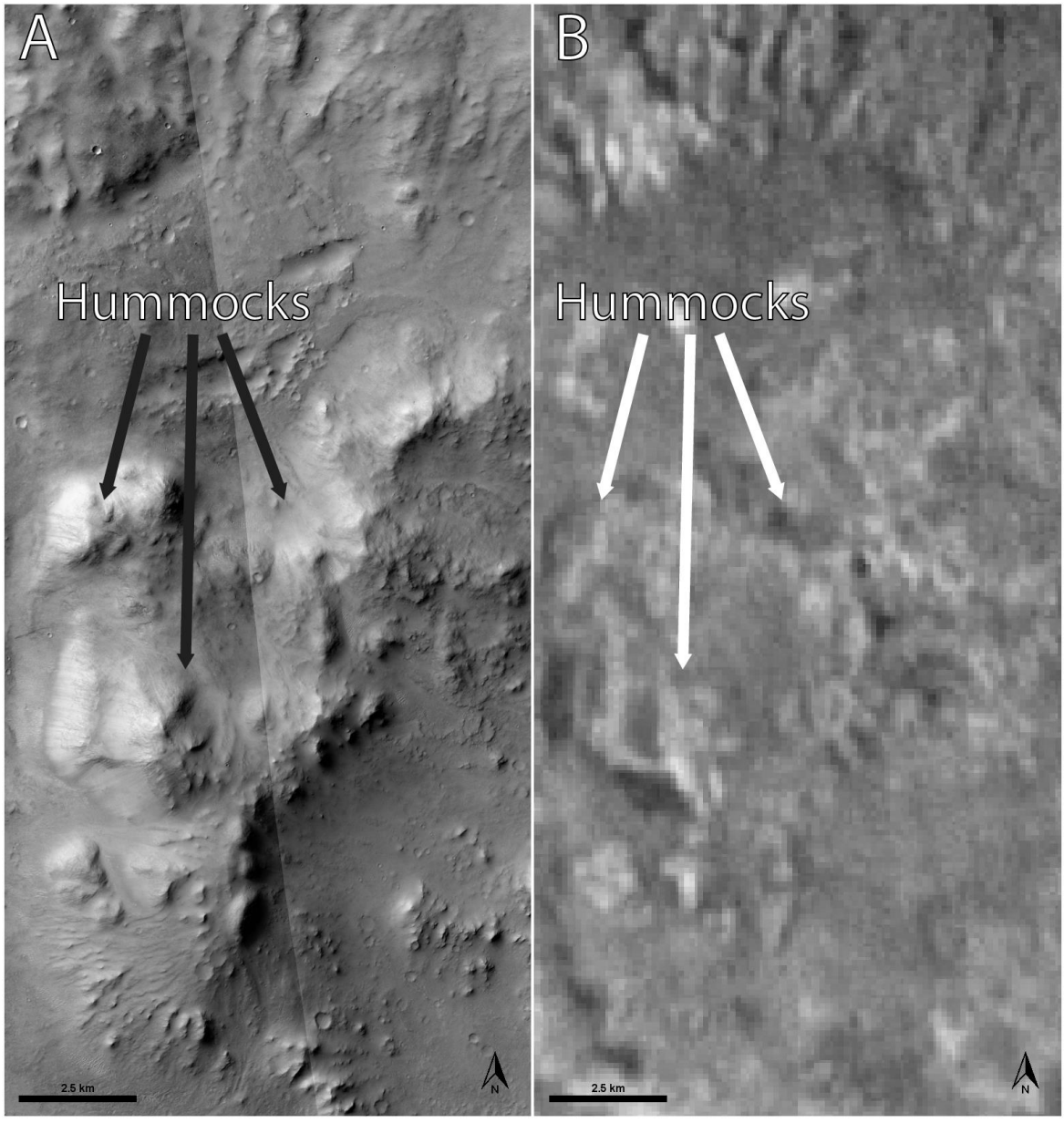

8. Cratered, Mottled Plains Unit - Cratered, mottled plains unit appears in between the hummocks and is visible between NGL and the rim of Gale Crater. The unit has a moderately cratered and mottled surface. It is mid toned in visible images and medium to dark in THEMIS Night IR.

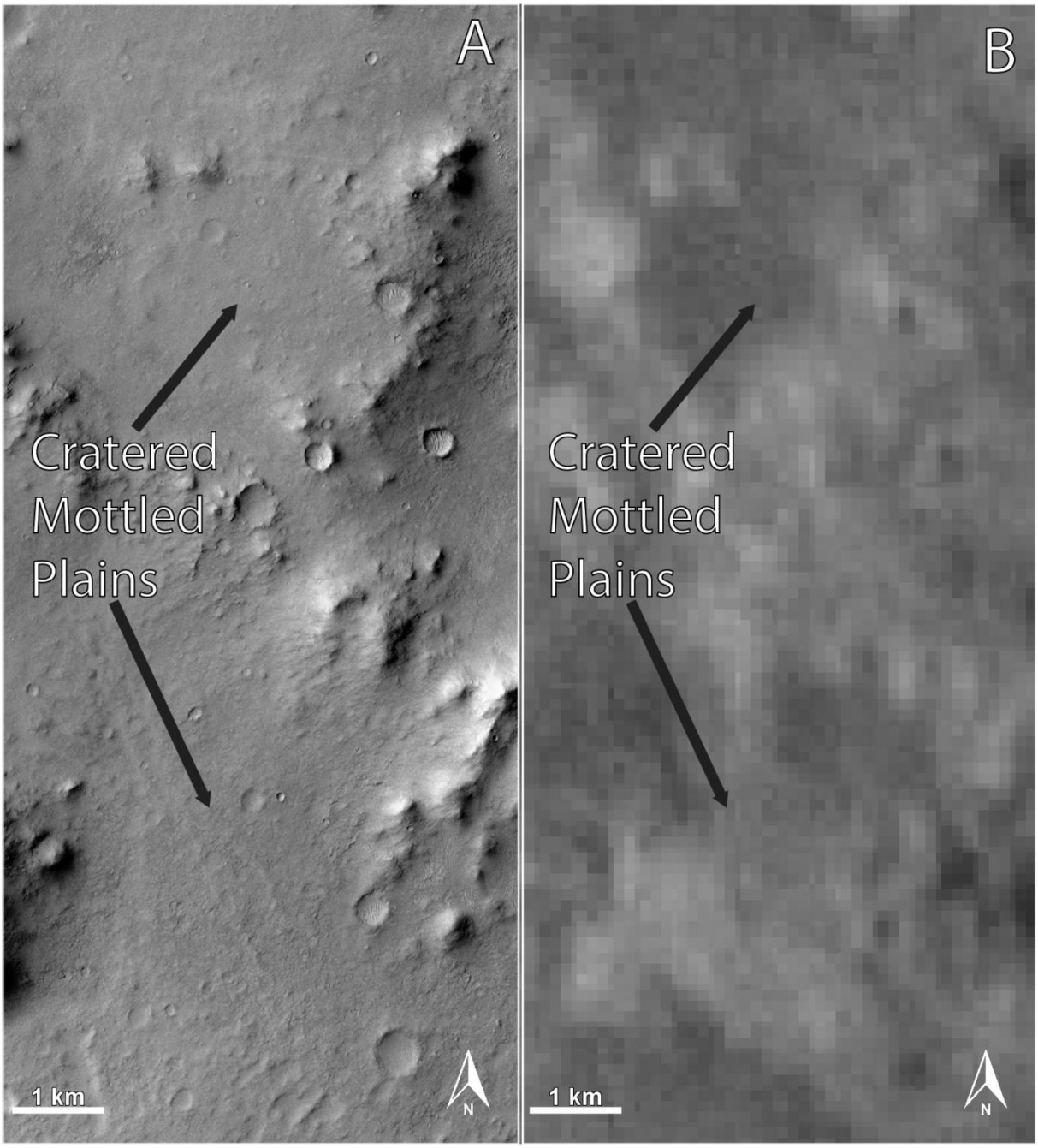

9. Pit Crater Chain Unit - Pit crater chain unit is ~40 km west-southwest of NGL. It is a linear series of craters that are connected together. Pit crater chains are features formed by the collapse of the surface into a significant void space below the surface (Wyrick, et al., 2004). The void spaces are thought to have several different methods of formation; several hypotheses include volcanic or tectonic processes: collapsing of a lava tube or magma chamber, dike swarms, and fissuring beneath a loose surface (Scott & Wilson, 2002; Wyrick, et al., 2004). The pit crater chain near NGL is oriented NE-SW; the same orientation as the regional fabric and perpendicular to the amphitheatre opening suggesting there may be some tectonic relationship with NGL.

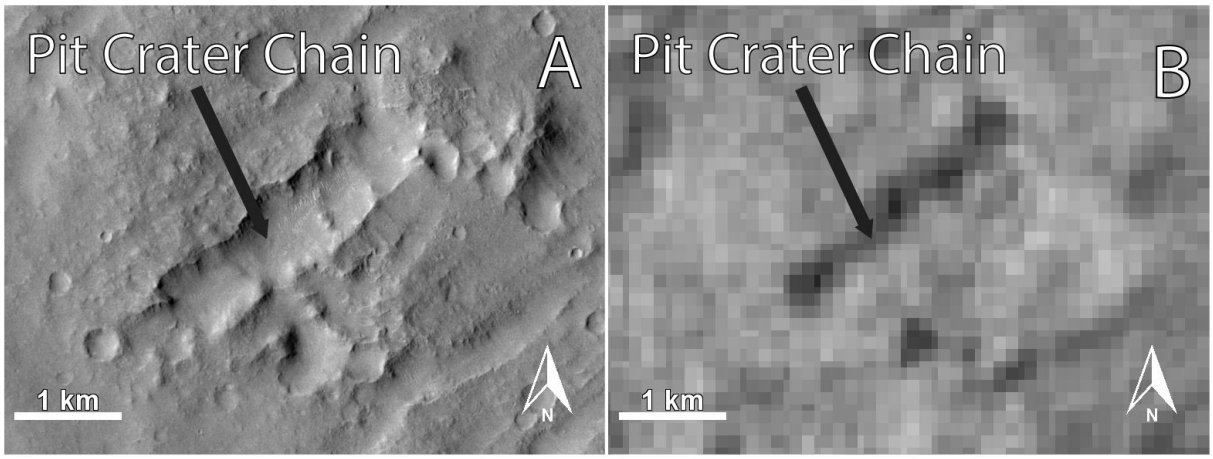

10. Chaotic Terrain Unit - Chaotic terrain unit is ~10 km southwest of NGL. It is a rounded rectangular area (15-km by 14 km) that has a surface broken into many polygonal blocks with quasi-linear depressions between them. The blocks are up to 1 km and there are a wide range of block sizes present (10s of m to ~1 km). The depressions are up to several 10s of meters below the blocks and up to 100s of meters wide. Chaotic terrain has been hypothesized to be the result of sublimation of ground ice due to reaction with a magma body, release of liquid CO_2 from gas hydrates or breach of confined subterranean aquifers (Meresse, et al., 2008).

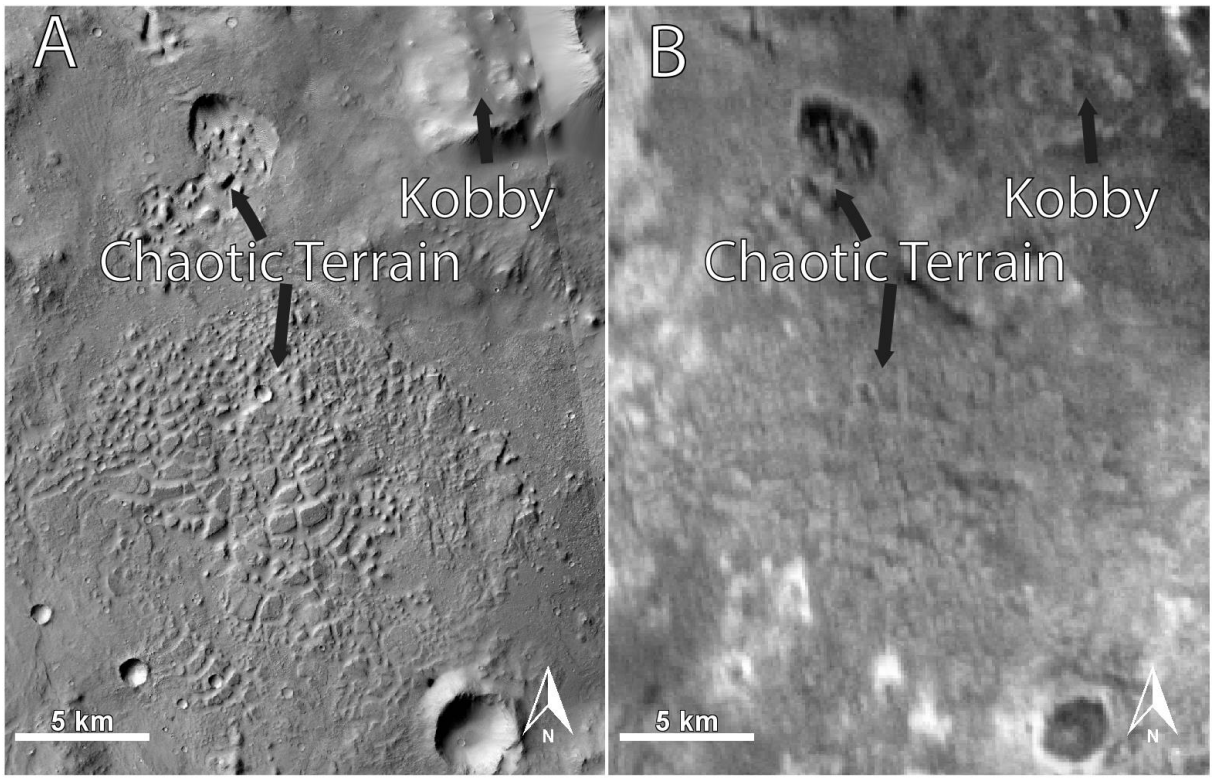

11. Dark Elevated Resistant Unit - The dark elevated resistant unit is raised relative to the cratered, mottled plains as indicated by shadows in CTX images; the elevation difference too small for MOLA interpretation. It has a higher relief than the cratered, mottled plains unit however it may be more resistant to deflation instead. It is darker tone than the other units as well. There are small craters covering the surface and it has irregular edges. There are large portions of this unit near the base of NGL and some other portions near Gale Crater. There are sections in the cratered, mottled plains between NGL and Gale Crater as well as in the cratered lowlands plains north of Gale Landform.

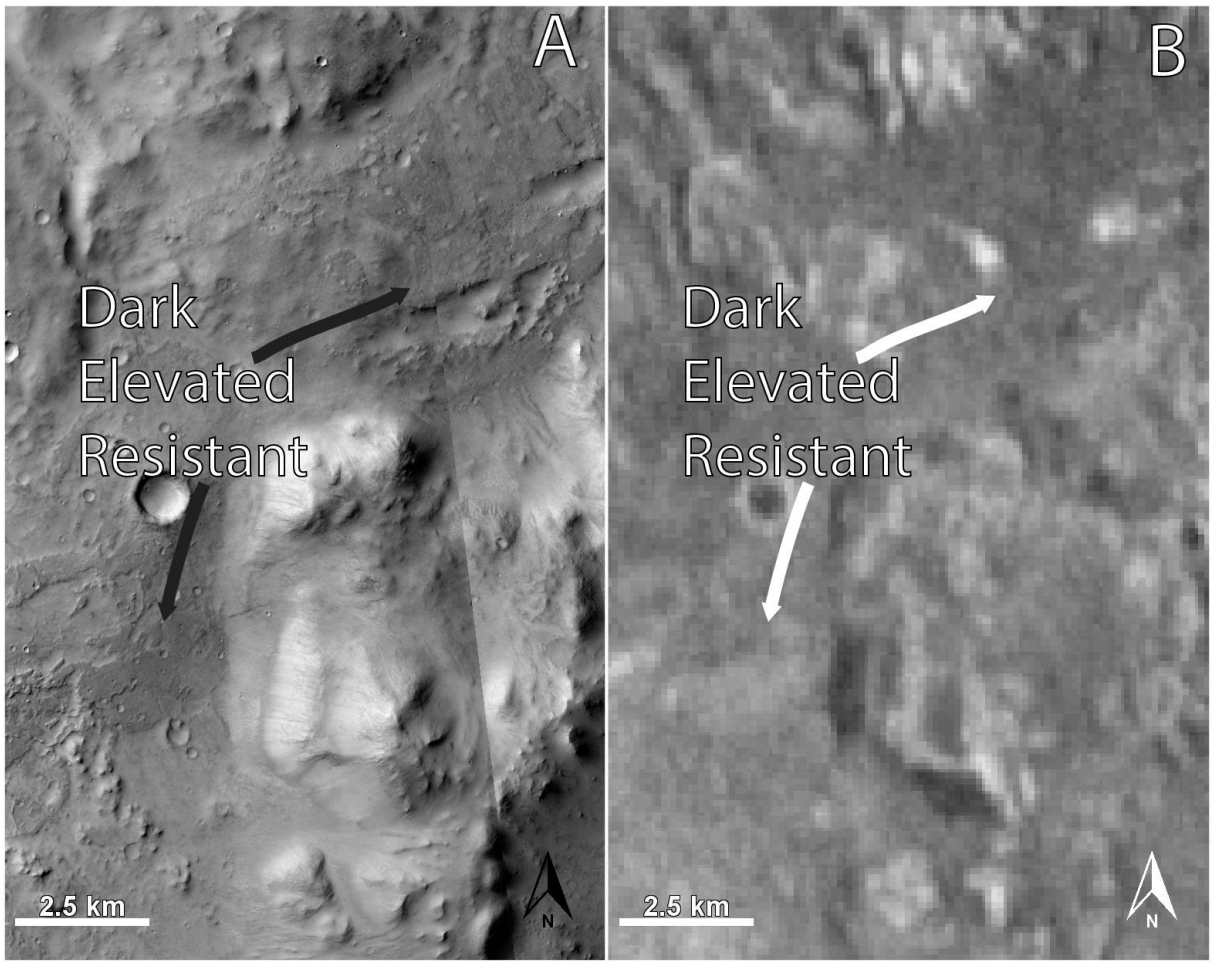

12. Colles Unit - Colles are small hills or knobs usually less than 1 km high and may be several km in diameter (Rotto & Tanaka, 1995). The colles often appear in groups but some can be spread out further. The colles can be solitary or very close to others. Colles appear in shapes ranging from square to circular to elongated. They could be associated with the mesas to the east, possibly as erosional remnants. They appear throughout the rough cratered highlands plains as well as the smoother cratered lowlands plains. They are a common feature in the Hesperian and Noachian transition unit from the USGS Geologic Map of Mars (Tanaka, et al., 2014).

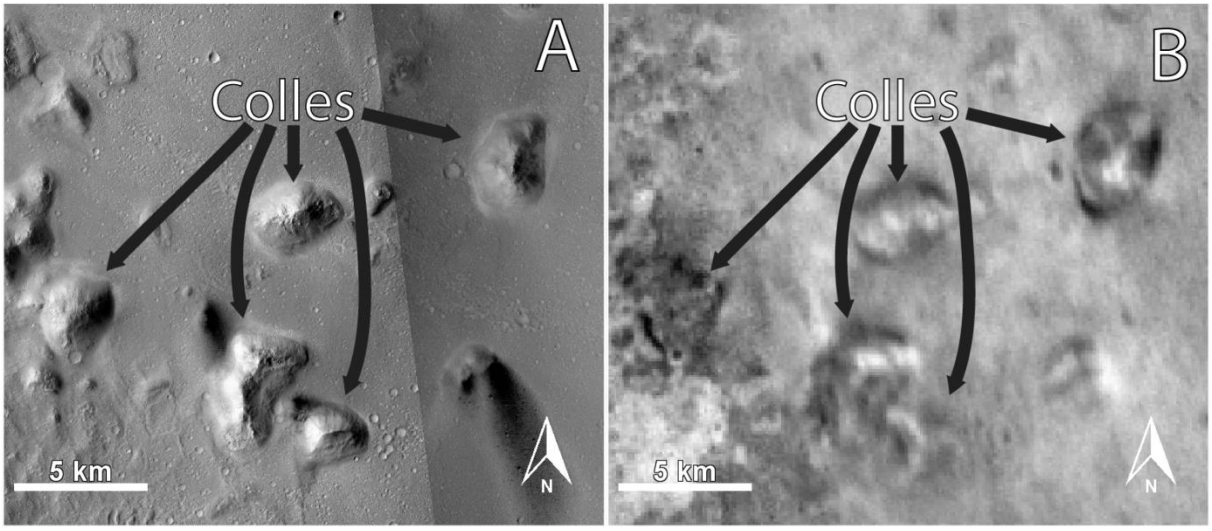

13. Gale Crater Rim Unit - The Gale Crater Rim unit is composed of the exposed rim of Gale Crater and Gale Crater ejecta directly adjacent to the rim. It is characterized by very dark spurs, talus slopes and some hilly ejecta just outside the rim. It has a sharper, more defined appearance than the hummocky terrain which is nearby. This unit is present only on and just outside the rim of Gale Crater in the morphological map area.

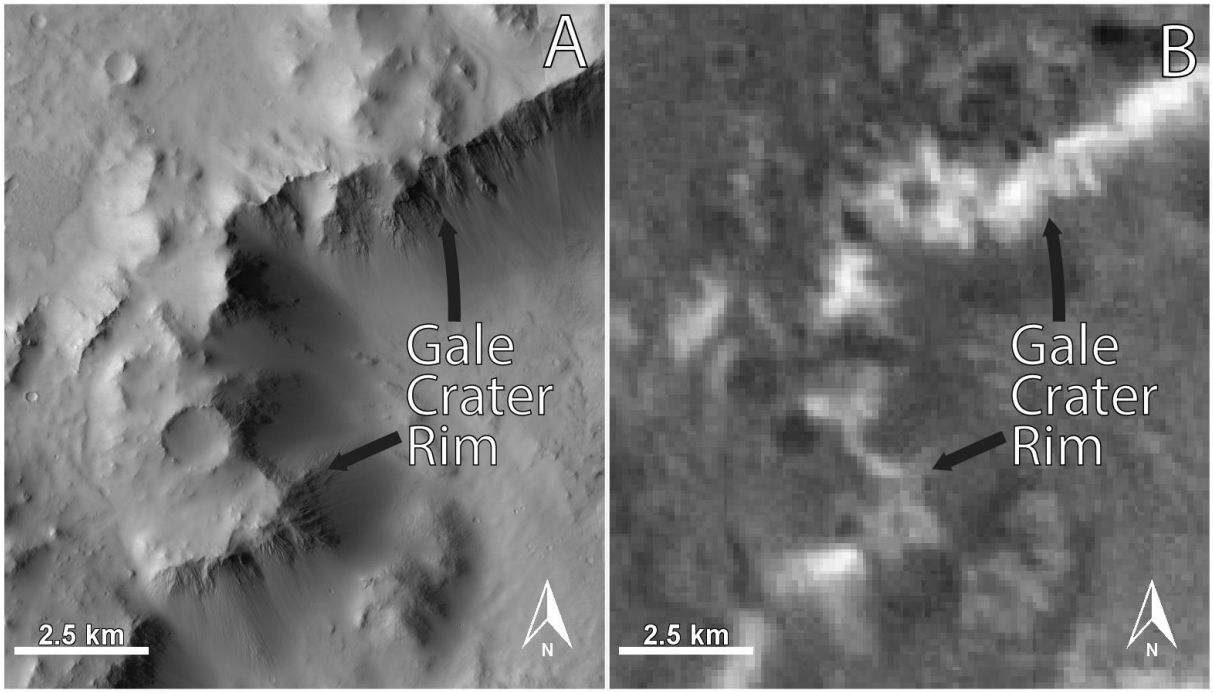

14. Highland Rugged Knobby Unit - The highland rugged knobby unit is a rough unit that exists on the edge of an elevated section of the cratered plains. It has an abundance of knobs and other small hills, in some locations it resembles the hummocky terrain and also has a similar appearance to Gale Crater rim. There are linear ridges of knobs/hills along with more rounded groupings. Ridges can be >10 km long and up to 300 m relief though generally smaller (5 km long, 100 m relief). Troughs between ridges appear smooth or channeled. Troughs and ridges may be related to channeling that appears in the unit. It is possible that some of it is ejecta from Gale Crater, colles or the result of the plains eroding into lower relief plains. It has many small craters and a few relatively large ones. It follows a ridgeline and has a different texture than the higher plains and lower plains.

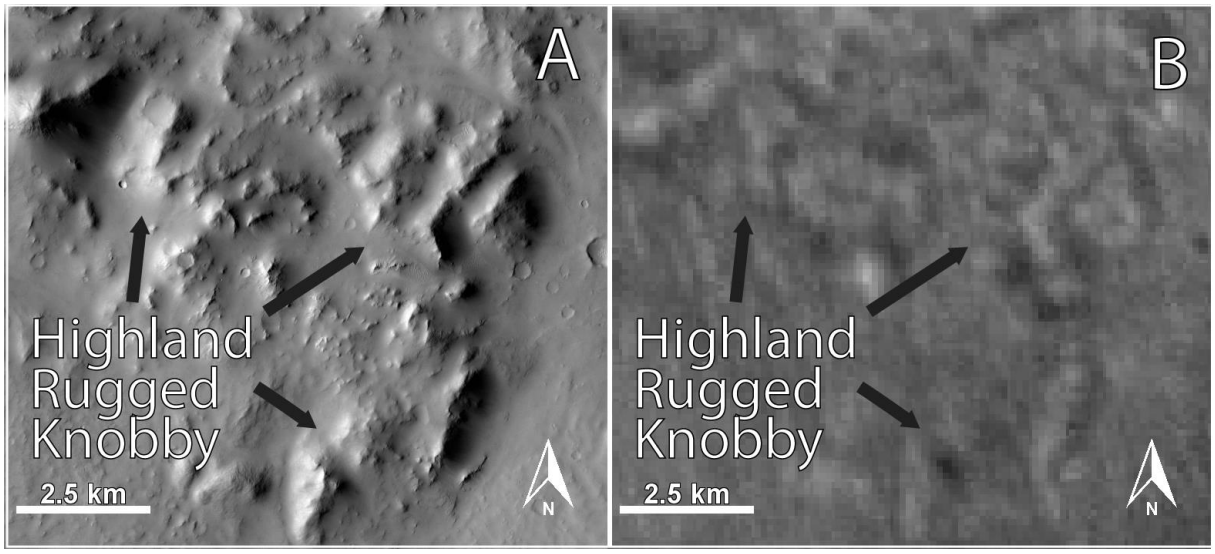

15. Cratered Highlands Plains Unit - A plains unit located to the west of North Gale Landform. It is at a higher elevation than the plains to the east of it. It contains hillier and rougher terrain than the cratered lowlands plains unit. It has a dark tone surface in CTX and bright surface in THEMIS Night IR.

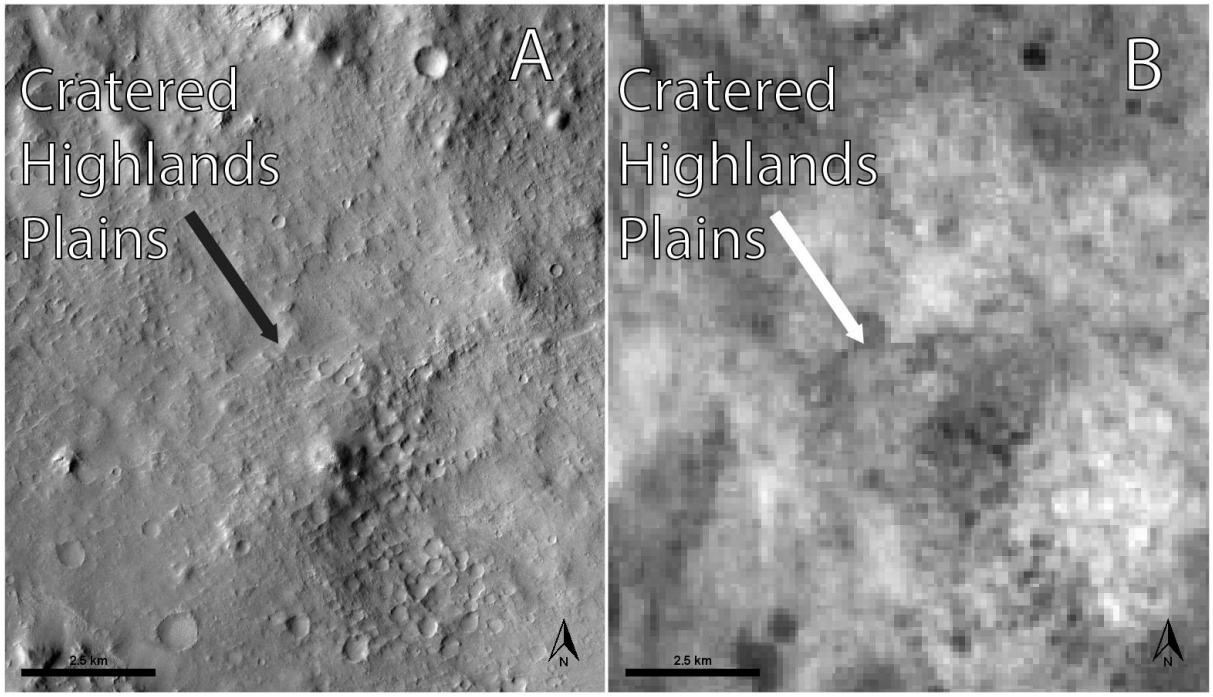

16. Cratered Lowlands Plains Unit - A flat plains unit that appears to the north of North Gale Landform. The surface is covered with small craters as well as some relatively large craters (up to 10 km diameter). There is a light tone and a dark tone component to this unit in CTX, the dark tone unit appears to be slightly elevated relative to the light tone. It is mid tone in THEMIS Night IR.

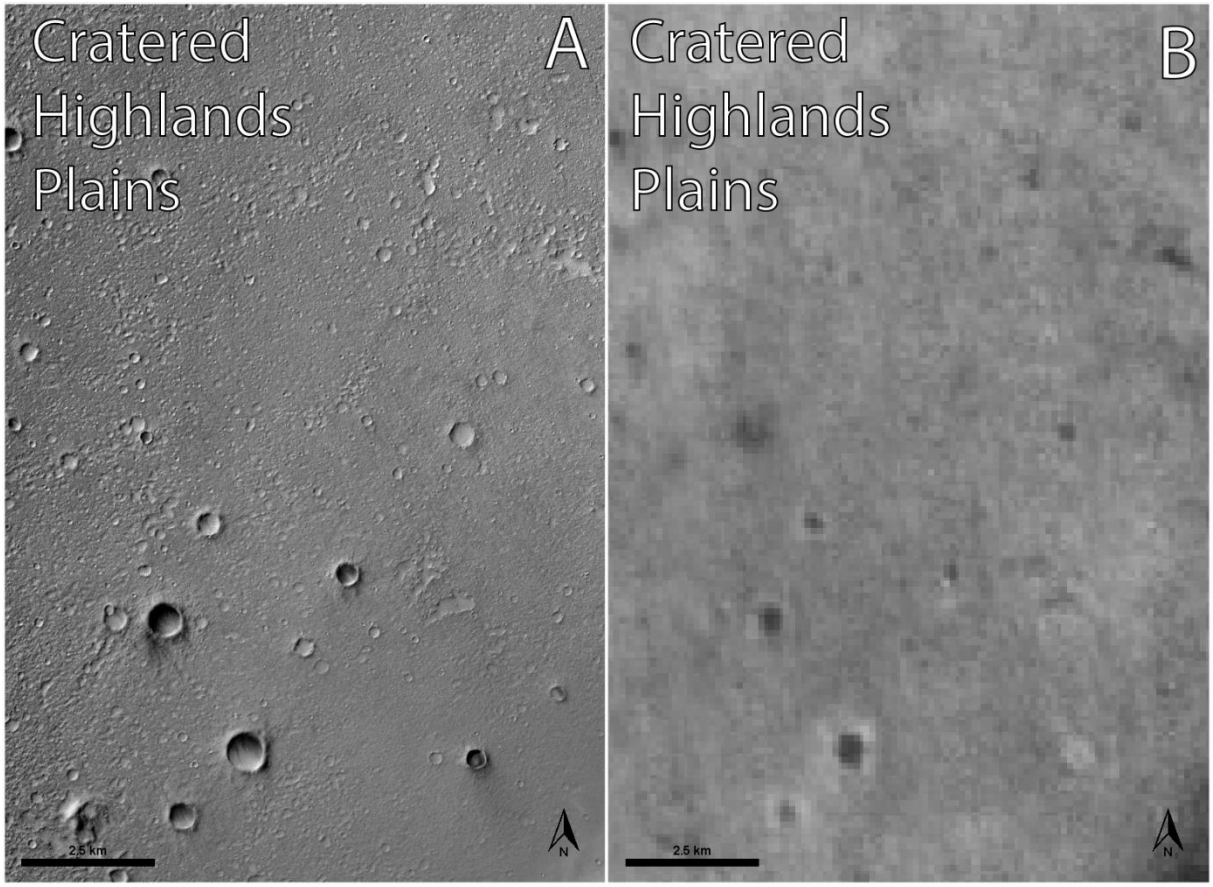

17. Cratered Light Tone Unit - A light tone unit with abundant small craters that wraps around the western side of North Gale Landform. This unit is smoother than the cratered lowlands plains to the north and cratered highlands plains to the west as well as lighter tone. It has a light tone under CTX and mid to light tone in THEMIS Night IR.

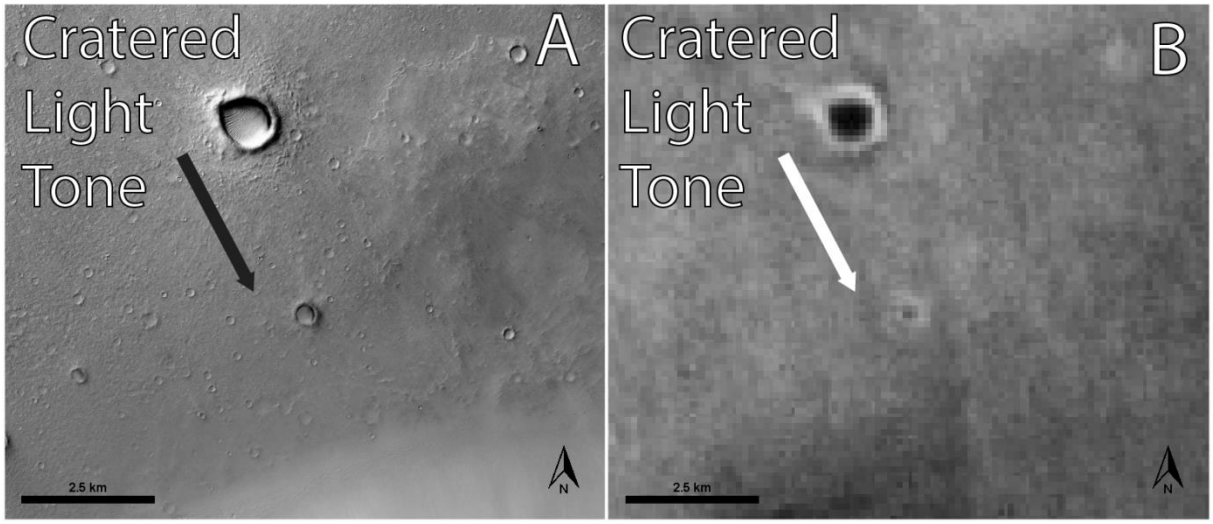

18. Cratered Mid Tone Unit - This unit contains lots of small craters and has a mottled surface texture. It has a mid range tone with some light toned lineations that are only visible in HiRISE, lineations that are mostly oriented roughly east-west. The light tone features may be the remains of an older surface that existed here before being taken away by erosion. This unit surrounds the chaotic terrain. It is bright under THEMIS Night IR.

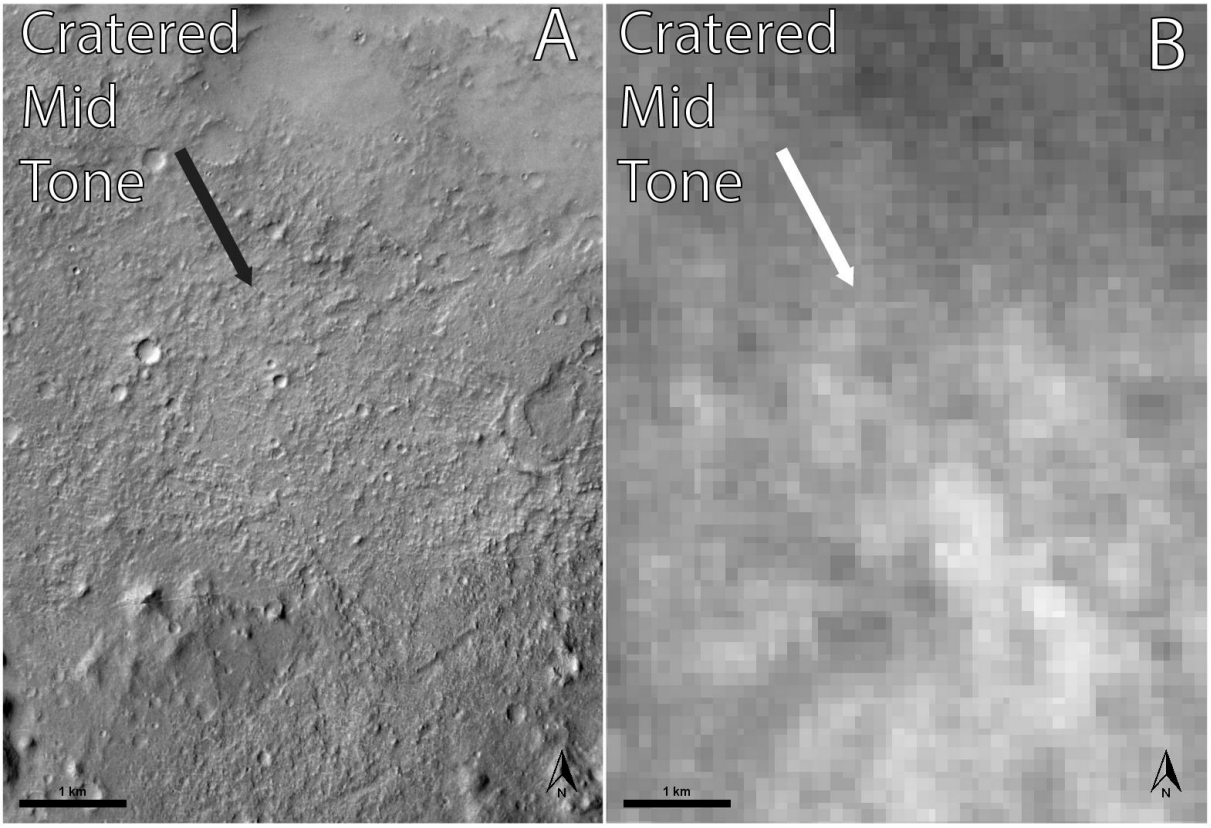

19. Mottled, Cratered, Dissected Mid Tone Unit - A mid tone unit, contains mottled terrain, abundant craters of varying sizes and some small colles features. It surrounds the large hill north of North Gale Landform. Some parts have been dissected with wide, shallow valleys that may have once carried water. There is a mixture of lighter and darker tone sections in CTX and appears mid to dark tone under THEMIS Night IR. There are several areas which appear to be depressions, may be related to volcanism or to sublimation of subsurface ice.

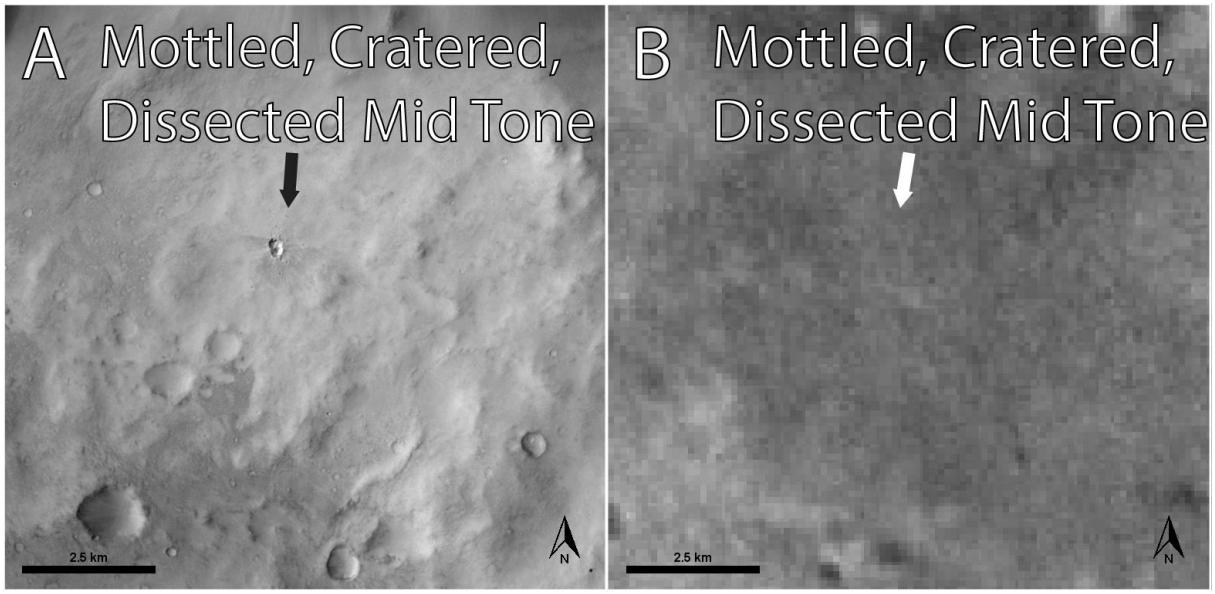

20. Shelf Unit - A “shelf” or ridge that is elevated above the smooth cratered lowlands plains to the northeast, it also has a different surface texture than the rougher cratered plains to the west. The surface has a cratered, mottled texture and tilted downslope to the west with up to a 100-m difference in elevation from the high point. The east side has a much steeper slope with up to 60-m difference in elevation and a channel alongside it. The channels cut through the northern part of the unit instead of along its edge. This unit may be related to the chaotic terrain. It is mid toned in CTX and THEMIS Night IR.

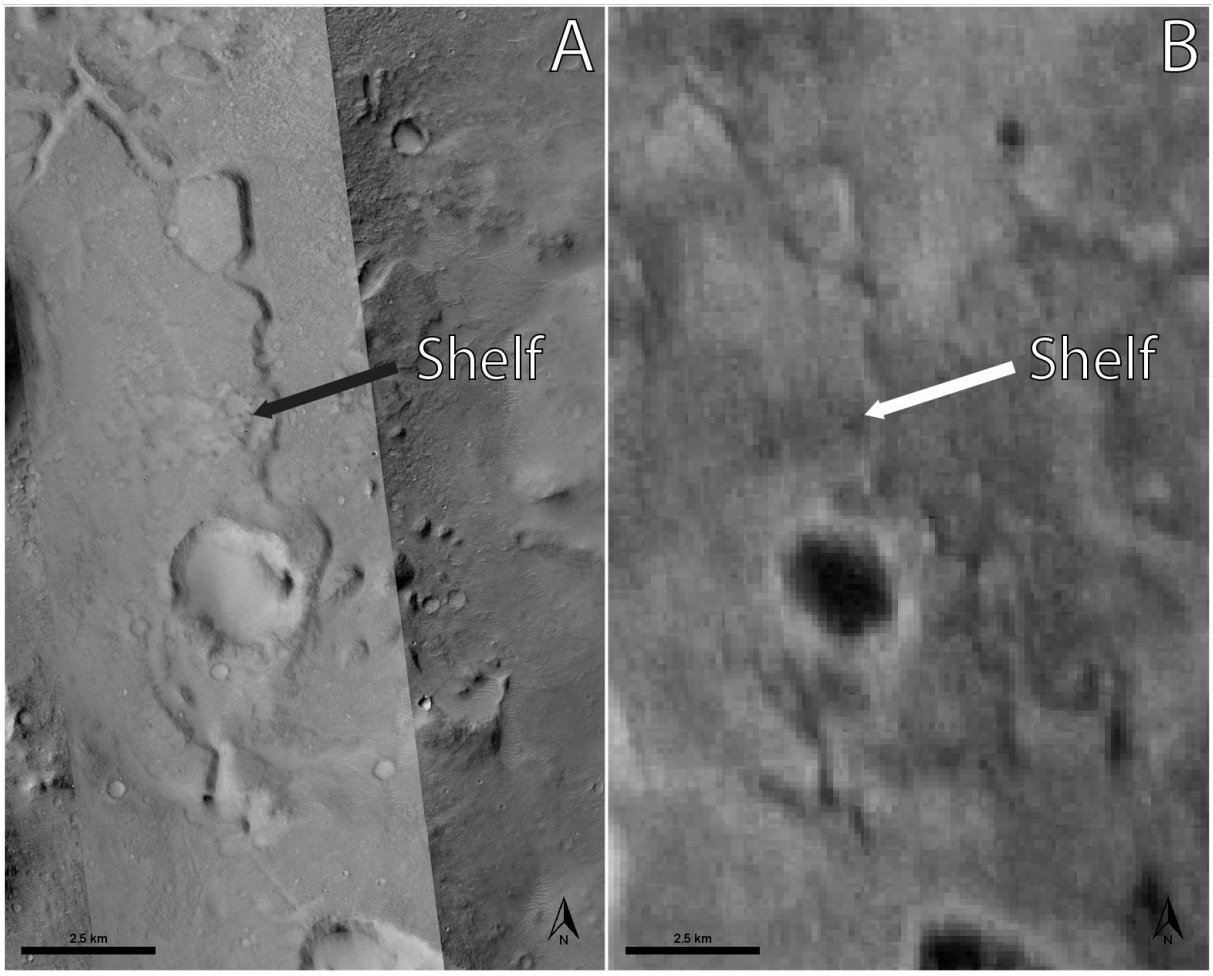

21. Dunes Unit - Large dune features, usually associated with colles or other forms of hills. There are up to 10s of meters in between crests though some have smaller distances. The light areas are crests of the dunes while dark areas are the troughs in CTX, it is dark under THEMIS Night IR.

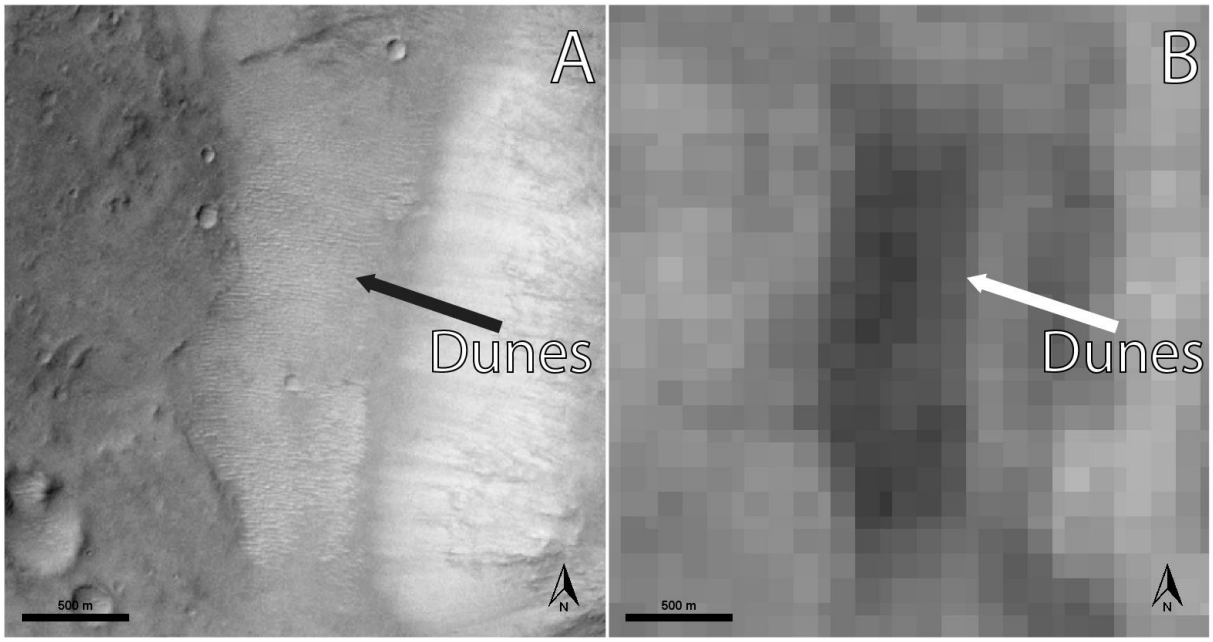

22. Crater Unit - Relatively large impact craters (>0.9 km, not including Gale Crater) with most having an associated visible ejecta blanket that at least partially surrounds the crater. Some of the craters have experienced infilling and some have spurs visible on the interior of the crater rim. The rim appears bright under THEMIS Night IR and the interior is mid to dark toned.

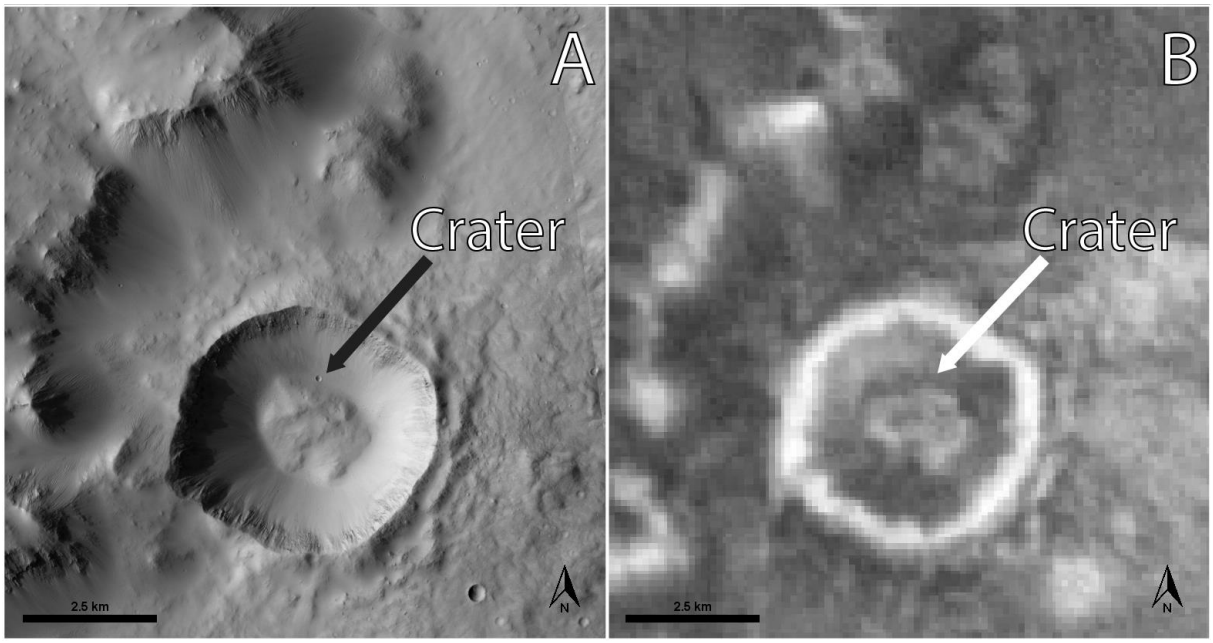

23. Ejecta Unit - The visible ejecta blankets from craters smaller than Gale Crater. They overlay the surface material and often have a radiating pattern spreading away from the center of the crater they surround. There are sometimes several waves of ejecta visible. This unit appears bright to mid toned under THEMIS Night IR.

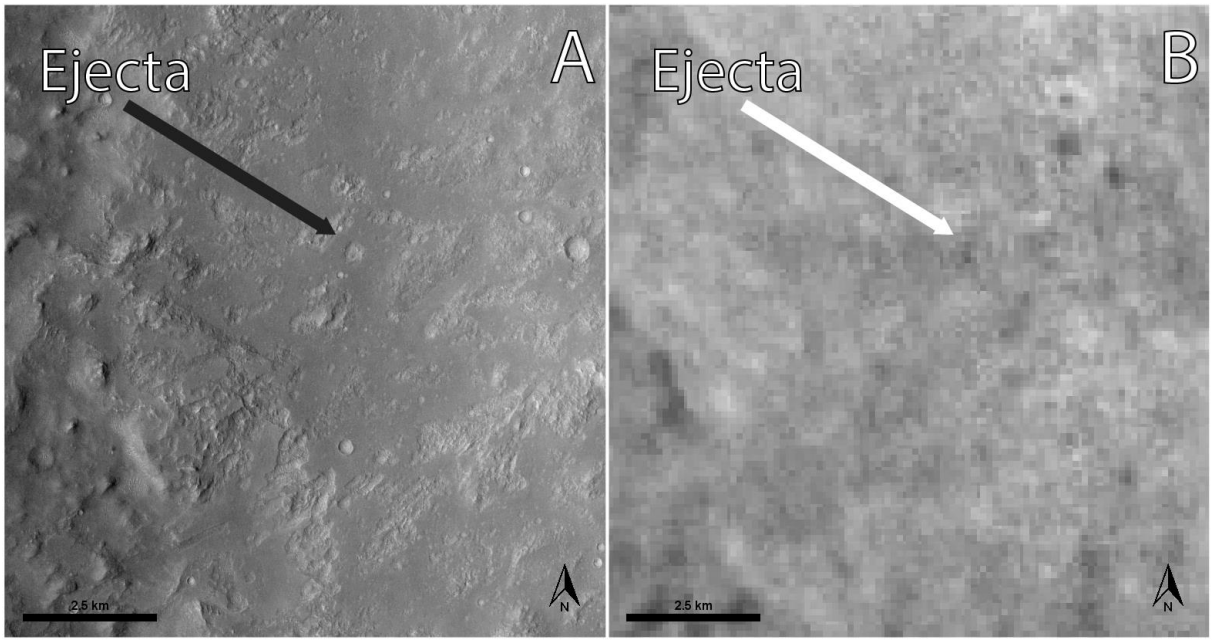

24. Alluvial Fan Unit - Alluvial fan in Gale Crater, end of the Peace Vallis drainage system. It has a cratered and smooth surface with mid tone in CTX and THEMIS Night IR. Some channeling is present.

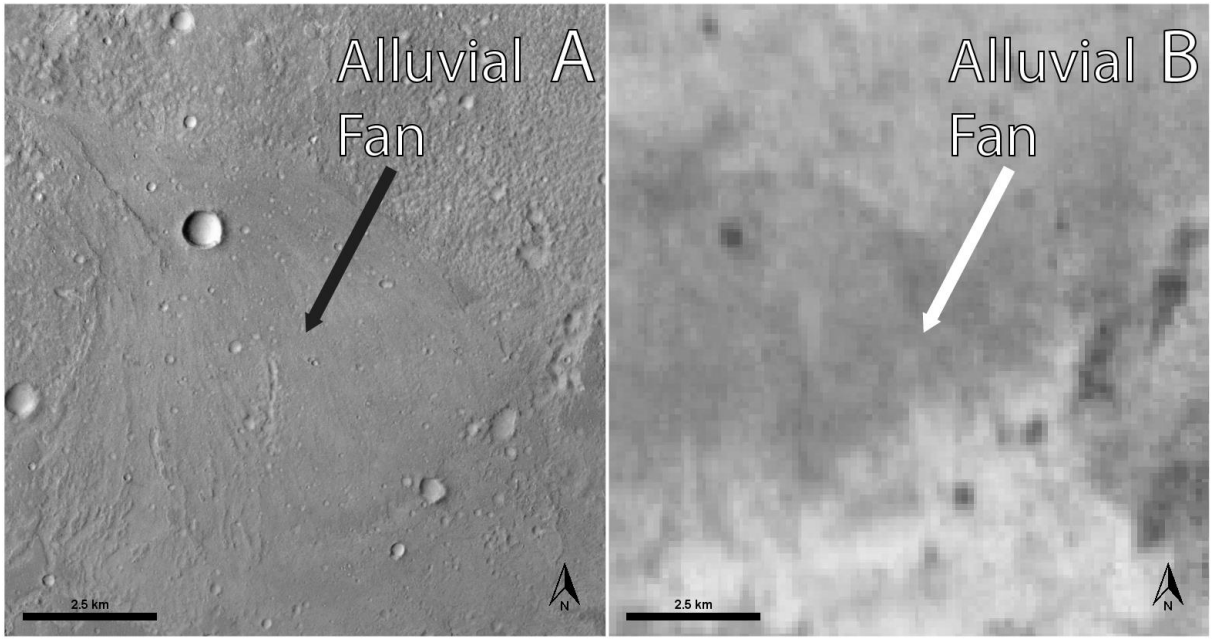

25. Gale Crater Interior Unit - The floor of Aeolis Palus between the rim and Mount Sharp in the northern part of Gale Crater. It is light and mid tone, has a mottled appearance and is dissected in portions as well. It appears bright under THEMIS Night IR. The unit contains many small craters as well as a few larger craters. There are inverted streams near the crater rim as well. The dark tone unit appears to be raised slightly when compared to the light tone unit.